Investigation of Au, Pd, and AuPd Nanoparticle Catalysts for Alcohol Oxidation Reactions

A Thesis Submitted to the College of

Graduate Studies and Research

In Partial Fulfillment of the Requirements

For the Degree of Master's of Science

In the Department of Chemistry

University of Saskatchewan

Saskatoon

By

Aimee Maclennan

Permission to Use

In presenting this thesis/dissertation in partial fulfillment of the requirements for a Postgraduate degree from the University of Saskatchewan, I agree that the Libraries of this University may make it freely available for inspection. I further agree that permission for copying of this thesis/dissertation in any manner, in whole or in part, for scholarly purposes may be granted by the professor or professors who supervised my thesis/dissertation work or, in their absence, by the Head of the Department or the Dean of the College in which my thesis work was done. It is understood that any copying or publication or use of this thesis/dissertation or parts thereof for financial gain shall not be allowed without my written permission. It is also understood that due recognition shall be given to me and to the University of Saskatchewan in any scholarly use which may be made of any material in my thesis/dissertation.

Requests for permission to copy or to make other use of materials in this thesis/dissertation in whole or part should be addressed to:

Head of the Department of Chemistry

University of Saskatchewan

Saskatoon, Saskatchewan (S7N 5C9)

Canada

Abstract

The focus of this thesis is on the synthesis, analysis, and applications of Au, Pd, and AuPd nanoparticle catalysts. The primary focus of this work is their use as catalysts for the oxidation of a variety of alcohols and the characterization of these materials by x-ray absorption spectroscopy to further understand their structure/property relationships.

The first project of this thesis consists of the synthesis of a series of Au, Pd, and AuPd nanoparticles by chemical reduction for the use in nanoparticle-catalyzed oxidations of a variety of α,β-unsaturated alcohols. It was seen that Pd NPs, K_2PdCl_4, AuPd nanoparticles, and Au nanoparticles mixed with K_2PdCl_4 were active catalysts for the oxidation of α,β-unsaturated alcohols in water at 60°C, with no added base, using O_2 as the oxidant. However, monometallic Au nanoparticles showed little to no activity for all substrates in this system. Monometallic Pd nanoparticles, in the absence of Au, showed high activities for reactions in ionic liquids due to the ease of Pd reduction in this environment. Structural analyses of the nanoparticles before and after reactions was performed by TEM and EXAFS. It was found that, during reactions catalyzed by Au nanoparticles and K_2PdCl_4, bimetallic AuPd nanoparticles were formed *in-situ* during the reaction. All of the other systems showed significant Ostwald ripening, indicating a redox mechanism for these reactions.

The second project focuses on the analysis of the formation of bimetallic AuPd NPs *in-situ* during the Au nanoparticle/K_2PdCl_4 catalyzed oxidation of α,β-unsaturated alcohols. The room temperature oxidation of crotyl alcohol using the aforementioned catalyst system was studied by *in-situ* x-ray absorption spectroscopy (both x-ray absorption near edge spectroscopy

and extended x-ray absorption fine structure spectroscopy). The mechanism by which this reaction occurs is poorly understood and remains unclear. Two proposed mechanisms for this system are a redox reaction involving Pd ions as the active species and a β-hydride elimination reaction. Studying the changes in Pd during the reaction by time-resolved, quick scan x-ray absorption spectroscopy allowed us to gain information about Pd speciation, and kinetics of the reduction reaction. It was determined that, upon addition of crotyl alcohol to an aqueous mixture of Au nanoparticles and K_2PdCl_4, the Pd(II) quickly and completely reduced onto the Au nanoparticles, forming bimetallic nanoparticles. The susceptibility of nanoparticles formed *in-situ* to oxidation was also tested. It was found that these particles are very stable, unaffected by exposure to molecular oxygen for up to seven hours. This suggests that Au in the system prevents the re-oxidation of Pd(0) from the surface of the bimetallic nanoparticles.

Acknowledgements

Throughout this crazy endeavour which has been my master's program there have been many people who've supported me with countless gestures of love and encouragement. Of these people, my family: Paulette, Gord, and Aaron Maclennan, have been the most endearing, holding my head up through times of stress and unease. I would like to thank them for all of the time, support, and love they've invested in me while going through the paces of being a grad student. I wouldn't have succeeded without their encouragement and support.

I would like to sincerely thank Dr. Robert W.J. Scott for taking on the challenge of being my supervisor. He is the most knowledgeable, encouraging, and patient supervisor I know. It couldn't have been an easy job motivating me into writing two papers, let alone a thesis. Thank-you for all of the knowledge and experiences you've helped me gain.

Thank-you to all of the Scott group members and fellow students of the Department of Chemistry. You all have made my M.Sc. experience a great one. Thank-you for the laughs, encouragement, knowledge, and advice!

My appreciation also goes out to Yongfeng Hu and Jeff Miller who helped with all of the *in-situ* work. Thank-you for sharing your expertise and knowledge about synchrotron analysis and XAFS. I appreciate all that I have learned by working with you both.

Lastly I'd like to thank my partner John Hayes for all of the laughs, love, and support he's given me over the last few years. I'm so lucky to have gone through this experience with you at my side, keeping me calm and focused. Without your support and encouragement I'd still be on chapter one.

To my family and friends

Thank-you for all of your love and support

Table of contents

Chapter 2

Aerobic Oxidation of α,β-unsaturated Alcohols Using Sequentially-Grown AuPd Nanoparticles in Water and Tetraalkylphosphonium Ionic Liquids

Chapter 3

In-Situ XAFS Analysis of Nanoparticles During the Oxidation of Crotyl Alcohol

List of Figures

List of Tables

List of Schemes

List of Abbreviations

β-H	Beta-hydride
BF	Bright Field
CTAB	Cetyl Trimethyl Ammonium Bromide
DCM	Dichloromethane
DF	Dark Field
EXAFS	Extended X-ray Absorption Fine Structure
HRTEM	High Resolution Transmission Electron Microscopy
ID	Insertion Device
IL	Ionic Liquid
LVCC	Laser Vaporization and Controlled Condensation
NMR	Nuclear Magnetic Resonance
NP	Nanoparticle
P[6,6,6,14]Cl	Trihexyl(tetradecyl)phosphonium Chloride
PAMAM	Poly(amido amine)
PEEK	Polyether Ether Ketone
PPI	Poly(propylene imine)
PVA	Polyvinyl Alcohol
PVP	Polyvinnylpyrrolidone
TEM	Transmission Electron Microscopy
THF	tetrahydrofuran
Uv-Vis	Ultraviolet Visible

XAFS	X-ray Absorption Fine Structure
XANES	X-ray Absorption Near Edge Spectroscopy
XAS	X-ray Absorption Spectroscopy

Chapter 1

Introduction and Review of Nanoparticles and Catalysis

1.1 Introduction

The study of catalysis is a diverse and constantly growing area of research which all leads to the same end goal; how to increase the rate of a reaction by adding another species which does not become consumed throughout the course of the reaction. A chemical species which increases the rate of reaction but is not consumed during the reaction is called a catalyst. There are many different types of catalysts which are used in a variety of reactions. Some of these catalysts include: organocatalysts, biocatalysts, electrocatalysts, and organometallic catalysts. Organocatalysts are small non-metal-containing molecules which play an important role in asymmetric synthesis reactions.[1] The majority of these catalysts are single molecules containing N, C, O, P, and S.[1] Biocatalysts are natural catalysts such as enzymes and lipases.[2] These catalysts are used in a variety of organic reactions such as transesterifications, ammoniolysis, and epoxidation reactions.[2] Electrocatalysts are metal-containing catalysts found in fuel cells and are used to increase the rate of oxygen reduction or fuel oxidation.[3] Electrocatalysts are generally composed of Pt, but Pd research is also on the rise for this class of catalyst.[3] Organometallic catalysts also contain metal species, but the metal is often incorporated into an organic framework. Common organometallic catalysts include N-heterocyclic carbenes, the Grubb's catalysts, Ziegler-Natta catalysts, and that used in the Monsanto process.[4]

Catalysts can be placed into two classes: homogeneous catalysts and heterogeneous catalysts. Homogeneous catalysts are those which are found in the same state as the reactants;

typically the catalyst and reactant are dissolved in the same solvent. Organocatalysts, biocatalysts, and organometallic catalysts can be classified as homogeneous catalysts. Heterogeneous catalysts are those that exist in a different state than the reactants. Electrocatalysts are considered to be heterogeneous catalysts because they are supported metal catalysts which are placed into a solution of reactants.

A third classification of catalyst which has not yet been discussed is a pseudo-homogeneous catalyst. Pseudo-homogeneous catalysts are those which appear to be in the same phase as the substrate, but are suspended in the solvent rather than dissolved in it. In pseudo-homogeneous catalysis, the catalytic species is often a metallic nanoparticle (NP) suspended in a solvent of a different phase. Pseudo-homogeneous NP catalysts have attracted a lot of interest in the catalytic community.

The focus of this thesis will be on gold, palladium, and gold-palladium NP catalysts, their use in oxidation reactions, and the means by which they are characterized.

1.2 Nanoparticle Catalysts

NPs have been found in applications dating back to the 19th century where they were used in photography and the decomposition of hydrogen peroxide.[5] However, it was not until much later when their use in catalytic applications was pioneered.[5] From 1941 to 1943, Nord *et al.* published a series of papers on polymer-stabilized Pt and Pd NPs and their use in hydrogenation reactions.[6, 7] By systematically studying NP catalytic efficiency on a variety of substrates using a range of NP stabilizers, pHs, and metal concentrations they paved the way for further development of NP catalysts. Two other pioneers in the world of NP catalysis were Parravano and Haruta. With influential works published in the 1970's and 1980's they outlined the use of

supported Au NPs on the oxidation of carbon monoxide (CO).[8-12] These works began the surge of Au NP catalyst research which has continued throughout the years.

NPs are small metal colloids with sizes of 10 nm or less. These particles are used to catalyze many reactions including oxidations,[13-18] hydrogenations,[9, 19] and C-C coupling reactions.[20, 21] The advantages of using NPs as catalysts include the large amount of surface area which they possess and their tuneability. Pseudo-homogeneous NP catalysts are desirable catalysts because they possess the potential for easy removal and regeneration of the catalytic species from a reaction compared to homogeneous systems. Traditional homogeneous catalysts require large amounts of solvent to separate the product from the catalyst, producing an excessive amount of waste. If the catalyst can be mechanically separated from the product it would provide a more efficient means of performing the reaction. The large amount of surface area which NPs possess coincides with their extremely small size. This is a very desirable trait because the increased surface area increases the amount of active sites on which the reaction can take place, subsequently increasing the rate of reaction. The size, shape, and morphology of NPs can be tuned using a variety of metals, metal precursors, solvents, stabilizers, and supports. Changing one variable in the synthetic technique can result in vastly different NPs. The ability to construct a NP with particular attributes is desirable because it affects the efficiency and selectivity of the catalyst for a particular reaction. Each of these NP traits is very important in the realm of catalysis. Because particular traits affect different reactions, it is important that a broad spectrum of NPs are synthesized and well-characterized in order to gain an understanding on how these materials work. Discussion on NP synthesis and characterization are included in detail below.

1.2.1. Monometallic Nanoparticle Catalysts

The most commonly used metal catalysts in today's industrial processes include Pt, Pd, and Rh.[22] These metals are commonly employed in the catalytic converters of cars, where they are present as nanocrystalline material layered on alumina, ceria, or silicate oxide supports. These noble metal particles are highly efficient catalysts because the metallic sites on the surfaces of the NPs serve as the active sites for both oxidation and reduction processes.[22] Although they are efficient catalysts, supported NPs do not always perform to their fullest potential because many of the active sites on the metal particle surface become partially hindered as the NP is bound to the oxide support. The development of NPs stabilized by alternatives to bulk oxide supports is currently underway in order to develop catalysts with more available surface area or active sites, thus increasing catalytic activity.

Aside from sequestering noxious chemicals from the environment by catalytic conversion, noble metal NPs are efficient catalysts for both oxidation and reduction processes. These chemical reactions are used in many industrial processes such as the production of pharmaceuticals and chemicals, and the conversion of waste by-products into usable species. NPs employed in these processes are often comprised of Pt, Pd, Ag, and Au.

When synthesizing metallic NPs it is common to use metals that are not susceptible to oxidation or degradation. If a catalyst becomes oxidized or degraded the catalytic activity decreases substantially, lowering the efficiency of the catalyst. Therefore, one must select the appropriate metal and stabilizers when synthesizing an efficient NP catalyst.

1.2.2 Bimetallic Nanoparticle Catalysts

Bimetallic NPs are those which contain two metals within one particle. Bimetallic NPs are often synthesized in order to reduce the cost of a catalyst[23-25] and/or to enhance the properties of a monometallic catalyst.[14, 16, 25-29] Many bimetallic NPs are composed of a noble metal and a transition metal. Common metal pairings for bimetallic NPs include a noble metal such as Au, and Pt and a 3d transition metal like Fe, Co, Ni, or Cu.[23-25] Making an NP out of a noble metal and a 3d-transition metal is beneficial because it reduces the amount of expensive noble metal required and thus, lowers the cost of NP synthesis. However, NPs consisting of two noble metals are also commonly made. Pairing Au and Pd or Au and Pt is often done to make highly active NP catalysts. When a NP is comprised of two metals a synergetic effect between the metals can occur, often creating a catalyst which is more efficient and selective than either of the metal species alone. The improved efficiency of bimetallic NPs is often attributed to electronic effects between the two metals. The non-active metal will withdraw electron density from the active species, altering its d-electron density, causing it to become a more efficient catalyst. Changing the electronic properties will also alter the interatomic distances between the metal atoms.[25] This can also play a role in catalytic efficiency and selectivity, resulting in a better catalyst than monometallic NPs.

For example, Prati *et al*. found that AuPd NPs were approximately 4.5 times more active for the selective oxidation of glycerol to glyceric acid than either of the monometallic species.[30] They concluded that the increase in activity is due to the change in morphology of the catalyst when the two metals were combined. They found that particles containing more Au than Pd were the most active for the oxidation of glycerol to glyceric acid. Particles with more Au had a multiply twinned structure with mostly active (111) surfaces. Particles with more Pd than Au

showed a large decrease in catalytic activity. These particles were not preferentially twinned, reducing the amount of active surfaces. This is an interesting display of the synergetic effect between metals because the authors concluded that the active site on the bimetallic particles was a Pd monomer surrounded by Au atoms. Therefore, Au plays a big role in increasing the activity of the Pd in the system.

1.2.2.1 Morphology of Bimetallic Nanoparticles

When synthesizing bimetallic NPs, there are a variety of morphologies which can be achieved. These morphologies arise from varying synthetic techniques and/or conditions, including the bimetallic composition of the NP.[30] The morphology of bimetallic NPs can also play a role in the efficiency of the catalyst. Depending if the catalytic species is present on the surface of the NP, accessible to the substrate, or hidden within the NP will have an effect on the efficiency of the catalyst.

Three common morphologies of bimetallic NPs are random alloy, cluster in cluster, and core-shell. (Figure 1.1) Random alloy NPs are those in which the two metals are distributed randomly throughout the NP. The cluster in cluster morphology of bimetallic NPs occurs when there are clusters of each metal distributed throughout the NP. Core-shell NPs are those which have a core of one metal species and a shell of the second metal around the well-defined core. Core-shell NPs are interesting in that, one can compose a core of a readily available, inexpensive material and surround it with an expensive, more catalytically active metal. For example, Zhang *et al*. showed an excellent case of AgAu NPs synthesized by galvanic exchange.[31] The production of NPs by galvanic exchange provided synthetic advantages such as independent

tuning of the size and composition of bimetallic NPs, production of NPs in high concentrations, and the general ability to synthesize NPs that cannot be made by the co-reduction method. An example of AgAu core-shell nanoprisms using the sequential reduction method was shown by Shahjamali *et al.*[32] They determined that the formation of a Au shell around a Ag core provided a strong stability against etching of the NPs. This can be beneficial for catalysts, preventing NP degradation. These works provide good examples of the benefits of alloy and core-shell morphologies of NPs.

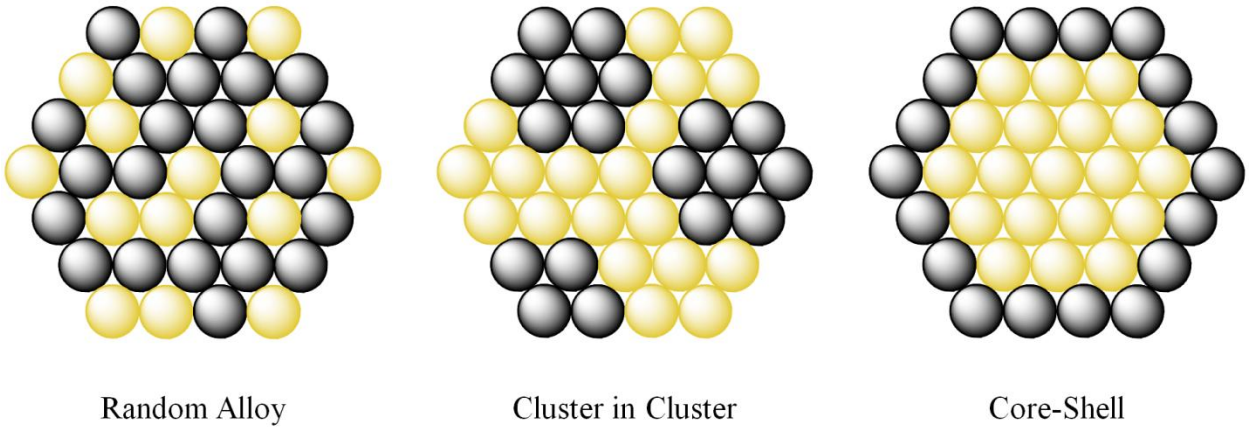

Figure 1.1. Common Morphologies of Bimetallic NPs

In an ideal catalyst the substrate is able to access the catalytically active species / active sites. Therefore, the core-shell morphology of bimetallic NPs can provide a catalyst morphology with a high atom economy. Since the catalytically active species is present as a shell around a transition metal core, there will be many available active sites to which the substrate can approach. Although the surface of a cluster in cluster NP is not entirely composed of the catalytically active material, it still possesses a high amount of accessible active sites. There are also cases in which cluster in cluster or random alloy morphologies are the desired NP species

because the active sites are determined to be at the interface between the two metals.[33, 34] Active sites are often thought to occur at surface defects (steps and edges) along NP surfaces. Under-coordinated atoms on these sites also may lead to significant changes in the electronic interactions on the NP surface, leading to changes in the NPs catalytic efficiency.[35, 36] However, independent of morphology, pairing two metals most often enhances the activity of a NP catalyst when compared to either of its monometallic species.[14, 16, 25-30, 37, 38]

1.2.3 Oxidation Catalysts

Both monometallic and bimetallic catalysts have been used to catalyze oxidation reactions. The catalysis of oxidation reactions is important because many industrial processes employ oxidation reactions in order to produce their desired products. Oxidation reactions are often performed using stoichiometric amounts of harsh or environmentally unfriendly chemicals.[39] The use of stoichiometric amounts of chemicals, as well as the organic solvents and hazardous wastes produced by traditional means of alcohol oxidation are not considered to be green chemistry by today's standards. Upon the use of NP catalysts, it has been found that the rate of oxidation reactions can be increased substantially while decreasing the amount of wastes and hazardous materials formed.

The oxidation of alcohols is a popular area of research in NP catalysis. Using NP catalysts for the oxidation of alcohols is preferred to traditional methods because these reactions can be performed at ambient temperatures, using molecular oxygen as the oxidant instead of harsh permanganates and chromates, as well as using benign solvents such as water, or even

under solventless conditions.[14, 27, 29, 40-43] It has also been found that, when oxidation reactions are catalyzed by NPs, the NPs can often selectively oxidize a certain hydroxyl group on a diol or polyol. The selectivity of the oxidation reaction can be tuned by NP size and morphology, as well as the support or stabilizer on the NP, and the reaction conditions such as temperature and oxidant. Selective oxidation becomes important when one wants to produce a desired product from an alcohol precursor such as an aromatic aldehyde.

1.3 Au, Pd and Bimetallic AuPd Nanoparticle Catalysts

Before the discovery of NPs, bulk Au was considered to be an inefficient catalyst.[44] It was especially inert for both oxidation and hydrogenation reactions. It was later determined that the inactivity of bulk gold is due to its smooth (111) surfaces which are unfavourable for the adsorption of H_2 and O_2.[45] Surface science and density functional theory calculations have been performed on bulk gold and proved that there is no dissociative adsorption of H_2 and O_2 onto the smooth (111) surfaces at temperatures below 473 K.[45] Therefore, in order to consider using bulk gold as a catalyst for these types reactions the temperature has to be above 473 K. Using high temperatures for catalytic reactions is not ideal because it is hard to get selective chemistry at high temperatures, and current science is constantly moving towards greener chemistry, including reactions done at ambient temperatures. It was later discovered that, while bulk gold is an inefficient catalyst, small gold particles were highly efficient for many reactions including hydrogenation and oxidation reactions. The catalytic activity of gold was found to increase as the size of the metallic particles decreases. This is mainly due to surface effects such as the enhanced surface area of small gold clusters versus that of bulk gold. Some of the pioneering scientists in

the area of Au NP catalysis include Bond,[19] Parravano,[8, 9] and Haruta.[10] These scientists were some of the first to discover that metallic gold on the order of 2-10 nm behaved much differently than its bulk counterpart. Currently, there are many research groups still analyzing the catalytic capabilities of Au NPs versus that of bulk gold.

It has also been found that Pd NPs can be highly efficient catalysts for a variety of oxidation reactions.[46-49] The Hutchings group has found that supported Pd NPs are active catalysts for the selective oxidation of glycerol to glyceric acid.[49] This is an important reaction because an increase in biofuel production will result in a surplus of glycerol. If the glycerol by-product can be efficiently converted into a commercial solvent such as glyceric acid, Pd NPs will become an invaluable catalyst on an industrial level.

Since the discovery of the enhanced activity of Au NPs over bulk gold, scientists have been pursuing other means of enhancing the activity of Au NPs. Many scientists have found that pairing Au and Pd to make bimetallic NPs forms a highly efficient catalyst for many oxidation reactions.[14, 29, 38, 50-54] Prati *et al*. used a series of AuPd NPs with varying ratios of the metals to catalyze the oxidation of a variety of alcohols.[55] They found that, for the oxidation of benzyl alcohol, cinnamyl alcohol, 2-octen1-ol, and 1-octanol catalyst efficiencies were increased by bimetallic NPs by 500 times as compared to their monometallic counterparts.[55]

The high catalytic efficiencies and selectivities of Au, Pd, and AuPd NPs make them very attractive materials to study. The synthesis, characterization, and use of these particles will be outlined below.

1.4 Synthesis of Nanoparticle Catalysts

There are two pathways one can follow when generating NPs: the top-down or the bottom-up approach. Both of these methods are capable of synthesizing particles on the nanometer scale, but the means by which it is accomplished is vastly different. In the top-down approach a bulk material is broken down by mechanical means until NPs are achieved. The bottom-up approach involves the building-up of NPs by chemical reactions from metal precursors.[33, 44, 56] An illustration of the top-down and bottom-up syntheses are shown in Figure 1.2

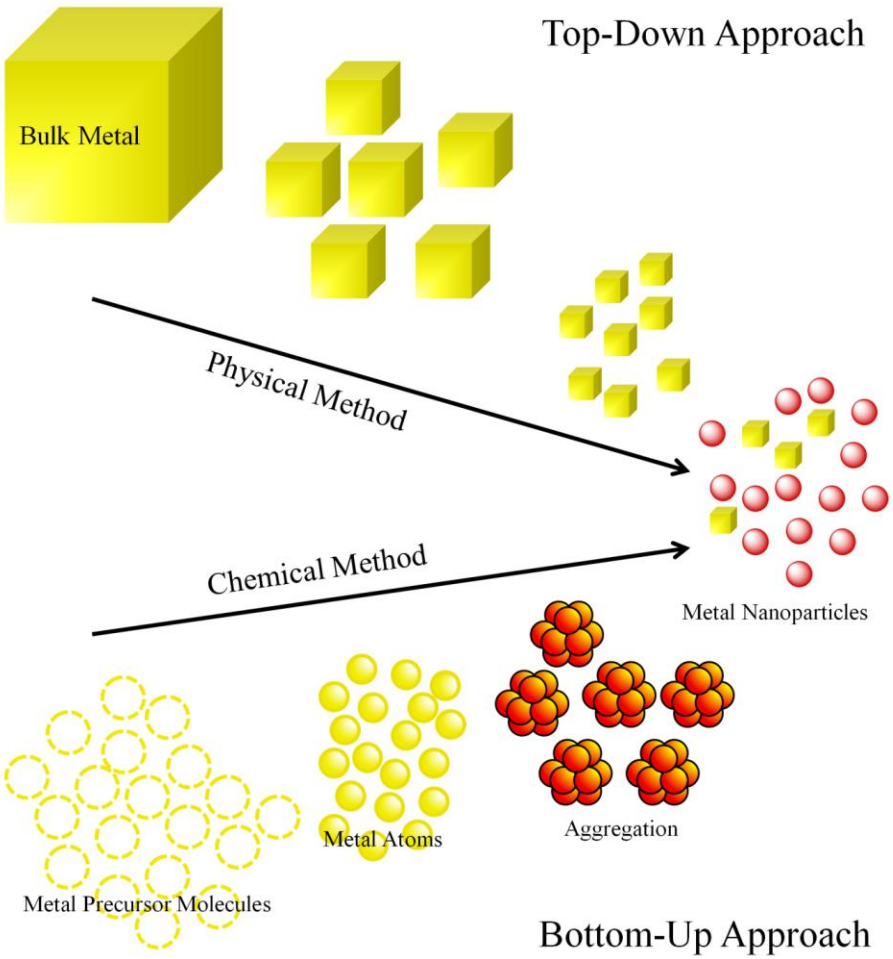

Figure 1.2. Illustration of the top down and bottom up approaches towards NP synthesis

Synthesis by means of the top-down approach is not a common way of making NPs. Synthesis by mechanical means often creates a sample of NPs which are not uniform in size or geometry.[56] Due to the nature of the synthesis, imperfections in the surface structure of the NPs also become an issue. This is due to the breaking apart of a larger material, causing stress fractures, cracks, and imperfections in the final nanosized product.[56] Often, there are also impurities found in the NPs which are a result of impure, low-grade bulk material.[56] Because synthesis by the top-down approach often produces a non-uniform, impure sample, the NPs created this way are not often ideal catalyst materials. Ideal NP catalysts are uniform in size and geometry, contain no impurities, and have well defined surfaces. Therefore, top-down synthesis of NPs will not be further discussed.

NP catalysts can be synthesized by the bottom-up method using many techniques which incorporate a variety of noble metal precursors, stabilizers, and supports. When synthesizing NPs the goal is to produce a sample of monodisperse and uniform particles which do not readily undergo degradation or agglomeration. Therefore, supports or stabilizers must be incorporated into the NP design in order to stabilize and sometimes enhance the activity of the particle. The synthetic procedure can often be tuned to produce a size-specific, monodisperse sample of NPs. This is advantageous because NPs of specific sizes, morphologies, and compositions often show high selectivities and reactivities towards many reactions. Common techniques used to synthesize NPs by the bottom-up approach include reduction of metal precursors, chemical vapour deposition, sonochemical irradiation, and photochemical irradiation. These methods, as well as the supports and stabilizers used to synthesize NPs will be discussed below.

1.4.1 Monometallic Nanoparticle Synthesis

As mentioned above, there are a variety of ways to synthesize NPs. Discussed below are common techniques used to produce monometallic NPs. Although these syntheses vary in methodology, they all aim to achieve the same end goal: to produce a sample of small, stable and monodisperse NPs with minimal to no surface defects.

1.4.1.1 Chemical Reduction

The most common technique of monometallic NP synthesis is reduction of a metal salt precursor.[57] Common metals used for this synthesis are Au, Ag, Pd, Pt, Ru, Rh, and Cu. In the case of Au NPs common salts are $HAuCl_4 \cdot 3H_2O$ and $NaAuCl_4 \cdot 3H_2O$. The synthesis often occurs in water, but can also be performed using non-aqueous solvents such as methanol and ethanol. When performed in non-aqueous solvent, it is often the solvent which is the reducing agent. For example, Hirai *et al.* made Rh NPs by refluxing rhodium a Rh salt and a polymeric stabilizer in methanol at 79°C for up 16 hours.[58, 59] The downside of synthesizing NPs in this manner is that the reaction must be done at high temperatures for long durations of time making the reaction environmentally unfriendly. A faster way to synthesize NPs via chemical reduction is to create an aqueous solution of metal precursor in water and reduce the metal ions with a reducing agent. Common reductants used to nucleate the metal include sodium borohydride, sodium carbonate, citrate anions, and ascorbic acid. The reductant is often used in a large excess in order to quickly reduce the metal salts into small NPs. NP size and morphology can be tuned using different types and of reductants. The size of NPs typically decreases with the increase in strength of reducing agent. A strong reducing agent will cause rapid nucleation of the precursor species, forming

many small NPs. A weak reducing agent will allow for slow nucleation, forming larger NPs. The type of reducing reagent can also affect the morphology of the NP. Miligan *et al.* found that when Au NPs are synthesized under the same conditions changing only the reducing agent, spherical NPs were formed when sodium citrate was used and prismatic NPs formed when citric acid was the reducing agent.[60] NP size is also dependant on the type and concentration of the stabilizer. The concentration and type of stabilizer will also affect the size and dispersity of NPs. Typically, as the concentration of stabilizer is increased, the size of NPs formed decreases. The stabilizer surrounds the NP preventing agglomeration of particles and typically quenches NP growth.

1.4.1.2 Electrochemical Synthesis

Electrochemical synthesis of NPs is used to produce pure, uniform, monodisperse samples of metal NPs. In order to produce NPs via electrochemical synthesis, a sacrificial metal precursor is selected as the anode in a simple two electrode cell.[61] The metal precursor at the anode becomes oxidized to metal ions when a current is applied to the system. The ions then migrate to the cathode where they are reduced and form metal NPs. The common electrolyte used in the cell is composed of tetraalklyammonium salts. These salts are used as the electrolyte because they act as a NP stabilizer, preventing agglomeration and metal plating onto the cathode surface.[61] Reetz *et al.* successfully synthesized Pd NPs using Pd metal as the anode material.[61] Tetraoctylammonium bromide in solution served as the electrolyte and stabilizer for the particles. Interestingly, the group found that as the current density was increased the size of the

nanoparticles decreased. Current densities of 0.1 mA/cm^2, 0.8 mA/cm^2, and 5.0 mA/cm^2 resulted in NPs of 4.8 nm, 3.1 nm, and 1.4 nm, respectively.[61]

Stabilizers such as polymer ligands can also be incorporated into the electrochemical synthesis, preventing agglomeration of NPs and electroplating of metals onto the cathode surface.[62] If a stabilizer is not incorporated into the cell during NP formation, metal NPs will have a tendency to form on the surface of the cathode. If this is the case, NPs are subsequently removed from the cathode via sonication in the presence of a surfactant which acts as the NP stabilizer.[63] Synthesis by electrochemical methods is a novel way to produce NPs because of the low reaction temperatures, the simplistic setup, as well as the ease of which NP size and morphology can be controlled.[64] NP size and morphology are easily controlled by adjusting the current density applied, the duration of electrolysis, and the type of electrolyte, stabilizers, and surfactants used.[65]

1.4.1.3 Chemical Vapour Synthesis

The process of synthesizing NPs via chemical vapour deposition begins with a metal precursor in the vapour phase. There are many ways to obtain a vapour precursor of metal including heating a solid until it vaporizes, pulsed laser ablation to vaporize a plume of material, or ion sputtering.[66] Synthesis of NPs using lasers is often referred to as laser vaporation and controlled condensation (LVCC).[67] Once in the gas form, the precursor vapour is often mixed with an inert gas. In their paper, Granqvist and Buhrman[68] reported how to synthesize metal particles less than 10 nm in size by inert-gas evaporation using a temperature-stabilized oven as a metal vapour source. They successfully synthesized NPs out of the transition metals Mg, Al, Cr,

Fe, Co, Ni, Cu, Zn, Ga, and Sn. From this publication it is seen that chemical vapour synthesis can be used to make a variety of metal NPs.

The driving force behind the chemical vapour synthesis of NPs is the establishment of a supersaturation of vapour. If the vapour phase is supersaturated with the metal precursor a high nucleation density occurs, causing the metal ions to nucleate and form NPs.[66] Mixing the precursor vapour with a cool, inert gas such as He or Ar also promotes NP formation by promoting condensation of the precursor vapour. NP size is controlled by nucleation time, the temperature of the vapour, the composition of the precursor, and well as the pressure at which the synthesis occurs.[69]

Although the NPs can be tuned by changing a variety of factors, gas-phase synthesis poses many problems. There are no stabilizers present during gas phase NP synthesis, causing excessive nucleation, sintering, and agglomeration of the NPs. In order to prevent or minimize these effects, the synthesis must be carried out using well defined temperatures and the reaction must be quenched very quickly by disrupting the high nucleation density of the system. Other common issues with vapour synthesis are precursor vapours interacting with oven materials and inhomogeneous heating of the vapour resulting in limitations with NP size control.[69] Although synthesis via the vapour method has the potential to produce a variety of metal NPs on many supports, it may still be beneficial to perform liquid synthesis via chemical reduction because it produces a monodisperse, well-defined sample of NPs.

1.4.1.4 Sonochemical and Photochemical Irradiation

Synthesis of NPs by irradiation is a less common, but an interesting means of making NPs. These syntheses involve the decomposition of a precursor by sonochemical or photochemical irradiation in order to produce well-defined NPs.

Sonochemical synthesis of NPs involves the subjection of a metal precursor dissolved in a high-boiling solvent to irradiation with a high-intensity ultrasound.[70] Ultrasonic treatment of the solution causes acoustic cavitation, resulting in the growth and collapse of bubbles within the solution. The collapse of the bubbles causes localized heating, which rapidly causes the organometallic precursor to decompose into metal atoms inside the collapsing bubble.[71] With the presence of stabilizers the metal atoms form small, monodisperse NPs.[70, 71] The NP size can be tuned by altering the frequency of sonochemical radiation, as well as the stabilizer present.

Synthesis of NPs via photochemical irradiation involves the reduction of metal precursors into metal NPs by UV irradiation. This method is beneficial for chemical reduction because less reducing agent is used, the reduction is performed uniformly in solution, and the rate of reduction is well known because the number of reducing equivalents generated by radiation is well defined.[72] The use of stabilizers is still required in order to produce small particles by preventing excess nucleation and agglomeration.[72] NP morphology using this method is dependent on photon flux, as well as the UV source.[73]

1.4.2 Bimetallic Nanoparticles

The synthesis of bimetallic NPs, like monometallic NPs, can be carried out using a variety of synthetic methods, including those used to make monometallic NPs. The morphology of bimetallic NPs can be controlled by the type of synthesis, as well as types of metals and metal precursors used. Similar to that of monometallic NPs, liquid synthesis is one of the most commonly used techniques used to produce bimetallic NPs. Two liquid syntheses: co-reduction and sequential reduction will be discussed in detail below.

1.4.2.1 Co-reduction

Co-reduction syntheses of bimetallic NPs involves the simultaneous reduction of two metal precursors via chemical reduction. Both core-shell and random alloy NP morphologies can by synthesized by the co-reduction of two metals.[14, 27, 33, 40, 74, 75] The morphology of the resulting NP depends on factors such as the affinity of the stabilizer towards one metal over the other, as well as the rates of reduction for each metal.[33] If a stabilizer has a higher affinity for one of the metal species in solution over the other, it is likely that the metal which is more attracted to the stabilizer will remain on the exterior of the NP (with the stabilizer bound to it) while the non-attracted species forms the core of the NP. Also, if one metal species has a faster rate of reduction, it is likely that this metal will form a "core" particle onto which the slower species will be reduced.[75] In these two cases, the NP will adopt a core-shell morphology. In the case that the stabilizer has no affinity towards a certain metal, and the metal ions reduce at the same rate, a random alloy NP may be produced. However, phase segregation of the metals can also occur, transforming alloy NPs into core-shell or cluster-in-cluster NPs.

Kuai *et al*. have developed methods to produce both core-shell and random alloy AuPd NPs by co-reduction.[74] They synthesized bimetallic NPs by mixing Pd(II) and Au(III) salt solutions with polyvinylpyrollidone (PVP) in the absence or presence of cetyltrimethylammonium bromide (CTAB). Ammonia was used as the reducing agent at hydrothermal conditions. They found that, in the absence of CTAB, core-shell NPs were formed. Due to the different reduction potentials of the metal salt precursors, Au reduced much faster than the Pd. This promoted the initial formation of Au NPs, followed by the reduction of Pd onto the NP surface, resulting in core-shell NPs. However, in the presence of CTAB, random alloy NPs were formed. They hypothesized that CTAB altered the reduction potentials of the metals, allowing both species to reduce simultaneously, creating small alloyed NPs.

1.4.2.2 Sequential Reduction

Although core-shell morphologies can be produced via co-reduction of metal precursors, it is more likely to produce a core-shell NP by the sequential reduction method. This method involves the initial formation of "seed" NPs from one metal, followed by the reduction of another metal onto the seed surfaces. Schmid *et al*. synthesized well-defined core-shell nanoparticles by reducing $HAuCl_4$ with sodium citrate to form Au "seed" particles, followed by the controlled reduction of H_2PdCl_4 by hydroxylamine hydrochloride onto the Au surface.[76]

Common problems with the sequential reduction method include the formation of secondary monometallic NPs and random alloy and cluster-in-cluster NPs. In order to prevent the formation of monometallic NPs, one must use a weak reducing agent in order achieve the controlled reduction of the second metal onto the "seed" particle. If a weak reducing agent is

used, the secondary metal will preferentially reduce onto the surface of the seed rather than forming a monometallic NP. Core-shell NPs are also often formed when a galvanic reaction takes place. These reactions occur when the two metals have different reduction potentials. The addition of a metal with a high reduction potential to one with a low reduction potential causes the atoms of the NP "seed" to be displaced from the NP by the incoming metal. This often forms core-shell NPs and metal ions from the seed material. A common example of the galvanic exchange reaction is the addition of Au salt to Pd NPs. As Au is introduced into the system, Pd from the "seed" particle becomes oxidized into Pd ions as Au is reduced onto the NP.[77]

1.4.3 Nanoparticle Stabilizers and Support Materials

NPs, because of their small size and high surface tension, are typically not thermodynamically stable. Due to their thermodynamic instability, NPs have a tendency to agglomerate, sinter, or precipitate during chemical reactions. A common form of NP degradation is known as Ostwald ripening. This is the phenomena by which surface atoms on a NP become oxidized to metal ions and redeposit onto other NPs, subsequently producing larger particles over time. Because NP size is related to catalyst efficiency, degradation and growth of NPs will decrease the catalytic ability of the material. Therefore, it is essential that a stabilizer is employed during NP synthesis in order to maintain the catalyst integrity. Stabilizers which are attached to the surface of the NPs are commonly surfactant or polymer and dendrimeric species. These capping agents preventing further nucleation or aggregation of the NPs during and after synthesis. NPs may also be embedded or encapsulated by a support material to prevent

agglomeration and precipitation. Common support materials include inert and redox active metal oxides, and carbon.

1.4.3.1 Polymers

Polymer stabilizers are used in NP synthesis to stabilize the particles. They form a protective monolayer on the surface of the NP, preventing aggregation and excessive nucleation. Common polymer stabilizers include polyvinylpyrollidone (PVP), polyvinyl alcohol (PVA), polyethyleneimine, and sodium polyacrylate.[56, 78] Two common polymer stabilizers are shown in Figure 1.3.

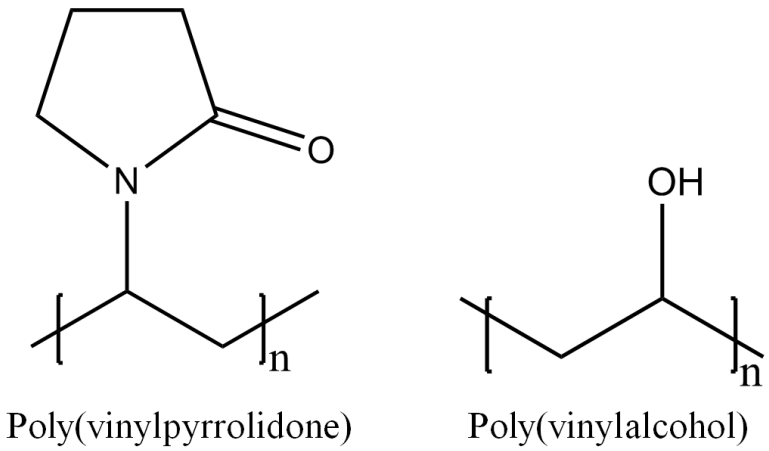

Figure 1.3. Examples of common polymers used for NP stabilization

Polymers provide stabilization by adding steric bulk to the NP surface, preventing agglomeration. These stabilizers are beneficial in the synthesis of NP catalysts because they provide the stabilization needed to prevent degradation of the catalyst while allowing access of the substrate to the NP surface. They do not provide so much steric bulk such that substrate cannot approach the active sites on the NP.

PVP is one of the most popular polymer stabilizers, providing stability to the NP through multiple coordination of its amido sites. It is one of the most desirable catalysts because it is low in cost, has low toxicity, comes in a variety of molecular weights, and it produces water-soluble NPs. Since NPs synthesized in PVP are water soluble, they can be used in environmentally friendly reactions, given that water is a benign solvent.

Polymer stabilizers also have an influence on the shape and size of NPs.[78, 79] Depending on the type of metal and the stabilizer, they can undergo various interactions which influence the final shape of the NP. A stronger preferential binding of a stabilizer to one of the NP planes may result in the growth or nucleation of other available planes, forming NPs with cubic or prismatic structures.[80] Full binding of the polymer to all planes on the NP would inhibit growth of the NP, leading to very small particles.

1.4.3.2 Dendrimers

Dendrimers, like polymers, are important stabilizers in NP synthesis because they stabilize the NP primarily through steric effects, which leaves a substantial amount of the NP surface open to participate in catalytic reactions.[81] Dendrimers also allow for the synthesis of monodisperse, size-specific NPs.[81, 82] An advantage of using dendrimers instead of linear polymeric stabilizers is that the branched dendrimers can determinedly act as a substrate filter, allowing access of particularly sized substrates to the NP surface.[81] Common dendrimers used in NP synthesis are PAMAM (poly(amidoamine)) and PPI (poly(propyleneimine) (Figure 1.4).

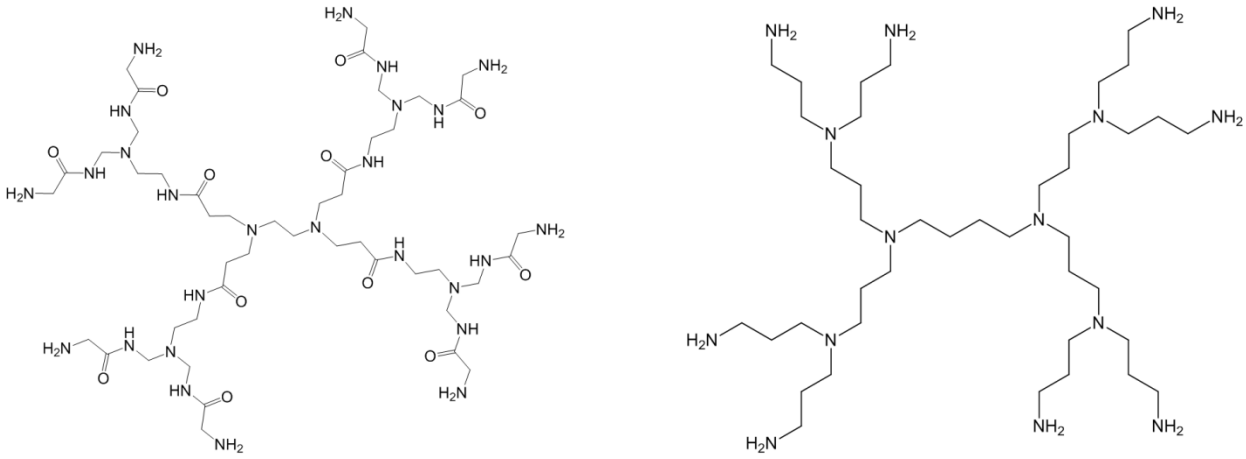

Figure 1.4. Examples of common dendrimers used for NP stabilization.

1.4.3.3 Surfactants

Nanoparticles can also be stabilized using surfactants.[5, 83] Surfactants stabilize NPs by binding tightly to the NP surface, providing steric hindrance around the NP. The long chain groups of the surfactant prevent the agglomeration of NPs.[84] Stabilization by surfactants also promotes the growth of very small NPs by slowing the rate at which material is deposited onto the NP surface during synthesis.[85] Two common surfactants used to stabilize NPs are tetraoctylammonium bromide (TOAB) and CTAB.[61, 86]

1.4.3.4 Solid Supports

Solid supports such as metal oxides and carbon can be used to stabilize NPs. These supports are different from polymers and dendrimers because, rather than being adsorbed to the

NP, solid supports provide a surface to which the NPs adhere or become embedded. These supports stabilize NPs by entrapping the NP and prevent it from interacting with neighbouring particles. One of the disadvantages of using oxide supports is that, once the NP becomes attached or embedded in the support, the available surface area of the NP typically decreases. Therefore, the amount of surface area/active sites decreases, which may lead to a decrease the activity of the NPs. However, some supports can also dramatically enhance the activity of the NPs. The benefit of using a solid support is that it provides a way to inhibit NP agglomeration and sintering during a reaction, allowing these materials to be used as heterogeneous catalysts. Common reactions which are heterogeneously catalyzed by supported NPs are hydrogenations, dehydrogenations, hydrocracking, and reduction/oxidation reactions in fuel cells.[87]

There are two common types of metal oxide supports: inert and redox active. Redox active supports can increase the activity of an NP by delivering a reactant such as molecular oxygen to the NP surface. Acid supports such as Al_2O_3 have been found to withdraw electron density from the active NP catalyst, making it more active for hydrogenation reactions.[88, 89]

1.5 Characterization of Nanoparticle Catalysts

The size, shape and morphology of NPs play an important role on their chemical properties. Therefore, it is important that we have a means of characterizing their physical properties. The ways in which we characterize NPs will be discussed below.

1.5.1 Uv-visible Spectroscopy

Ultraviolet visible (UV-Vis) spectroscopy is an important tool in the characterization of NPs. The metals Ag, Au, and Cu exhibit characteristic surface plasmon resonance bands in the visible region of the light spectrum. These bands are characteristic of the type of metal, as well as the NP size. They arise due to freely mobile conduction electrons which show a characteristic collective oscillation frequency.[70] When the size of the NP is smaller than the wavelength of light, a surface plasmon resonance band is generated.[56] Monitoring the plasmon band and the wavelength of light at which it arises can provide information about the size and morphology of a NP. When a particle consists of the same metal but decreases in size, the wavelength of the surface plasmon resonance band blue shifts, or shifts towards shorter wavelengths.[90]

When synthesizing NPs of metals which have visible plasmon bands it is useful to monitor the change in the UV-Vis spectra in order to determine that the metal has been successfully reduced. Although this is often accompanied by a visible colour change, the change in the UV-Vis spectrum will provide evidence that all of the metal precursor has been reduced, as well as provide some indication of the NP shape. If a NP is of zeroth dimension (*i.e.* spherical) it will only have one plasmon band. This is because all the directions in which the electrons can oscillate are equivalent. Two or three dimension particles such as rods or prisms produce UV-Vis spectra with two or three absorption peaks, respectively.[56] The formation of multiple resonance bands is due to the propagation of electrons in multiple directions. For example, electrons can propagate along the diameter of the rod or along the length, resulting in two absorption bands. Considering this phenomena, the number of plasmon bands present in the spectra will provide some indication of the NP shape. However, there are cases where extra bands arise in the spectra

due to quadripolar interactions. One must take this into consideration when using UV-Vis to determine the dimensionality of NPs.

In the synthesis of bimetallic NPs with Au seeds, one can analyse the spectrum of the seed NP before the addition of the second metal. Once the second metal is reduced onto the seed particle, the UV-Vis spectra can then be collected and the difference between the two can be analyzed. In the case of Au-Pd NPs, the addition of Pd to the Au surface dampens the plasmon band produced by Au. This is because the plasmon band of NPs is surface dependant; therefore once the particle is covered by a Pd shell the plasmon band from Au is dampened. As Pd does not have a plasmon band in the visible region of the spectrum, the spectrum of the bimetallic NPs have no visible absorption band. If the characteristic plasmon band of Au still appears in the UV-Vis spectrum after the reduction of Pd, it may be indicative that there are monometallic Au NPs still present in the system. Therefore, the Pd would not have been successfully reduced onto the Au seeds. This method of analysis was performed by Scott *et al.* in the formation of Au-Pd bimetallic NPs.[91]

1.5.2 Transmission Electron Microscopy

Transmission Electron Microscopy (TEM) is a common technique used to determine the size, geometry, and crystal shape of NPs.[56] In this form of microscopy, high energy electrons are directed at and passed through a very thin sample of material. The atoms within the material absorb or scatter the incoming electrons.[92] Common TEM imaging techniques include dark field (DF) and bright field (BF) imaging. The difference between these two techniques is determined by the source of electrons that are imaged. If the non-scattered/absorbed electrons are imaged,

they will appear as a bright spot on the film. This essentially creates a shadow image of the material being analyzed. Therefore the background or "field" which consists of non-absorbed/scattered electrons will form a bright field image, leaving the image of the sample as a dark spot, much like a shadow. Imaging the electrons diffracted by the sample produces a dark-field image. The areas which diffract electrons will appear to be bright spots on the film, leaving areas which did not diffract electrons dark. Dark and light field images are essentially the same image with opposing contrasts. Dark and light field images of silicon NPs synthesized by Yasar-Inceoglu *et al.* are shown in Figure 1.5.[93]

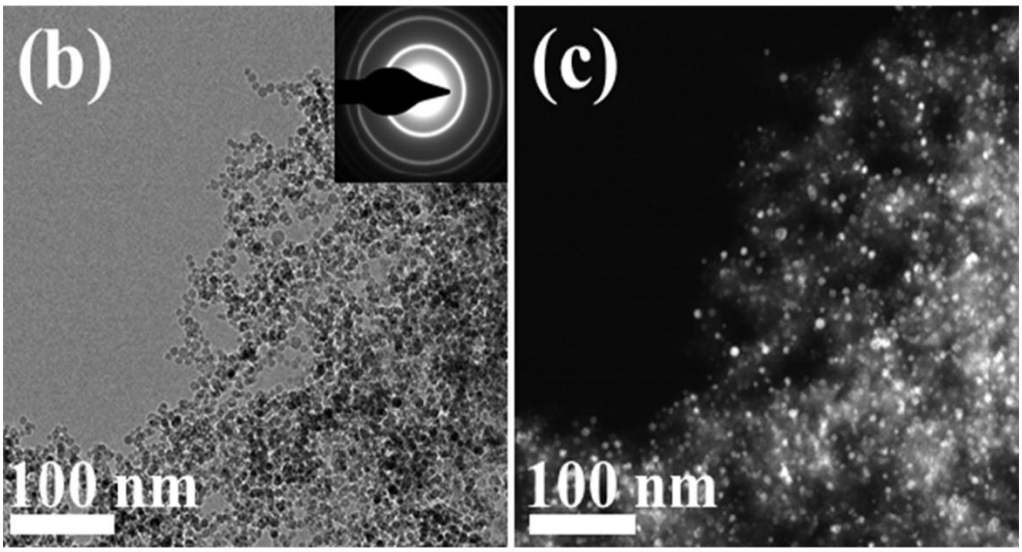

Figure 1.5. TEM images of silicon NPs in (b) Bright Field (c) and Dark Field modes. (Figure adapted from reference 81 with permission)

Since NPs are composed of metals which are high in electron density, there is a high contrast between the metal NP and the carbon TEM grid on which it is placed. Therefore, the NPs are easily detected by TEM and the size and geometry of the particles can clearly be seen in the resulting image. NP sizes are measured from the image, often with the aid of imaging programs and particle size counting programs such as Image J.[94] If enough particles are

analyzed, information about the average size and distribution of the particles can be calculated. This information is invaluable for NP analysis and characterization since properties such as catalytic ability and selectivity depend highly on their size and structure.[95] If a NP consists of two materials with different electron densities, the morphology of the particle can sometimes be seen. An example of this would be a metal particle with an oxide shell. Since the two materials of the NP have vastly different electron densities they produce images with different contrasts. An example of Au NPs with an iron oxide shell synthesized by Shevchenko *et al*. and shown in Figure 1.6.[96] The morphology of the particles can be seen because the Au appears darker than the oxide shell in the image. Unfortunately, when a bimetallic NP is composed of two similar metals such as Au-Pd or Au-Pt, the electron densities are often too similar to detect any difference in contrast. Thus, only the size and shape of this type of NP can be detected.

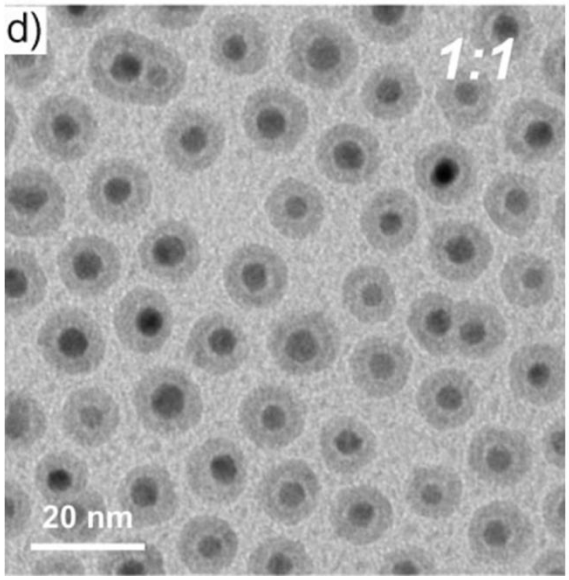

Figure 1.6. TEM image of Au-core, iron oxide-shell NPs. (Image adapted from reference 84 with permission)

General TEM analysis often does not provide a high enough resolution to determine the crystallinity and ordering of atoms within a nanomaterial. However, high resolution transmission electron microscopy (HRTEM) can be performed on a sample, resulting in atomic level resolution, as well as the possibility of a well-defined electron diffraction pattern, much like an X-ray diffraction pattern. This helps gain insight into the ordering of metal atoms within a NP as well as highlight any defects within the NP. This information can lead to insight about the surface structure of the NPs.

TEM analysis is one of the key tools that one must use when characterizing NPs. Although it does not provide information about the oxidation state of metals within the material, or information about the structure of a bimetallic NP consisting of two electron dense metals, it still provides the much needed information about NP size and distribution.

1.5.3 X-ray Absorption Fine Structure Analysis

X-ray Absorption Fine Structure (XAFS) analysis is an element specific technique, which can be used to determine local atomic structure around a metal centre.[97] This analysis involves the excitation of electrons from a core-level orbital of an atom and the detection of the resulting photoelectron. When a core electron is excited with an incoming energy higher than its binding energy the electron will be ejected from the atom, resulting in the relaxation of outer shell electrons into the newly formed core hole. The relaxation of electrons into the core hole results in the expulsion of a photoelectron. The photoelectron that is emitted from the absorbing species is reflected by the electrons of neighbouring atoms. When the reflected photoelectron propagates back towards the absorbing atom, the two oscillating waves can interact constructively or

destructively, producing a spectrum with characteristic oscillations. An illustration depicting how XAFS spectra are formed is shown in Figure 1.7.

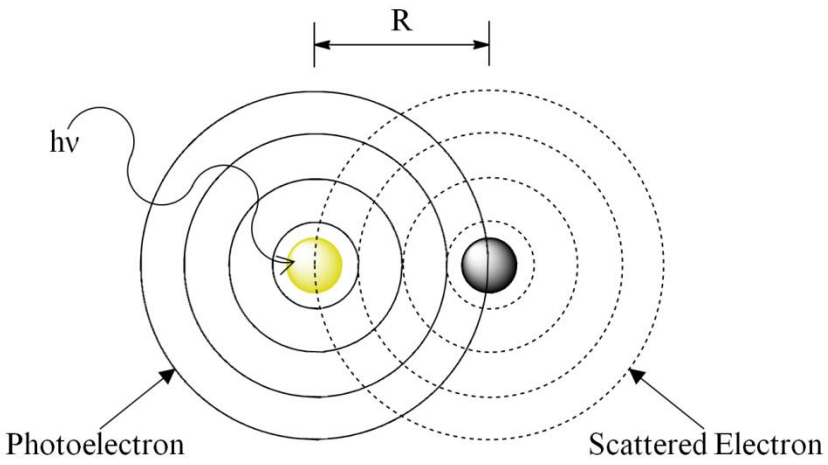

Figure 1.7. Constructive and destructive interference of scattered electrons, resulting in XAFS spectra.

The oscillating spectrum of the absorption coefficient versus photon energy produces a characteristic graph of the element being studied. This XAFS graph can be broken down into two energy regions: X-ray Absorption Near Edge Spectroscopy (XANES) and Extended X-ray Absorption Fine Structure (EXAFS) analysis. The XANES region is typically considered to be ~50 electron volts (eV) before and after the absorption edge and the EXAFS region comprises of energies higher than ~50 eV above the absorption edge. An example of a XAFS spectra, showcasing both the XANES and EXAFS regions is shown in Figure 1.8.

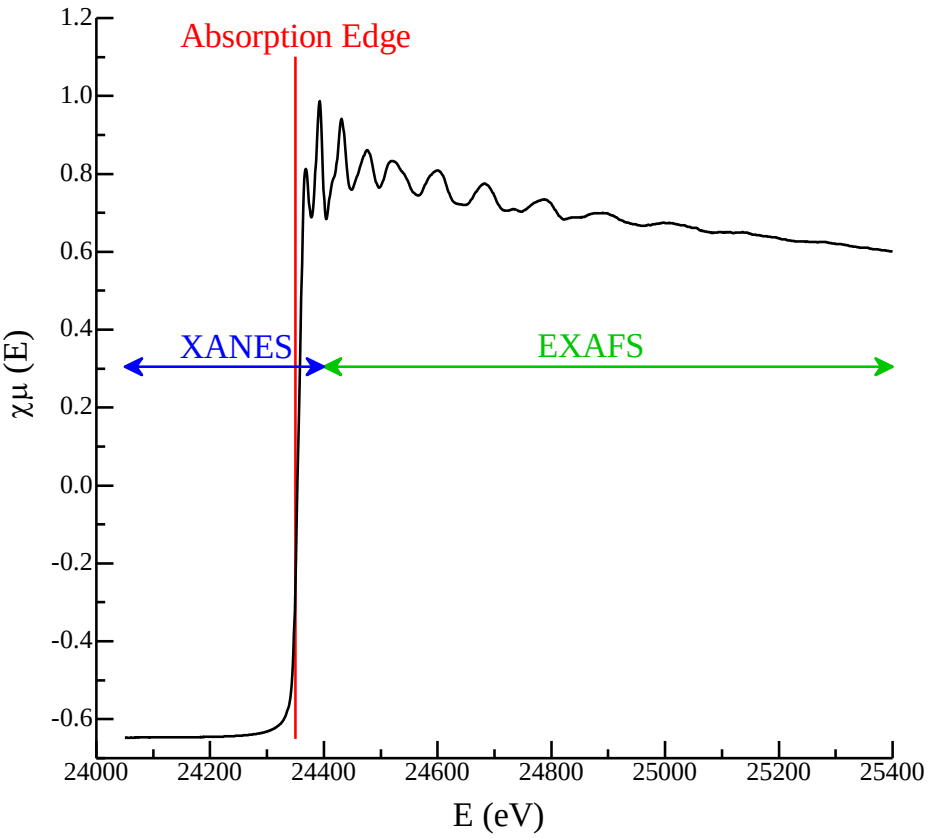

Figure 1.8. Summary of XANES and EXAFS spectra of the Pd-K-edge.

XAFS is an element-specific analysis because the energy required to excite a core electron, or the binding energy, is determinate of the element being analyzed. It also takes a specific energy to excite the different core-electrons of a particular element. The two most studied absorption edges for NP catalysts are the K-edge and the L_{III}-edge of an element. The K and L_{III} edges correspond to excitations from the 1s to valence p orbital and the 2p to valence d orbital, respectively. In the case of Au, the K-edge is a 1s to 6p transition and the L_{III}-edge is a 2p to 5d transition. Once the XAFS spectra for the specific edge of an element is collected, one can analyze the XANES and EXAFS regions to determine the structural properties of the material analyzed. How this analysis is performed and the information which is obtained from each region of the spectrum is discussed below.

1.5.3.1 X-ray Absorption Near Edge Spectroscopy (XANES)

XANES analysis, as mentioned before, is the low-energy region of an XAFS spectrum. Ranging from ±50 eV from the absorption edge, the low energy data collected in this range can provide information on the oxidation state, the coordination number, the charge, and the d-occupancy of a material. Since the photons directed at the material are low energy, they experience much stronger multiple scattering and curved wave effects.[97] Therefore, there are often strong features in the pre-edge region that are characteristic of a material. Analysis of a material via XANES is most often done by comparison of a standard material with known oxidation state and coordination numbers to the spectrum obtained from the unknown material.[97] Comparing the changes between the standard and unknown spectra provides characteristic information about the material. If an unknown spectrum is compared to a standard and a feature within the unknown is shifted to higher energies, one can deduce that the unknown material likely has a higher oxidation state than the standard. This is because, as electrons are removed from the atom, it becomes harder to promote further electrons from said atom, resulting in higher binding energies to excite the core electrons of the oxidized species. If one knows the oxidation state of the element within the standard material, it can be easy to deduce the oxidation state of the unknown material. Reference spectra with known coordination numbers can also be used to determine the coordination number of atoms around the absorbing species. Four coordinate and six coordinate species provide different pre-edge characteristics due to the different amount of neighbouring atoms which can scatter the excited electron. Therefore, by comparing the unknown spectrum to two spectra of determinate valency one can deduce the coordination number of an element. Since XANES can provide a lot of information about structural properties, it is an invaluable tool in the world of NP catalysis. Knowing the coordination number and

oxidation state of metal atoms in a NP can provide insight into how they work as catalysts, allowing for development of even more efficient catalysts.

1.5.3.2 Extended X-ray Absorption Fine Structure Analysis (EXAFS)

EXAFS analysis provides valuable information about the local atomic structure of a material in terms of bond lengths of the first few coordination shells, coordination numbers, and the level of ordering or rigidity of those bonds.[97] Unlike XANES, EXAFS data is analyzed by fitting the unknown spectrum to a structural model, rather than comparing it to a spectrum with known references. By building a model of the unknown material and fitting the spectrum to that of the model, one can extrapolate the structural information mentioned above. This analysis can be difficult, as one must construct an adequate model of the material using estimations such as bond lengths between atoms and coordination environment around the absorbing atom. A poorly constructed model will lead to poor information from the fit about the material in question.

Before the sample spectrum can be fit to the constructed model, data reduction must be performed on the spectrum. Data reduction is often performed using the IFEFFIT software package,[98] though other software is available. The pre-edge background is removed using a linear function. This is done in order to remove signal contributions from instrumental background, lower energy absorption edges and scattering.[97, 99] The post-edge background is also fit in order to determine the jump size of the absorption edge. This is most often fit with a cubic spline function, but can be done with other functions as well. The goal of post-edge background removal is to obtain a spectrum which is equally weighted above and below the zero line.[97] Once background removal is complete, the spectrum can then be fit to a theoretical model.

The fit between the model and unknown is be performed in k-space and R-space. The k-space of a spectrum is the wavenumber of the photoelectron and is determined by Equation 1.1:

$$k = \sqrt{\frac{2m(E-E_0)}{\hbar^2}} \tag{1.1}$$

where m is the mass of an electron, E and E_0 are the measured absorption energy and absorption edge energy, respectively.[99] Converting the energy data to k-space provides a spectrum with a series of oscillations which are correlated to different near-neighbour coordination shells around the absorbing atom. To emphasize higher energy and often more important oscillations k-space is multiplied by a power of k, resulting in values of k^2 and k^3. The data is also fit to the model in R space, which is the Fourier transform of k-space. This data is used to isolate and identify different coordination spheres around the absorbing atom. Figure 1.9 shows a sample XAFS spectrum and its conversion to k-space and R-space.

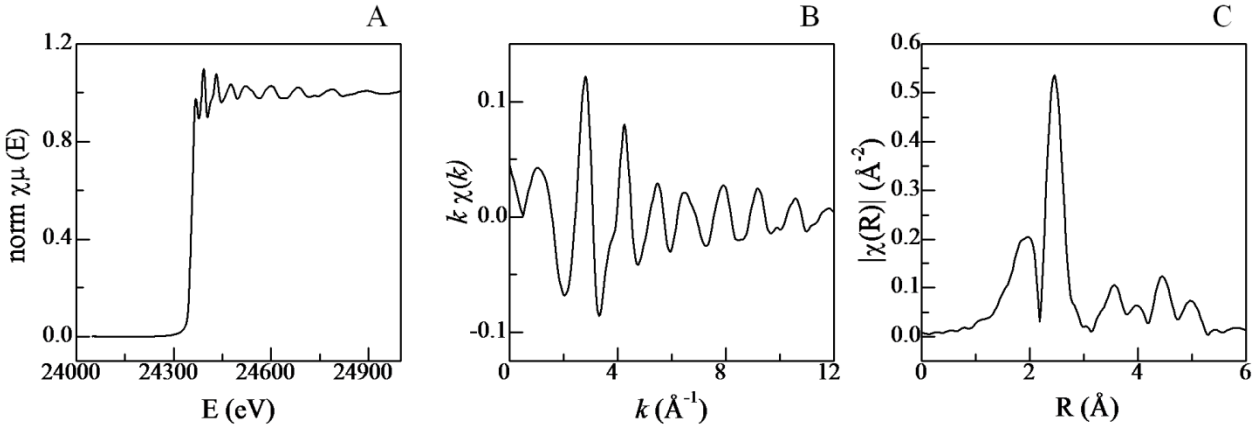

Figure 1.9 Depiction of data in (A) normalized E-space, (B) k-space, and (C) R-space for the Pd-K-edge.

Once the fit has been successfully performed with a high value of correlation ($R^2 < 0.02$), the values for coordination number (N), bond length (R), and the mean square of disorder (σ^2) from the absorbing atom can be determined. From this information, the morphology of a NP sample can be determined. For example, Balcha *et al.* used EXAFS analysis to determine the morphology of Au, Pd, and Au-Pd NPs.[14] In a bulk material of Au or Pd, there are significantly more atoms within the NP than on the surface. Therefore, the coordination number for these atoms would be near 12. However, due to the high amount of surface atoms on NPs, it is expected that the coordination number is less than 12. This is precisely what was seen; monometallic NPs have coordination numbers of approximately 10, indicating a high concentration of surface atoms. It was also noted that the Au-Au and Pd-Pd distances were much shorter in the NPs than in the bulk material, indicating increased d-d hybridization. When determining the morphology of the Au-Pd bimetallic NPs, it was noted that the coordination number around Au atoms was much higher than that around Pd. From this information, it was determined that Au must be located inside the NP (resulting in a total coordination number near 12) while Pd remained on the surface of the atom, exhibiting coordination numbers lower than 12. Many other groups have also studied a variety of NPs by EXAFS. They too have used similar methods to determine the structural properties and morphologies of NPs.[37, 100, 101]

1.5.3.3 In situ XANES and EXAFS

Due to limitations in equipment such as mirrors and detectors, XANES and EXAFS analysis have traditionally been performed on solid samples using long scan times. Solid materials are generally used because the concentration of the absorbing element is high enough

to produce an adequate signal while maintaining a short path length for the incoming X-rays to penetrate. Liquid and gas samples are difficult to analyze because they are often too dilute to achieve an adequate signal. Beam attenuation from the solvent is also a major issue that has to be overcome.[102] The solvent often absorbs the incoming X-ray, decreasing its energy as well as the depth to which the beam can penetrate. This makes it difficult to promote enough electrons from the target absorber to be detected, resulting in poor data. Therefore, analysis of non-solid samples is difficult and not often performed. Since most reactions occur quickly and are not carried out in the solid phase, *in situ* XAFS studies are also rarely performed. Typically it is only possible to study a material (such as a catalyst) before and after a reaction, leaving information about the active state of the catalysts during the reaction unknown. In addition, since many catalysts are air sensitive, *ex-situ* measurements may lead to incorrect assumptions about the catalyst nature due to oxidation of the active species.

Recent advances in synchrotron technology have overcome these limitations, allowing for *in situ* analysis of a material to be performed. *In situ* analyses are those that are performed while a reaction is taking place. However, the reaction conditions may not be identical to those used during a true catalytic trial. For example, as discussed in further chapters, the *in situ* XAFS analyses performed on our catalysts are carried out at much higher metal concentrations than would be used during the analysis of catalytic reactions. This is due to the high metal concentrations needed for XAFS analysis, while much less material is needed when studying the efficiency of our catalysts. *In-operando* studies are those which are performed under identical conditions for both XAFS analyses and catalytic reactions.

One of the most important advances for *in situ* XAFS is the development of liquid cells.[102-105] These cells are designed to be X-ray-transparent and used in transmission and/or

fluorescence detection. Ideal cells allow for temperature control over a range of temperatures, easy loading especially under inert atmosphere, exposure to different atmospheres, and easy addition of reagents to the cell if required.[102] Common materials used for these liquid cells are polyether ether ketone (PEEK), Teflon, and Vespel.[102] These materials are chemically inert, X-ray penetrable, and can be heated or cooled to a variety of temperatures. Some liquid cells require the use of thin-film windows for fluorescence detection. Windows are commonly made of thin films of polymeric species such as Kapton, Mylar, Polypropylene, and Ultralene.[106] All of these materials are X-ray penetrable, causing little to no attenuation of the beam. Figure 1.10 shows images of two cells used in this thesis. The high energy cell is made of PEEK, while the low energy cell is composed of chemically inert material (undisclosed by the supplier), covered by a 5μm Ultralene window.

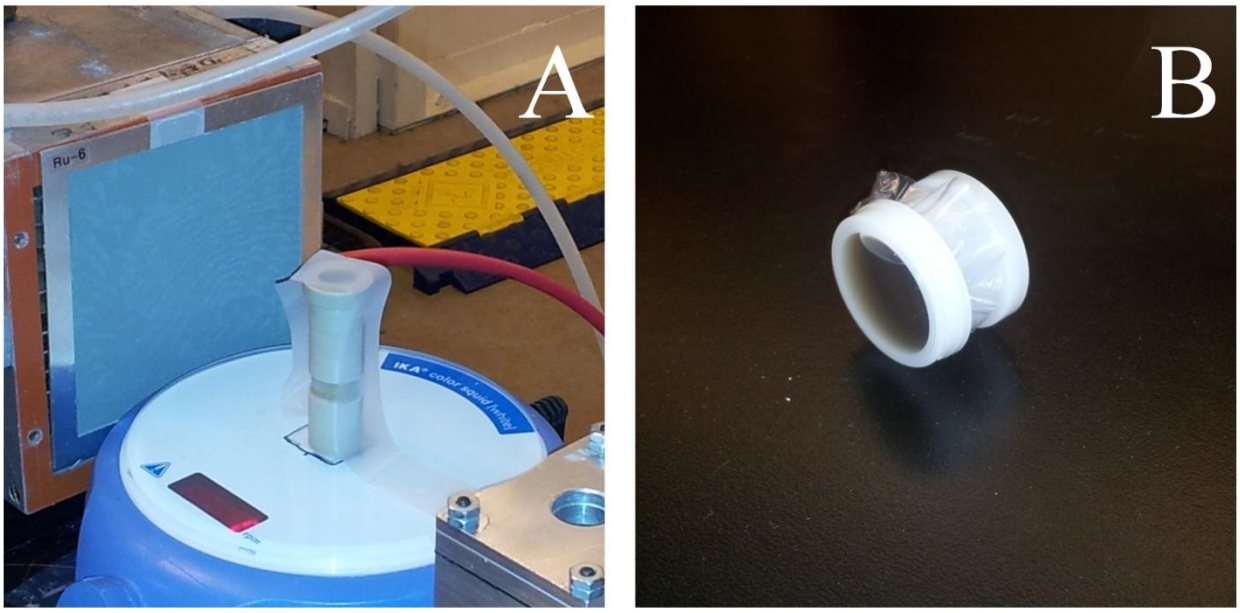

Figure 1.10. Examples of liquid cells for (A) high energy radiation (B) and low energy radiation.

In situ XAFS methods of analyzing catalysts during *in situ* conditions have been employed by a few research groups. Fulton *et al.* have used *in situ* XAFS to determine the

catalytic species in Rh catalyzed reactions for the decoupling of amine boranes and the hydrogenation of benzene.[106-109] Beale *et al.* used *in situ* XANES to study the Mo catalyzed dehydrogenation of propane in order to analyze the catalyst behaviour and determine its active sites and deactivation pathways.[110] By studying the time-resolved XANES spectra they noted that, throughout the reaction, Mo(VI) was becoming reduced to Mo(IV). Therefore, they concluded that the catalytically active species in their reaction involved the dispersion of Mo(IV) over a solid support. They were also able to determine that the catalyst deactivation was due to the formation of large MoO_3 clusters, which were much harder to reduce than the small MoO_3 clusters that are present at the beginning of the reaction. Melke *et al.* studied the effects of adsorbates and the structural changes to carbon supported Pt, PtRu, and PtSn catalysts during the oxidation of ethanol.[111] Another popular use for *in situ* XAS analysis has been for the study of electrode catalysts in fuel cells.[112-114] Imai *et al*. studied Co-Pt core-shell nanoparticles in aqueous solutions by *in situ* XAFS.[114] By monitoring the Pt-L_{III}-edge, they were able to observe the Pt-O bond formation during electrochemical treatments of Co core, Pt shell NPs. They found that surface oxidation of the Pt shell of bimetallic NPs occurs much faster than surface Pt of monometallic NPs. They also determined that the Pt shell became oxygen saturated at a certain point, while Pt NPs showed no saturation point for oxidation. From this information it was determined that CoPt core-shell NPs may have a higher resistance to corrosion, making them more desirable catalysts.[114]

Using *in situ* XAS technology to study materials under reaction conditions has already proven to be an invaluable technique. From the information gathered by time resolved XAS, one has the potential to determine the active form of a catalyst species and its active sites, the cause of catalyst deactivation, the mechanism of the reaction, and the kinetics of a particular reaction.

All of this information can help to understand how NP catalysts work, as well as how they can be improved. Therefore, it is imperative that further development of *in situ* XAS analysis occurs.

1.6 Research Objectives

Catalysis involving Au, Pd, and Au-Pd NPs have been performed by many research groups, especially for the oxidation of α,β-unsaturated alcohols.[13-15, 17, 28, 38, 40, 50, 51, 54, 55, 115-120] However, many of these reactions have been performed using the addition of a base, harmful oxidants, organic solvents, and high reaction temperatures. It has only been recently that the NP catalyzed oxidation of α,β-unsaturated alcohols has been performed under environmentally benign conditions such as aqueous media or solventless conditions,[29, 43] no added base,[14] molecular oxygen as the oxidant, and at room temperature.[14] However, the scope of these reactions has been limited to only a few α,β-unsaturated alcohols such as allyl, benzyl, and crotyl alcohol, using a variety of supported NPs. The first objective of this thesis is to study a larger scope of NP catalyzed oxidation reactions of α,β-unsaturated alcohols. This will be done using PVP-stabilized Au, Pd, and Au-Pd NPs in aqueous solutions. The stability and efficiency of these NPs were compared to similar reactions performed in ionic liquids, rather than water. This work is outlined in Chapter 2.

The second objective of this work was to gain insight into the mechanism by which these oxidation reactions take place. There are two main mechanisms within the literature which outline how α,β-unsaturated alcohols are oxidized using Au/Pd catalysts: a redox mechanism involving the formation of an active Pd(II) species, and a β-hydride (β-H) elimination over a zero-valent species.[14, 40, 47, 121] In order to determine the active species of this reaction, *in situ*

XAFS analysis was performed on the NP-catalyzed oxidation of crotyl alcohol. The Pd-K and Pd-L_{III} edges were analysed by quick-scan XAFS during the addition of crotyl alcohol to a mixture of Au NPs and Pd(II) salt. The changes in the Pd spectra were analyzed and linear combination analyses were performed in order to gain insight into the reaction. Determination of the active species will help gain insight into the mechanism by which this reaction occurs. This work can be seen in Chapter 3.

1.7 References

1 J. Seayad, B. List, *Org. Biomol. Chem.* **2005**, *3*, 719-724.

2 R. A. Sheldon, R. M. Lau, M. J. Sorgedrager, F. van Rantwijk, K. R. Seddon, *Green Chem.* **2002**, *4*, 147-151.

3 S. J. Bae, K. S. Nahm, P. Kim, *Curr. Appl Phys.* **2012**, *12*, 1476-1480.

4 W. A. Herrmann, *Angew. Chem. Int. Ed.* **2002**, *41*, 1290-1309.

5 D. Astruc, F. Lu, J. R. Aranzaes, *Angew. Chem. Int. Ed.* **2005**, *44*, 7852-7872.

6 L. D. Rampino, F. F. Nord, *J. Am. Chem. Soc.* **1941**, *63*, 2745-2749.

7 K. E. Kavanagh, F. F. Nord, *J. Am. Chem. Soc.* **1943**, *65*, 2121-2125.

8 D. Y. Cha, G. Parravano, *J. Catal.* **1970**, *18*, 200-211.

9 G. Parravano, *J. Catal.* **1970**, *18*, 320-328.

10 M. Haruta, T. Kobayashi, H. Sano, N. Yamada, *Chem. Lett.* **1987**, *16*, 405-408.

11 M. Haruta, S. Tsubota, T. Kobayashi, H. Kageyama, M. J. Genet, B. Delmon, *J. Catal.* **1993**, *144*, 175-192.

12 M. Haruta, Y. Yamada, T. Kobayashi, S. Iijima, *J. Catal.* **1989**, *115*, 301-309.

13 M. Alhumaimess, Z. Lin, W. Weng, N. Dimitratos, N. F. Dummer, S. H. Taylor, J. K. Bartley, C. J. Kiely, G. J. Hutchings, *ChemSusChem* **2012**, *5*, 125-131.

14 T. Balcha, J. R. Strobl, C. Fowler, P. Dash, R. W. J. Scott, *ACS Catal.* **2011**, *1*, 425-436.

15 S. Carrettin, P. McMorn, P. Johnston, K. Griffin, G. J. Hutchings, *Chem. Commun.* **2002**, 696-697.

16 N. Dimitratos, A. Villa, L. Prati, *Catal. Lett.* **2009**, *133*, 334-340.

17 Y. Kon, Y. Usui, K. Sato, *Chem. Commun.* **2007**, 4399-4400.

18 A. Villa, G. M. Veith, L. Prati, *Angew. Chem. Int. Ed.* **2010**, *49*, 4499-4502.

19 G. C. Bond, P. A. Sermon, G. Webb, D. A. Buchanan, P. B. Wells, *J. Chem. Soc., Chem. Commun.* **1973**, 444b-445.

20 A. Balanta, C. Godard, C. Claver, *Chem. Soc. Rev.* **2011**, *40*, 4973-4985.

21 S. K. Beaumont, *J. Chem. Tech. Biotech.* **2012**, *87*, 595-600..

22 M. S. Hegde, G. Madras, K. C. Patil, *Acc. Chem. Res.* **2009**, *42*, 704-712.

23 Y. X. Jin, C. N. Ma, M. Q. Shi, Y. Q. Chu, Y. H. Xu, T. Huang, Q. Huang, Y. W. Miao, *Int. J. Electrochem. Sci.* **2012**, *7*, 3399-3408.

24 P. He, X. Wang, Y. Liu, X. Liu, L. Yi, *Int. J. Hydrogen Energy* **2012**, *37*, 11984-11993.
25 M.-H. Shao, K. Sasaki, R. R. Adzic, *J. Am. Chem. Soc.* **2006**, *128*, 3526-3527.
26 X. Yang, Q. Yang, J. Xu, C.-S. Lee, *J. Mater. Chem.* **2012**, *22*, 8057-8062.
27 P. Dash, T. Bond, C. Fowler, W. Hou, N. Coombs, R. W. J. Scott, *J. Phys. Chem. C.* **2009**, *113*, 12719-12730.
28 N. Dimitratos, J. A. Lopez-Sanchez, G. J. Hutchings, *Chem. Sci.* **2012**, *3*, 20-44.
29 D. I. Enache, J. K. Edwards, P. Landon, B. Solsona-Espriu, A. F. Carley, A. A. Herzing, M. Watanabe, C. J. Kiely, D. W. Knight, G. J. Hutchings, *Science* **2006**, *311*, 362-365.
30 D. Wang, A. Villa, F. Porta, L. Prati, D. Su, *J. Phys. Chem. C.* **2008**, *112*, 8617-8622.
31 Z. Qingbo, L. Jim Yang, Y. Jun, B. Chris, Z. Jixuan, *Nanotechnology* **2007**, *18*, 245605.
32 M. M. Shahjamali, M. Bosman, S. Cao, X. Huang, S. Saadat, E. Martinsson, D. Aili, Y. Y. Tay, B. Liedberg, S. C. J. Loo, H. Zhang, F. Boey, C. Xue, *Adv. Funct. Mater.* **2012**, *22*, 849-854.
33 N. Toshima, T. Yonezawa, *New J. Chem.* **1998**, *22*, 1179-1201.
34 B. J. Auten, H. Lang, B. D. Chandler, *Applied Catalysis B: Environmental* **2008**, *81*, 225-235.
35 L. Y. Chang, A. S. Barnard, L. C. Gontard, R. E. Dunin-Borkowski, *Nano Lett.* **2010**, *10*, 3073-3076.
36 K. Honkala, A. Hellman, I. N. Remediakis, A. Logadoltir, A. Carlsson, S. Dahl, C. H. Christensen, J. K. Norskov, *Science* **2005**, *307*, 555-558.
37 A. M. Molenbroek, S. Haukka, B. S. Clausen, *J. Phys. Chem. B.* **1998**, *102*, 10680-10689.
38 P. Miedziak, M. Sankar, N. Dimitratos, J. A. Lopez-Sanches, A. F. Carley, D. W. Knight, S. H. Taylor, C. J. Kiely, G. J. Hutchings, *Catal. Today* **2011**, *164*, 315-319.
39 D. G. Lee, U. A. Spitzer, *J. Org. Chem.* **1970**, *35*, 3589-3590.
40 W. Hou, N. A. Dehm, R. W. J. Scott, *J. Catal.* **2008**, *253*, 22-27.
41 Y. T. Chen, H. M. Lim, Q. H. Tang, Y. T. Gao, T. Sun, Q. Y. Yan, Y. H. Yang, *Appl. Catal., A* **2010**, *380*, 55-65.
42 D. I. Enache, D. W. Knight, G. J. Hutchings, *Catal. Lett.* **2005**, *103*, 43-52.
43 L. Kesavan, R. Tiruvalam, M. H. A. Rahim, M. I. bin Saiman, D. I. Enache, R. L. Jenkins, N. Dimitratos, J. A. Lopez-Sanchez, S. H. Taylor, D. W. Knight, C. J. Kiely, G. J. Hutchings, *Science* **2011**, *331*, 195-199.

44 C. Binns, *Introduction to nanoscience and nanotechnology*. Editor, Wiley, Hoboken, NJ, **2010**.

45 M. Haruta, *ChemInform* **2003**, *34*, 75-87.

46 J. Muzart, *Tetrahedron* **2003**, *59*, 5789-5816.

47 C. Keresszegi, D. Ferri, T. Mallat, A. Baiker, *J. Phys. Chem. B* **2005**, *109*, 958-967.

48 W. P. Zhou, A. Lewera, R. Larsen, R. I. Masel, P. S. Bagus, A. Wieckowski, *J. Phys. Chem. B.* **2006**, *110*, 13393-13398.

49 S. Carrettin, P. McMorn, P. Johnston, K. Griffin, C. J. Kiely, G. J. Hutchings, *Phys. Chem. Chem. Phys.* **2003**, *5*, 1329-1336.

50 A. J. Frank, J. Rawski, K. E. Maly, V. Kitaev, *Green Chem.* **2010**, *12*, 1615-1622.

51 A. F. Lee, S. F. J. Hackett, G. J. Hutchings, S. Lizzit, J. Naughton, K. Wilson, *Catal. Today* **2009**, *145*, 251-257.

52 W. B. Hou, N. A. Dehm, R. W. J. Scott, *J. Catal.* **2008**, *253*, 22-27.

53 N. Dimitratos, J. A. Lopez-Sanchez, D. Lennon, F. Porta, L. Prati, A. Villa, *Catal. Lett.* **2006**, *108*, 147-153.

54 M. Sankar, E. Nowicka, R. Tiruvalam, Q. He, S. H. Taylor, C. J. Kiely, D. Bethell, D. W. Knight, G. J. Hutchings, *Chem. Eur. J.* **2011**, *17*, 6524-6532.

55 A. Villa, N. Janjic, P. Spontoni, D. Wang, D. S. Su, L. Prati, *Appl. Catal., A* **2009**, *364*, 221-228.

56 G. Cao, *Nanostructures & Nanomaterials: Synthesis, Properties & Applications*. Editor, Imperial College Press, London, **2004**, pp. 433.

57 C. B. Murray, C. R. Kagan, M. G. Bawendi, *Annu. Rev. Mater. Sci.* **2000**, *30*, 545-610.

58 H. Hirai, Y. Nakao, N. Toshima, K. Adachi, *Chem. Lett.* **1976**, *5*, 905-910.

59 H. Hirai, Y. Nakao, N. Toshima, *J. Macromol. Sci. Part A Pure Appl. Chem.* **1978**, *12*, 1117-1141.

60 W. O. Milligan, R. H. Morriss, *J. Am. Chem. Soc.* **1964**, *86*, 3461-3467.

61 M. T. Reetz, W. Helbig, *J. Am. Chem. Soc.* **1994**, *116*, 7401-7402.

62 M. Zhou, S. Chen, H. Ren, L. Wu, S. Zhao, *Physica E* **2005**, *27*, 341-350.

63 C. Huang, Y. Wang, P. Chiu, M. Shih, T. Meen, *Mat. Lett.* **2006**, *60*, 1896-1900.

64 C. Huang, P. Chiu, Y. Wang, K. Chen, J. Linn, C. Yang, *J. Electrochem. Soc.* **2006**, *153*, D193-D198.

65 J. Cha, K. Kim, S. Choi, S. Yeon, H. Lee, C. Lee, J. Shim, *Korean J. Chem. Eng.* **2007**, *24*, 1089-1094.

66 M. T. Swihart, *Curr. Opin. Colloid Interface Sci.* **2003**, *8*, 127-133.

67 V. Abdelsayed, M. S. El-Shall, T. Seto, *J. Nanopart. Res.* **2006**, *8*, 361-369.

68 C. G. Granqvist, R. A. Buhrman, *J. Appl. Phys.* **1976**, *47*, 2200-2219.

69 G. Glaspell, V. Abdelsayed, K. M. Saoud, M. S. El-Shall, *Pure Appl. Chem* **2006**, *78*, 1667-1689.

70 G. Schmid, *Nanoparticles: from theory to application*. Editor, Wiley-VCH, Weinheim, **2010**, 521.

71 K. S. Suslick, M. Fang, T. Hyeon, *J. Am. Chem. Soc.* **1996**, *118*, 11960-11961.

72 S. Dong, C. Tang, H. Zhou, H. Zhao, *Gold Bull.* **2004**, *37*, 187-195.

73 S. Yang, Y. Wang, Q. Wang, R. Zhang, B. Ding, *Colloids Surf., A* **2007**, *301*, 174-183.

74 L. Kuai, X. Yu, S. Wang, Y. Sang, B. Geng, *Langmuir* **2012**, *28*, 7168-7173.

75 A. Roucoux, J. Schulz, H. Patin, *Chem. Rev.* **2002**, *102*, 3757-3778.

76 A. F. Lee, C. J. Baddeley, C. Hardacre, R. M. Ormerod, R. M. Lambert, G. Schmid, H. West, *J. Phys. Chem.* **1995**, *99*, 6096-6102.

77 A. Murugadoss, K. Okumura, H. Sakurai, *J. Phys. Chem. C.* **2012**, *just accepted manuscript* doi: 10.1021/jp307377r.

78 S. Porel, S. Singh, T. P. Radhakrishnan, *Chem. Commun.* **2005**, 2387-2389.

79 A. Mayer, M. Antonietti, *Colloid. Polym. Sci.* **1998**, *276*, 769-779.

80 T. S. Ahmadi, Z. L. Wang, T. C. Green, A. Henglein, M. A. El-Sayed, *Science* **1996**, *272*, 1924-1925.

81 R. M. Crooks, M. Zhao, L. Sun, V. Chechik, L. K. Yeung, *Acc. Chem. Res.* **2000**, *34*, 181-190.

82 R. W. J. Scott, O. M. Wilson, R. M. Crooks, *J. Phys. Chem. B* **2004**, *109*, 692-704.

83 A. Corma, H. Garcia, *Chem. Soc. Rev.* **2008**, *37*, 2096-2126.

84 H. Bönnemann, G. Braun, W. Brijoux, R. Brinkmann, A. S. Tilling, K. Seevogel, K. Siepen, *J. Organomet. Chem.* **1996**, *520*, 143-162.

85 C. Burda, X. B. Chen, R. Narayanan, M. A. El-Sayed, *Chem. Rev.* **2005**, *105*, 1025-1102.

86 T. Y. Dong, C. N. Chen, H. Y. Cheng, C. P. Chen, N. Y. Jheng, *Inorganica Chimica Acta* **2011**, *367*, 158-165.

87 A. T. Bell, *Science* **2003**, *299*, 1688-1691.

88 A. Y. Stakheev, L. M. Kustov, *Appl. Catal., A* **1999**, *188*, 3-35.

89 Z. Guo, C. Zhou, D. Shi, Y. Wang, X. Jia, J. Chang, A. Borgna, C. Wang, Y. Yang, *Appl. Catal., A* **2012**, *435–436*, 131-140.

90 S. Link, M. A. El-Sayed, *Int. Rev. Phys. Chem.* **2000**, *19*, 409-453.

91 R. W. J. Scott, O. M. Wilson, S.-K. Oh, E. A. Kenik, R. M. Crooks, *J. Am. Chem. Soc.* **2004**, *126*, 15583-15591.

92 R. F. Egerton, *Physical Principles of Electron Microscopy: An Introduction to TEM, SEM, and AEM*. Editor, Springer, **2005**.

93 O. Yasar-Inceoglu, T. Lopez, E. Farshihagro, L. Mangolini, *Nanotechnology* **2012**, *23*, 255604.

94 C. A. Schneider, W. S. Rasband, K. W. Eliceiri, *Nat Meth* **2012**, *9*, 671-675.

95 A. I. Frenkel, C. W. Hills, R. G. Nuzzo, *J. Phys. Chem. B* **2001**, *105*, 12689-12703.

96 E. V. Shevchenko, M. I. Bodnarchuk, M. V. Kovalenko, D. V. Talapin, R. K. Smith, S. Aloni, W. Heiss, A. P. Alivisatos, *Adv. Mater.* **2008**, *20*, 4323-4329.

97 G. Henderson, D. R. Baker, *Synchrotron Radiation: Earth, Environmental and Materials Sciences Applications*. Editor, Canada, **2002**.

98 M. Newville, *J. Synchrotron Radiat.* **2001**, *8*, 322-324.

99 M. Newville, *Fundamentals of XAFS*. Editor, Chicago, IL, **2004**, pp. 41.

100 F. Liu, D. Wechsler, P. Zhang, *Chem. Phys. Lett.* **2008**, *461*, 254-259.

101 K. Asakura, C. R. Bian, S. Suzuki, W. J. Chun, N. Watari, S. Ohnishi, P. Lu, N. Toshima, *Physica Scripta* **2005**, *2005*, 781.

102 R. C. Nelson, J. T. Miller, *Catal. Sci. Technol.* **2011**, *2*, 461-470.

103 J. L. Fulton, Y. Chen, S. M. Heald, M. Balasubramanian, *Rev. Sci. Instrum.* **2004**, *75*, 5228-5231.

104 J. L. Fulton, J. G. Darab, M. M. Hoffmann, *Rev. Sci. Instrum.* **2001**, *72*, 2117-2122.

105 S. R. Bare, N. Yang, S. D. Kelly, G. E. Mickelson, F. S. Modica, *Catal. Today* **2007**, *126*, 18-26.

106 Y. Chen, J. L. Fulton, J. C. Linehan, T. Autrey, *J. Am. Chem. Soc.* **2005**, *127*, 3254-3255.

107 J. L. Fulton, J. C. Linehan, T. Autrey, M. Balasubramanian, Y. Chen, N. K. Szymczak, *J. Am. Chem. Soc.* **2007**, *129*, 11936-11949.

108 E. Bayram, J. C. Linehan, J. L. Fulton, J. A. S. Roberts, N. K. Szymczak, T. D. Smurthwaite, S. Özkar, M. Balasubramanian, R. G. Finke, *J. Am. Chem. Soc.* **2011**, *133*, 18889-18902.

109 R. Rousseau, G. K. Schenter, J. L. Fulton, J. C. Linehan, M. H. Engelhard, T. Autrey, *J. Am. Chem. Soc.* **2009**, *131*, 10516-10524.

110 A. M. Beale, A. M. J. van der Eerden, K. Kervinen, M. A. Newton, B. M. Weckhuysen, *Chem. Commun.* **2005**, 3015-3017.

111 J. Melke, A. Schoekel, D. Dixon, C. Cremers, D. E. Ramaker, C. Roth, *J. Phys. Chem. C* **2010**, *114*, 5914-5925.

112 N. Ishiguro, T. Saida, T. Uruga, S.-i. Nagamatsu, O. Sekizawa, K. Nitta, T. Yamamoto, S.-i. Ohkoshi, Y. Iwasawa, T. Yokoyama, M. Tada, *ACS Catal.* **2012**, *2*, 1319-1330.

113 H. Imai, K. Izumi, M. Matsumoto, Y. Kubo, K. Kato, Y. Imai, *J. Am. Chem. Soc.* **2009**, *131*, 6293-6300.

114 H. Imai, M. Matsumoto, T. Miyazaki, K. Kato, H. Tanida, T. Uruga, *Chem. Commun.* **2011**, *47*, 3538-3540.

115 A. F. Lee, C. V. Ellis, J. N. Naughton, M. A. Newton, C. M. A. Parlett, K. Wilson, *J. Am. Chem. Soc.* **2011**, *133*, 5724-5727.

116 A. F. Lee, C. V. Ellis, K. Wilson, N. S. Hondow, *Catal. Today* **2010**, *157*, 243-249.

117 J. Naughton, A. F. Lee, S. Thompson, C. P. Vinod, K. Wilson, *Phys. Chem. Chem. Phys.* **2010**, *12*, 2670-2678.

118 L. Prati, A. Villa, C. E. Chan-Thaw, R. Arrigo, D. Wang, D. S. Su, *Faraday Discuss.* **2011**, *152*, 353-365.

119 A. Villa, D. Wang, P. Spontoni, R. Arrigo, D. Su, L. Prati, *Catal. Today* **2010**, *157*, 89-93.

120 D. Wang, A. Villa, P. Spontoni, D. Su, L. Prati, *Chem. Eur. J.* **2010**, *16*, 10007-10013.

121 H. Tsunoyama, H. Sakurai, Y. Negishi, T. Tsukuda, *J. Am. Chem. Soc.* **2005**, *127*, 9374-9375.

Chapter 2

Aerobic Oxidation of α,β-Unsaturated Alcohols Using Sequentially-Grown AuPd Nanoparticles in Water and Tetraalkylphosphonium Ionic Liquids

A series of Au, Pd, and AuPd catalysts systems were studied for the oxidation of a series of allylic alcohol substrates. Turnover frequencies and selectivities of the reactions were monitored by gas chromatography. Similar reactions were performed in both aqueous media and ionic liquids and the results were compared between the two systems. Nanoparticle characterization was also performed by EXAFS analysis and fitting.

This paper was co-authored by Abhinandan Banerjee and accepted in Catalysis Today in June 2012. The paper is currently in press:

Maclennan, A.; Banerjee, A.; Scott, R.W.J., Aerobic oxidation of α, β-unsaturated alcohols using sequentially-grown AuPd nanoparticles in water and tetraalkylphosphonium ionic liquids, *Catal. Today* (**2012**), http://dx.doi.org/10.1016/j.cattod.2012.04.053.

All NP synthesis and reactions performed under aqueous conditions were done by myself. Abhinandan Banerjee performed all of the synthesis and reactions in ionic liquids. All gas chromatography analysis (aqueous and ionic liquid systems) and synchrotron work, including experiments and data analysis (EXAFS data reduction and fitting) were also performed by myself. Writing and editing of this manuscript was performed by myself, Abhinandan, and Dr.

Robert W. J. Scott. The final manuscript was submitted after thorough revisions by Dr. Robert W.J. Scott.

Aerobic Oxidation of α,β-Unsaturated Alcohols Using Sequentially-Grown AuPd Nanoparticles in Water and Tetraalkylphosphonium Ionic Liquids

Aimee Maclennan[1], Abhinandan Banerjee[1], and Robert W.J. Scott*

2.1 Abstract

Metallic and bimetallic nanoparticles (NPs) (Au, Pd, and AuPd) were synthesized in water with PVP as a polymer stabilizer, as well as in tetraalkylphosphonium halide ionic liquids (ILs). A borohydride reduction technique was used for the preparation of the monometallic NPs, while a sequential reduction strategy was seen to generate the putative core-shell varieties. Pd and sequentially grown Au-Pd NPs were seen to serve as efficient catalysts for the oxidation of α,β-unsaturated alcohols, while the Au NPs themselves showed minimal activity. However, a system with both Au NPs and a Pd(II) salt (K_2PdCl_4) also efficiently catalyzed the oxidation reaction in water. A number of aliphatic and aromatic unsaturated alcohols were oxidized using oxygen as an oxidant with these as-prepared catalysts at 60^{o}C in the absence of base. TEM and EXAFS studies of the nanoparticle catalysts before and after the oxidation reaction revealed that the Pd(II) salt was reduced in situ during catalytic conditions, and that there was large changes in particle size and morphology after catalysis, which suggests Ostwald ripening and the presence of a redox mechanism. In the IL system, the ease of Pd reduction led to high activities for many α,β-unsaturated alcohols in the absence of the Au promoter.

2.2 Introduction

The oxidation of alcohols to their respective carbonyl compounds, although known to the scientific community since the 19th century[1], continues to represent a major challenge as far as the industrial implementation of such processes is concerned. Traditionally, in the laboratory, such conversions have been performed using highly toxic transition metal compounds (such as chromium salts) in volatile and flammable organic solvents[2]. Such systems are rife with disadvantages: the reaction mixtures are inherently toxic, often corrosive, and the process can pose a serious threat to the environment if performed regularly on a large scale[3]. Another point worth noting is the probability of "over-oxidation" of primary alcohols in such systems, where the reaction proceeds to give the carboxylic acid rather than halt at the aldehyde stage. Moreover, from the standpoint of green chemistry, catalytic processes are preferred over stoichiometric ones. While the application of novel sources of oxygen such as ozone, PhOI, N-morpholine-N-oxide, or urea-hydrogen peroxide have notable utility, for industrial processes either air or oxygen are the oxidants of choice if they can be used safely, simply for the sake of accessibility and cost-effectiveness[4].

Our group and many others are examining the "greening" of important chemical reactions by developing methods by which reactions of industrial importance (such as oxidations, hydrogenations, and so on) can be carried out in solvents ear-marked as "green", and with catalysts that are readily recyclable, with high yields and minimal waste products (e.g. high selectivities). Stable metal nanoparticles (NPs) in solvents such as water, supercritical carbon dioxide, ionic liquids, or eutectic mixtures provide an alternative route to traditional homogeneous or heterogeneous catalysis[5]. In fact, such pseudo-homogeneous nanocatalysis involving suspended nanoparticle catalysts in liquid media straddles the boundaries between

homogeneous and heterogeneous catalysis, combining some of the advantages of both approaches. While the catalytic versatility of metal NPs is well-known, their tendency to agglomerate and precipitate in the absence of stabilizers can restrict their catalytic uses: however, several strategies have been successfully applied to minimize such catalyst deactivation, and many different reactions have been screened for potential application of pseudo-homogeneous nanocatalysis.

After the pioneering work by Haruta, it is now well-known that Au NPs below a certain critical size are capable of efficient catalysis of oxidation reactions at low temperatures[6]. In 2005, Tsunoyama *et al.* showed that PVP-stabilised Au NPs in water selectively catalyze the oxidation of benzyl alcohol to benzaldehyde in the presence of base[7-9] and many other groups have also reported alcohol oxidations with Au NPs[3, 10-15], as well as enhanced activities for AuPd NPs for mild alcohol oxidations[16-26]. We previously studied alcohol oxidations in aqueous solutions using Au, Pd, and bimetallic AuPd NP catalysts in aqueous solutions, and determined that AuPd systems were much more reactive than their monometallic Au and Pd counterparts[18]. Recently, both ourselves[25], and others[21, 24], have shown that core-shell AuPd NPs (either as-synthesized or synthesized *in situ* during reaction conditions) are particularly active for alcohol oxidations, with substantial activities and selectivities for α,β-unsaturated alcohols such as crotyl alcohol at room temperature in the absence of bases. However, it was not apparent how generic such results were to other alcohol systems, and what the dominant mechanism was in the reaction. In addition, little to no studies are available detailing the recyclability of such nanoparticle systems. Catalytic oxidations in ionic liquids (ILs) are rather less-well-known than those in other media: even in cases where such studies have been carried out, the actual catalytic species are often transition metal complexes (such as methyltrioxorhenium[27], OsO_4[28], $RuCl_3$[29], and so on), and/or the oxygen

is harvested from novel oxidants rather than using molecular oxygen or air. Heteropolyacids have been immobilised on imidazolium IL modified SBA-15 for alcohol oxidations[30], and ILs such as choline hydroxide have also been used to stabilize Ru NPs on MgO supports for oxidations[31]. However, AuPd systems have not been well explored in IL systems to date.

In this study, the oxidation of a variety of α,β-unsaturated alcohols (aliphatic as well as aromatic) in the presence of molecular oxygen have been investigated. The catalytic systems of choice are Au, Pd, Au/Pd(II), and sequentially grown AuPd NPs, while the reaction media include water in the presence of PVP stabilizer as well as a tetraalkylphosphonium chloride IL (P[6,6,6,14]Cl) capable of inherent NP stabilisation. Careful growth of Pd shells on Au seeds using mild reductants such as ascorbic acid have been used to generate sequentially grown AuPd NPs while minimizing secondary nucleation of Pd NPs. *In situ* formation of Pd shells on Au cores may also be achieved by the oxidation of the substrate itself, and concurrent reduction of Pd(II) in the presence of Au NPs, while individually each of these show very little catalytic activity. Similar catalytic NP systems are generated in trihexyl(tetradecyl)phosphonium halide ILs in the absence of any external stabilizers, and the resulting Pd NPs show high activities even in the absence of the Au promoter. Tentative mechanisms for α,β-unsaturated alcohol oxidation in water and in trihexyl(tetradecyl)phosphonium halide ionic liquids have been suggested, and the influence of the anion of the ionic liquid on the catalytic activity of the NPs is noted. Finally, TEM and EXAFS studies of core-shell catalyst before and after reaction, as well as of Au NP/Pd(II) salt after reaction has been conducted to study the structure of these NP catalysts, and results suggest that the initial step of the oxidation reaction with Au NPs in the presence of Pd (II) salts leads to in situ formation of AuPd catalysts. Since allylic aldehydes are valuable fine chemicals finding extensive use in the pharmaceutical, agrochemical and cosmetic industries, we

believe it is worthwhile to seek clean technologies for their synthesis via atom-efficient oxidations that also address issues of catalyst reusability, environmental impact, waste disposal, and renewable feedstock.

2.3 Experimental

2.3.1 Materials

All chemicals except for the ones listed below were purchased from Sigma Aldrich and used as received. Poly(vinylpyrrolidone) (PVP) (M.W. 58,000 g/mol), tetrachloroauric acid, $HAuCl_4.4H_2O$ and potassium tetrachloropalladate, K_2PdCl_4, (both 99.9%, metals basis) were all obtained from Alfa Aesar, and the metal salts were stored under vacuum and flushed with nitrogen after every use. Commercial samples of the trihexyl(tetradecyl)phosphonium chloride (P[6,6,6,14]Cl) room-temperature ionic liquid (IL) were generously donated by Cytec Industries Ltd. Commercial samples of ILs were dried under vacuum at 70^{o}C for 10-12 hours with stirring before use. Deuterated solvents were purchased from Cambridge Isotope Laboratories. 18 MΩcm Milli-Q water (Millipore, Bedford, MA) was used throughout.

2.3.2 Synthesis of PVP Stabilized Pd, Au and AuPd NPs in Water

PVP-stabilized metallic and sequentially grown bimetallic NPs were synthesized by previously reported procedures[18,25]; metallic NPs were reduced using sodium borohydride while sequentially grown AuPd NPs were synthesized using ascorbic acid as the selective reducing agent for the Pd shell. To prepare the Au NPs (also used as "seed" particles), 50 mL of 0.35 mM

PVP (1.75×10^{-5} mol) was added to 5 mL of 10 mM $HAuCl_4 \cdot 3H_2O$ (5×10^{-5} mol) and stirred at 800 rpm for 30 minutes. The solution was then placed on ice, stirring set to 1200 rpm, and 5 mL of 100 mM $NaBH_4$ (5×10^{-4} mol) was added quickly to the solution. The reaction was left to stir for 30 min on ice, then stirred for another 30 minutes at room temperature. To quench the reaction, 5 mL of 100 mM HCl (5×10^{-4} mol) was added to the solution and stirred for 30 min. To further stabilize the NPs, 35 mL of 1.0 mM PVP (3.5×10^{-4} mol) was added to the final solution and stirred for 30min. The particles were dialyzed overnight using cellulose dialysis membrane with a molecular cut off of 12,400 g/mol under N_2. Pd NPs were synthesized using the same procedure, but K_2PdCl_4 was used instead of $HAuCl_4 \cdot 3H_2O$. The sequentially-grown 1:3 AuPd NPs were synthesized by mixing 100 mL of previously made Au "seed" particles (5×10^{-5} mol) with 15 mL of 100 mM ascorbic acid (1.5×10^{-3} mol) on ice, stirring at 800 rpm. To this solution, 15 mL of 10 mM K_2PdCl_4 (1.5×10^{-4} mol) was added then left to stir at 800 rpm on ice for 1 hour. Upon completion, the particles were dialysed overnight in the same manner as the Au seed particles. For the generation of the Au NP/ Pd(II) system, an identical procedure was followed, except for the addition of ascorbic acid and the second dialysis step.

2.3.3 Synthesis of Pd, Au and AuPd NPs in IL

For the synthesis of Pd NPs in IL, 1.6 mg of K_2PdCl_4 (5.0×10^{-6} mol) was added to a 10 mL sample of the trihexyl(tetradecyl)phosphonium chloride IL mixed with 2 mL 1,4-dioxane at room temperature, and vigorously stirred. To this solution, an excess of $LiBH_4$ reagent (1.0 mL, 2.0M in THF) was injected drop-wise over a period of five minutes[32]. A brisk effervescence followed, and the entire solution turned brown, indicating nanoparticle formation. After the

addition of $LiBH_4$, volatile impurities including the dioxane were removed by vacuum-stripping the system at 70^{o}C. The Pd NP solution thus obtained was stored under nitrogen in capped vials until use. For the synthesis of Au NPs, a similar procedure was followed. Tetrachloroauric acid (2.0 mg, 5.0 x 10^{-6} mol) was dissolved in 10 mL P[6,6,6,14]Cl diluted with 2 mL 1,4-dioxane at room temperature to give a golden yellow solution which turned colorless, violet and then wine-red upon drop-wise addition of 1.0 mL of a 2.0 M $LiBH_4$ reagent. Excess $LiBH_4$ was quenched with methanol and volatiles were subsequently removed by vacuum-stripping. For the synthesis of sequentially grown AuPd NPs, a sequential reduction procedure was followed using the Au NP seeds as synthesized above, followed by the addition of 200 mg ascorbic acid added to the reaction medium. While stirring this mixture under ice, a 5 mL solution of K_2PdCl_4 (15.0 x 10^{-6} mol) dissolved in methanol was added to it all at once. The mixture was then stirred under ice for ~1h, and volatiles were removed from it by vacuum-stripping. For the generation of the Au NP/ Pd(II) system, an identical procedure was followed, except for the addition of ascorbic acid.

2.3.4 General Procedure for Oxidation Reactions

Oxidation reactions were carried out in a 25 mL round-bottomed flask, sealed with a septum. In a general procedure, 10 mL of the NP solution (in water or IL) was stirred and heated to 60^{o}C under a vigorous flow of oxygen for about 10 min for aqueous systems, and for about 1 h in IL systems to compensate for the higher viscosity of the IL. After this, 500 or 5000 equivalents (based on 1 equivalent of metal catalyst) of the alcohol substrate was injected into the flask. For aqueous work, at incremental times 1.0 mL of the reaction mixture was sampled and the products were then extracted from the aqueous catalyst layer by two, 0.5 mL aliquots of ethyl acetate,

shaking in 1 minute intervals for 5 minutes per extraction. For IL samples, after ~12 h, the reaction vessel was removed from the constant temperature bath, and subjected to vacuum-stripping while being heated for extraction of the products and/or unreacted substrate. Conversion and selectivity were determined by GC-FID (Agilent Technologies 7890A) equipped with a HP-Innowax capillary column. Two reactions were typically run for each sample. The neat organic liquids extracted were subsequently characterised by ^{1}H NMR, ^{13}C NMR, and GC-FID techniques. For GC-FID analysis, 25µL of a neat extract was mixed with 1 mL ethyl acetate in a GC-vial, and subjected to analysis.

2.3.5 Characterization

UV-Vis spectra were obtained using a Varian Cary 50 Bio UV-Visible spectrophotometer with a scan range of 200-800 nm and an optical path length of 1.0 cm. ^{1}H and ^{13}C NMR spectra were obtained using a Bruker 500 MHz Avance NMR spectrometer; chemical shifts were referenced to the residual protons of the deuterated solvent. TEM analyses of the NPs in IL and water, both before and after catalytic cycles, were conducted using a Philips 410 microscope operating at 100 kV. The samples in IL were prepared by ultrasonication of a 1% solution of the NP/IL solution in DCM followed by drop-wise addition onto a carbon-coated copper TEM grid (Electron Microscopy Sciences, Hatfield, PA). To determine average particle diameters, a minimum of 100 particles from each sample were manually measured from several TEM images using the ImageJ program. The Hard X-ray MicroAnalysis beamline (HXMA) 061D-1 (energy range, 5-30 keV; resolution, 1 x 10^{4} $\Delta E/E$) at the Canadian Light Source was used for recording X-ray absorption spectra at the Pd K-edge and the Au L_{III}-edge. The beamline optics include

water-cooled collimating KB mirrors (Rh for the Au LIII-edge and Pt for Pd K-edge), and a liquid nitrogen cooled double crystal monochromator housing two crystal pairs [Si (111) and Si (220)]. The X-ray measurements were conducted in ion chamber filled with a helium and nitrogen mixture for the Au LIII-edge and pure helium for the Pd K-edge. The energy scan range for the measurement was between -200 eV to +1000 eV at each edge. Pd and Au foils were used for the respective edges as references. All EXAFS measurements were conducted in transmission mode at room temperature using samples trapped in alumina at 2.5% by weight metal and pressed into pellets[33]. The software package IFEFFIT was used for data processing which included fitting the pre-edge region to a straight line, and the background above the edge was fit to a cubic spline function[34, 35]. The EXAFS function, χ, was obtained by subtracting the post-edge background from the overall absorption and then normalizing with respect to the edge jump step. The EXAFS fitting was performed in R-space between 1.4 to 3.4 Å for the Au edge and 1.4 to 3.0 Å for the Pd-edge using theoretical phase-shifts and amplitudes generated by FEFF. fcc bulk lattice parameters (i.e., first shell coordination numbers of 12) were used to determine the amplitude reduction factor, S_o^2, for Au and Pd by analyzing Au and Pd reference foils[36].

2.4 Results and Discussion

2.4.1. Oxidation Reactions in Water

PVP-stabilized Au, Pd, sequentially grown 1:3 AuPd NPs and Au NP/Pd(II) 1:3 mixtures were synthesized. Figure 2.1(A, B) shows representative TEM images of samples of PVP-stabilized Au NPs and sequentially grown 1:3 AuPd NPs.

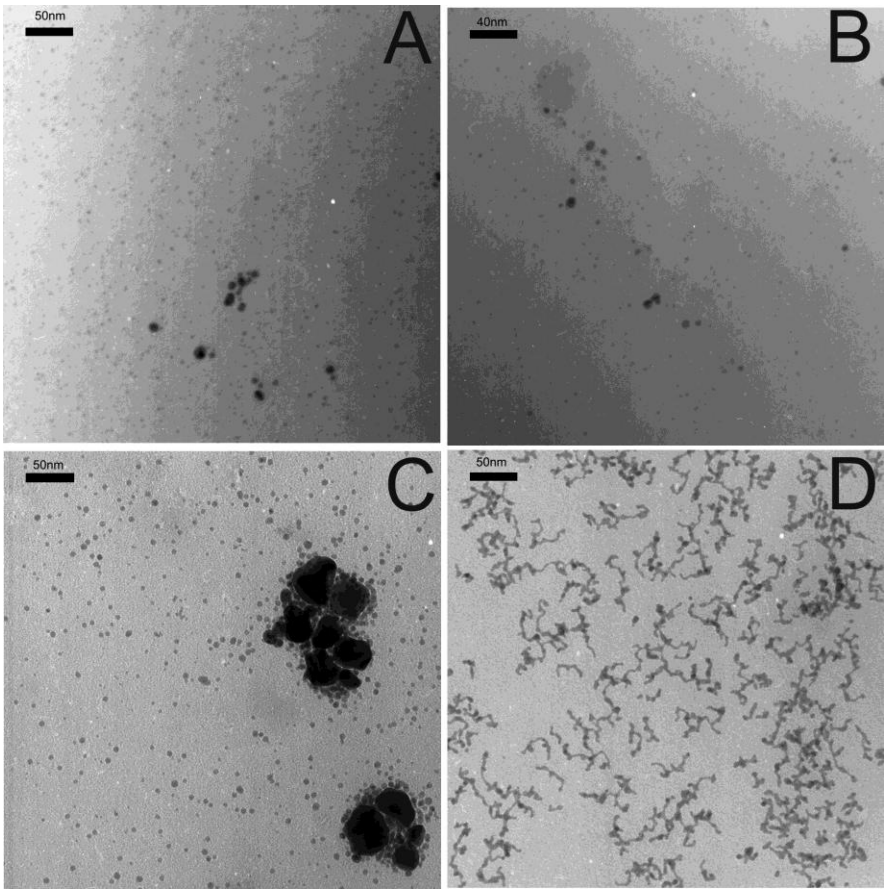

Figure 2.1 TEM images of PVP-stabilized (A) as-synthesized Au NP seeds and (B) as-synthesized sequentially-reduced 1:3 AuPd NPs and (C) Au NP/Pd(II) 1:3 mixture after 24 h reaction with cinnamyl alcohol and (D) sequentially-grown 1:3 AuPd NPs after 24 h reaction with cinnamyl alcohol.

Average particle sizes were found to be 2.9 nm ±1.4 nm and 3.9 nm ± 1.7 nm for these systems, respectively, which is in general agreement with previous work, although the Au NP sample showed some larger particles present and thus were not as monodisperse as could be desired. Pd NPs were 2.7 nm ± 1.0 nm, which within error is similar to that of the Au NPs; particle sizes of all samples by TEM are listed in Figure 2.1. The ca. 1 nm increase of size for the sequentially-grown particles is consistent with, but does not in itself prove, core-shell type growth of the particles. The UV-Vis spectra of Au, Pd, and sequentially grown 1:3 AuPd NPs are shown in Table 2.1.

Table 2.1: Summary of Nanoparticle Sizes obtained by TEM

Nanoparticle	**Size (nm)**	
	Water	**Ionic Liquid**
Au NPs	2.9 (1.4)	2.2 (0.8)
Pd NPs	2.7 (1.0)	4.3 (1.3)
1:3 AuPd Seq. Grown NPs	3.9 (1.7)	3.7 (1.0)
1:3 AuPd Seq. Grown NPs after reaction	--- [a]	8.0 (5.0)[b]
1:3 Au NPs/Pd(II) after reaction	6.4 (7.8)[b]	8.7 (3.9)
Pd NPs after reaction	---	9.0 (2.9)

[a] Particles formed worm-like structures; [b]Bimodal distribution of particles

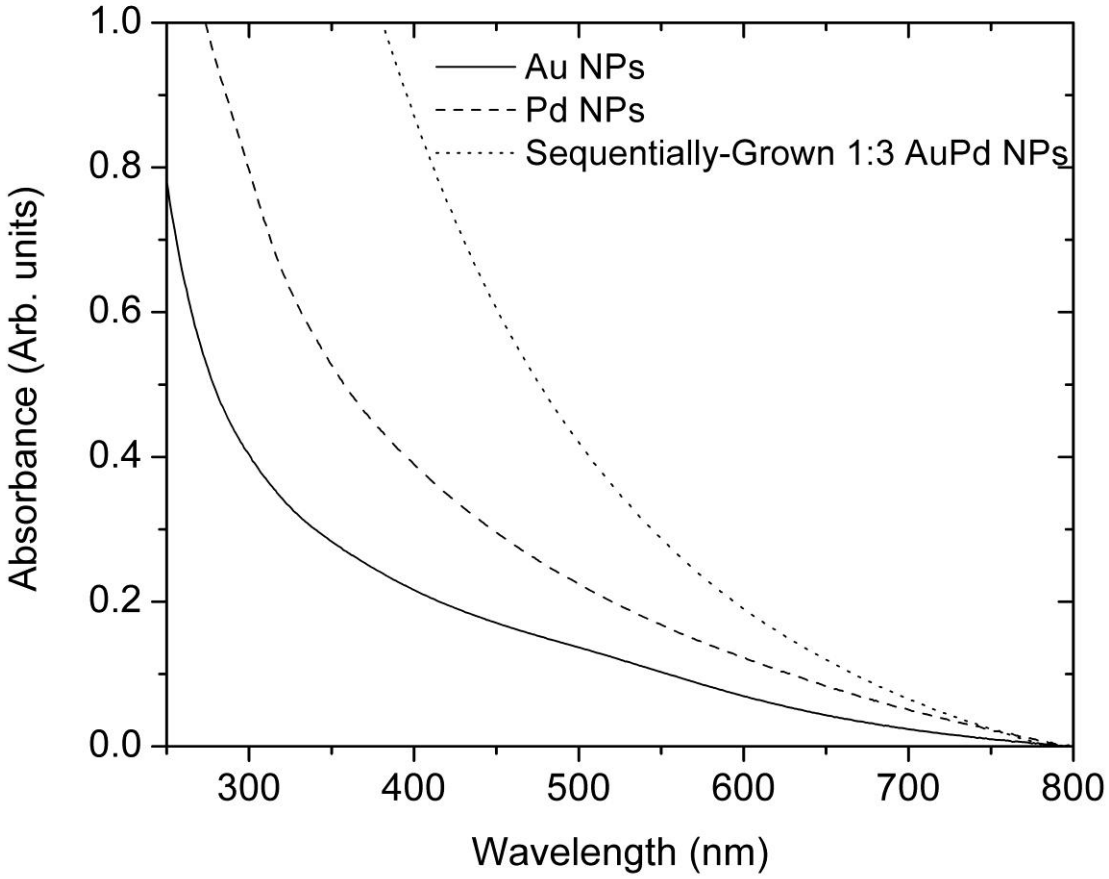

Figure 2.2. UV-Vis spectra of PVP-stabilized Au, Pd, and sequentially-grown 1:3 AuPd NPs.

There is a slight plasmon shoulder at ~530 nm in the Au NP sample, which is no longer apparent in the sequentially grown AuPd NP sample, which is similar to results seen before in this system[25, 33, 37], and is in agreement with TEM results which suggest Pd growth on the Au NP seeds. However, no information about whether the final particles have specific structures (core-shell, cluster on cluster, etc) can be obtained from this TEM and UV-Vis information alone.

Previous work has shown that sequentially-grown PVP-stabilized 1:3 AuPd NPs were optimal catalysts for the room-temperature oxidation of crotyl alcohol in water in the absence of base[25]; however, it was noted in the previous study that crotyl alcohol was an unusual substrate in this regard (e.g. room temperature/base free activation) and other allyl and benzyl alcohols showed much lower activity at these conditions. We also noted in the previous study that Au NPs in the presence of Pd(II) salts (specifically K_2PdCl_4) also showed tremendous activity for crotyl alcohol oxidation activation at room temperature while the individual Au NPs and Pd(II) salts showed next to no activity, and hypothesized that in situ reduction of Pd onto the Au NPs was responsible for this activity[25]. Thus in this study we wished to test the generality of both the high activity of sequentially-grown 1:3 AuPd NPs for other allylic and benzylic alcohols (e.g. α,β-unsaturated alcohols) and whether the Au NP/Pd(II) salt mixtures showed strong activities for other substrates as well. In order to activate other allylic and benzylic alcohols with moderate conversions, it was necessary to increase reaction temperatures to 60^{o}C using 1 atm oxygen as the oxidant (but no external base has been added to the system). Catalysis results for the five chosen α,β-unsaturated alcohols are shown in Table 2.2, and the major and minor products are shown in Scheme 2.1. For all the systems studied, Au NPs showed no or next to no activity under these conditions. Results for the K_2PdCl_4 salt by itself were non-uniform; both cinnamyl alcohol and crotyl alcohol showed significant conversions over 24 hours in the presence of the Pd(II) salt alone, while the other substrates did not react to any significant extent. Similarly, Pd NPs by themselves did not show significant activities for many substrates, although nearly 12% conversion was seen for allyl alcohol.

Table 2.2: Summary of Catalytic Results for the Oxidation of α,β-Unsaturated Alcohols using PVP-stabilized NPs in water [a]

Substrate	**NP Catalyst**	**Conversion[1]**	**Selectivity (%)**	
			Aldehyde or Ketone	Other
Allyl Alcohol	Au NPs	0	0	0
	K_2PdCl_4	2	66	34
	Pd NPs	11.6	29	71[3]
	1:3 AuPd Seq. NPs	19.9	14	86[3]
	1:3 Au/Pd(II)	17.1	9	91[3]
Benzyl Alcohol	Au NPs	0	0	0
	K_2PdCl_4	2.3	100	0
	Pd NPs	2.7	100	0
	1:3 AuPd Seq. NPs	4.3	100	0
	1:3 Au/Pd(II)	3.1	100	0
Cinnamyl Alcohol	Au NPs	0	0	0
	K_2PdCl_4	34.3	96	4
	Pd NPs	6.8	100	0
	1:3 AuPd Seq. NPs	34.2	89	11
	1:3 Au/Pd(II)	29.3	90	10
Crotyl Alcohol	Au NPs	-	-	-
	K_2PdCl_4	14.0	34	66
	Pd NPs	-	-	-
	1:3 AuPd Seq. NPs	36.9	73	27
	1:3 Au/Pd(II)	37.9	65	35
1-Hexen-3-ol	Au NPs	0	0	0
	K_2PdCl_4	trace amounts	~97	~3
	Pd NPs	trace amounts	~37	~63
	1:3 AuPd Seq. NPs	17.3[2]	29	71[4]
	1:3 Au/Pd(II)	35.1[2]	27	73[4]

[a] Reaction conditions: All reactions are carried out at 60°C with a substrate:catalyst ratio of 500:1. **[1]**Conversions and selectivities listed over 24h. [2]Conversions and selectivities listed after 4h. [3]Major product for allyl alcohol reaction 1-propanal (isomerization product), α,β-unsaturated ketone (prop-2-en-1-al) was minor product. [4]Major product for 1-hexen-3-ol reaction is 3-hexanone (isomerization product), α,β-unsaturated ketone (1-hexen-3-one) was minor product.

Scheme 2.1. Schematic Illustration of the major and minor products formed from the oxidation of α,β-unsaturated alcohols.

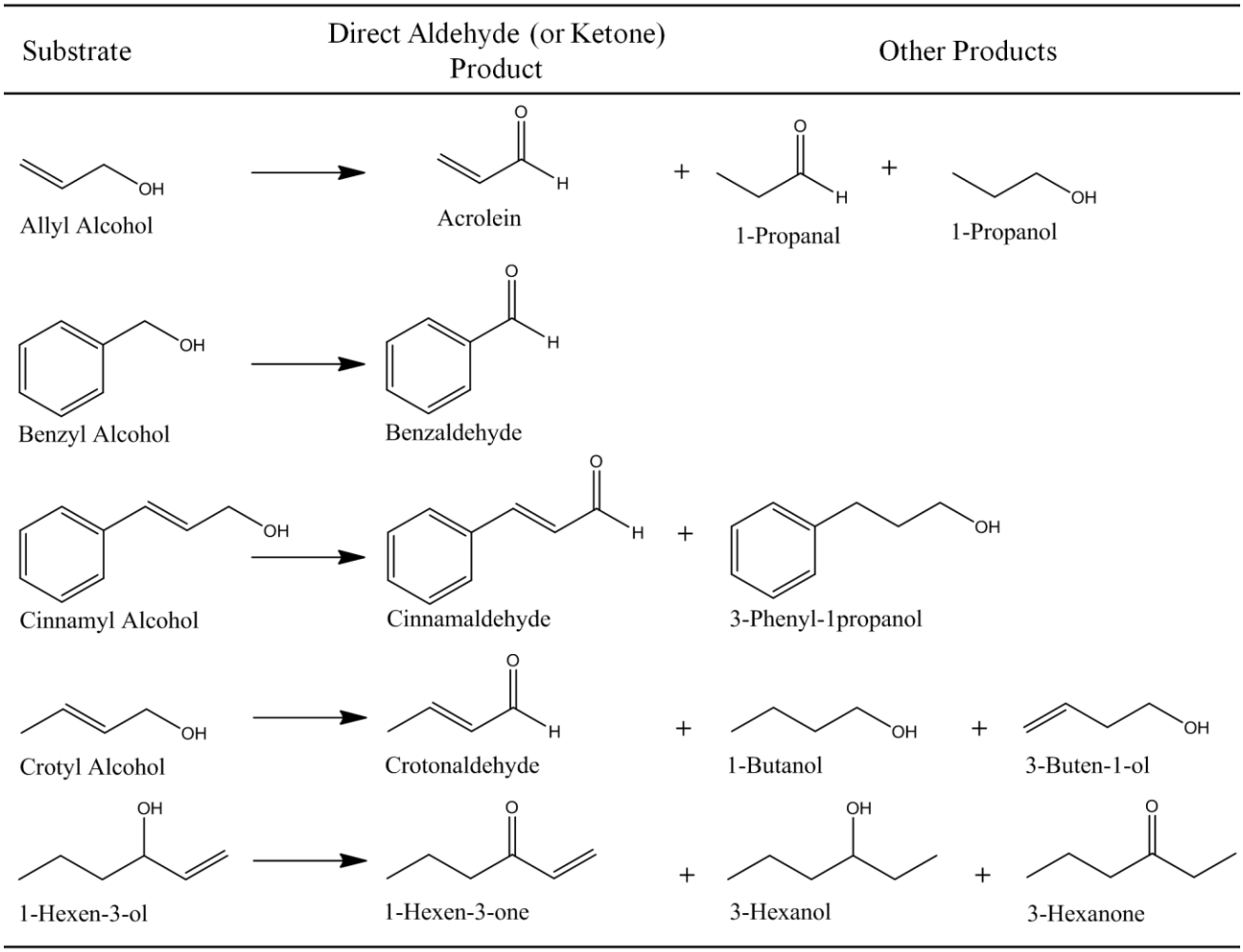

Interestingly, both the sequentially-grown 1:3 AuPd NPs and the 1:3 Au NP/Pd(II) mixtures showed moderate activity for most substrates, typically with similar conversions and selectivities towards the aldehyde (or ketone in the case of 1-hexen-3-ol) product. For 1-hexen-3-ol, the 1:3 Au NP/Pd(II) mixture showed significantly higher reactivity, for reasons that are not known at this time. High selectivities towards the aldehyde product were seen for benzyl and cinnamyl alcohols, while moderate selectivities were seen in the crotyl alcohol reaction, in which significant hydrogenation and isomerization products were also seen at short time periods. For 1-

hexen-3-ol, the major product of the reaction was actually the saturated ketone, 3-hexanone, which is an isomerization/tautomerization product (or a hydrogenation+oxidation product)[38, 39]; while the expected oxidation product, 1-hexen-3-one was formed in much lower amounts. Similarly, the major product for the allyl alcohol oxidation reaction was the isomerization/tautomerization product, 1-propanal. Similar reactivity of allyl alcohol to give large amounts of 1-propanal has been previously documented by our group using Pd catalysts under hydrogenation conditions[39]. The formation of minor hydrogenation products in many reactions can be attributed to a partial hydrogen coating on the NP surface, since it has been shown by Schwabe that even during oxidation of alcohols, the potential of Pt-group metals lie in the "hydrogen region"[40].

Interestingly, for crotyl alcohol, which we have previously shown can be activated at room temperature in the absence of base with excellent conversions and a high selectivity to crotonaldehyde[25], the harsher reaction conditions (60^{o}C) here generally lead to lower overall conversions for both the AuPd NPs and Au NP/Pd(II) systems with moderate selectivities to crotonaldehyde; also, moderate decompositions to CO and propene were seen after 8 hours[21, 41]. The reaction has a TOF of 120 moles product/moles catalyst h^{-1} over the first hour, which is comparable to earlier room-temperature work[18, 25], followed by a drastic reduction in the reaction rate after 1 hour. We believe that the decrease in TOF after one hour and thus the lower overall conversions after 24 h seen at these higher temperature conditions are due to significant Ostwald ripening of the particles during the catalyst experiment. To further explore this, the nanoparticle catalysts were examined after the catalytic reaction. Figure 2.2.1(C, D) show the final TEM images of the Au NP/Pd(II) and sequentially-grown AuPd NP systems, respectively, after 24 h reaction. Significant growth in the NPs are seen in both systems; the Au NP/Pd(II)

system showed a bimodal distribution with the presence of extremely large particles and an average particle size of 6.4 nm ± 7.8 nm, while the sequentially-grown AuPd NP system showed wormlike particles after the 24 h reaction (no particle size is reported due to the change in morphology). In the absence of a catalytic reaction (e.g. just heating to 60^{o}C) there is typically no change in average particle sizes in these systems. Both of these results suggest significant ripening of particles during the catalytic reaction, likely due to an Ostwald ripening mechanism. Previously we indicated that the mechanism for this reaction may be a redox mechanism in which the Pd is oxidized to Pd(II) and reformed upon reaction with the alcohol substrate[25]; and others have also supported an Pd(II) oxidation mechanism[24]. Such a mechanism is likely to lead to homogeneous Pd(II) species in solution during the catalytic reaction which would greatly enhance Ostwald ripening. Indeed, others have shown that Pd(II) species can react stoichiometrically with many α,β-unsaturated alcohols[42, 43]. Thus the lower activities seen for crotyl alcohol at 60^{o}C seems mostly due to the large changes seen in particle size during the reaction; at lower temperatures the Ostwald ripening is much slower, thus allowing for higher-surface area NPs to remain active for longer periods of time. We believe the role of the Au in this reaction is to destabilize the Pd to oxidation by oxygen, thus allowing the reaction to turnover.

Finally, in order to further examine both the structure of the sequentially grown AuPd NPs and the reaction product in the Au NP/Pd(II) system, these systems were examined via EXAFS analysis of these systems was performed. Figure 2.3 shows the Au L_{III}-edge and Pd K-edge EXAFS spectra in k-space for the pure Au and Pd NPs, sequentially grown AuPd NPs, and the reaction product in the Au NP/Pd(II) system (after 24 h reaction with crotyl alcohol); high quality data was collected over a k-range from 0 to 14 for the Au edge and 0 to 10 for the Pd edge.

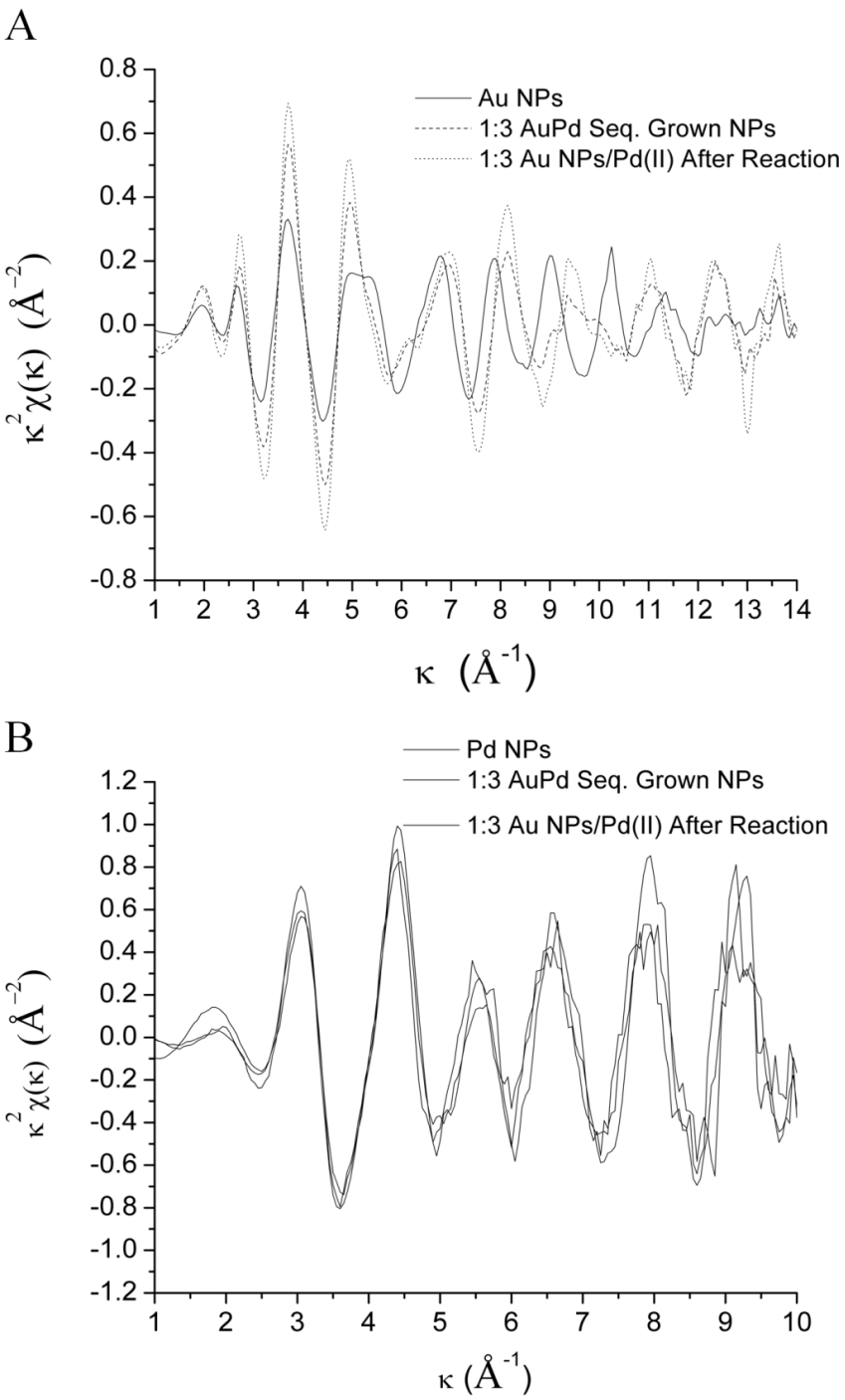

Figure 2.3. EXAFS spectra in k-space for monometallic Au, Pd and sequentially-grown 1:3 AuPd NPs and Au NP/Pd(II) 1:3 mixture after 24h reaction with crotyl alcohol. (A) Pd K-edge (B)Au-L_{III} edge.

Both the Pd and Au edge k-space data show that the the reaction product in the Au NP/Pd(II) system has similar chemical environments around the Au and Pd absorber atoms as the as-synthesized sequentially grown AuPd NPs. The shift in periodicity in the Au k-space data suggests some alloying of Au and Pd in both the bimetallic samples[33, 44, 45]. Figure 2.4 shows the experimentally obtained EXAFS data in R-space with the single-shell theoretical fits for sequentially grown AuPd NPs and the reaction product in the Au NP/Pd(II) system.

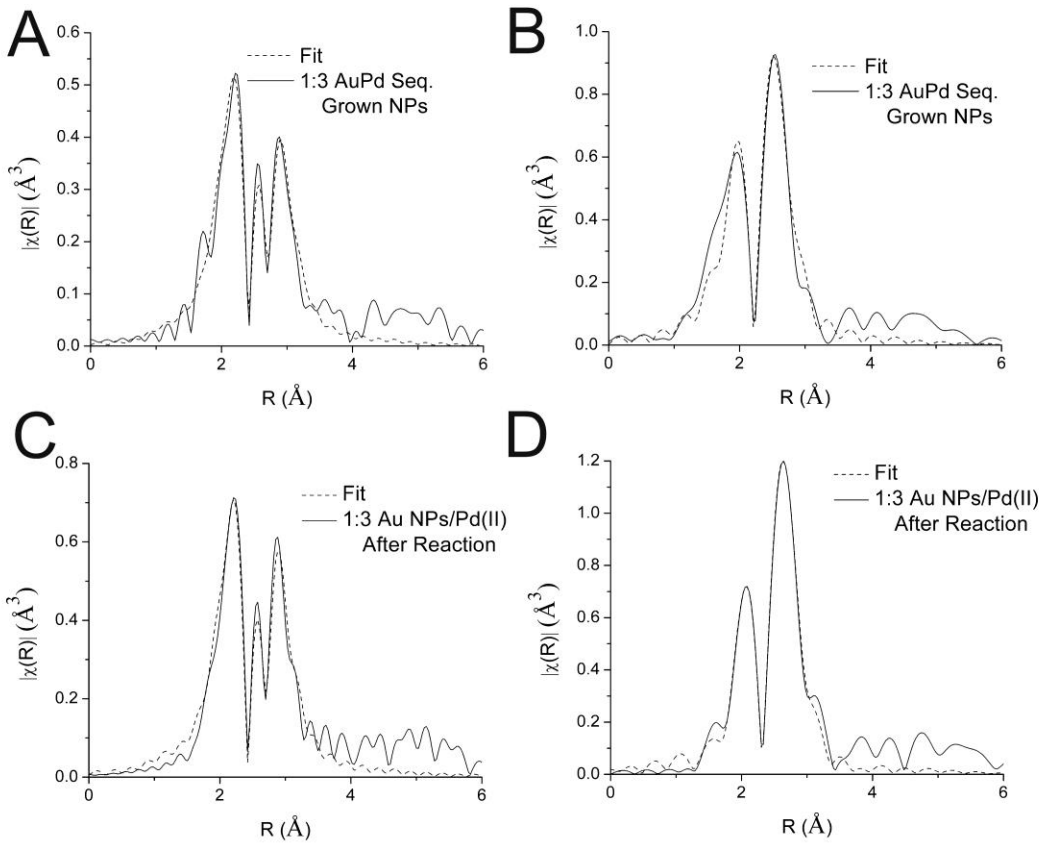

Figure 2.4. EXAFS single-shell fits in r-space for sequentially-reduced 1:3 AuPd NPs at the (A) Au-L_{III} and (B) Pd K edges and Au NP/Pd(II) 1:3 mixture after 24h reaction with crotyl alcohol at the (C) Au-L_{III} and (D) Pd K edges .

For the bimetallic NPs, the Au and Pd EXAFS data of the same sample were simultaneously fit using the IFEFFIT software package[35]. High-quality fits have been obtained for both the bimetallic AuPd samples. We note that the Pd data shows significant Pd-Pd and Pd-Au coordination environments but minimal Pd-O and/or Pd-Cl contributions (a very small shoulder can be seen on the low r-side of the Pd data); thus during the reaction, the Pd(II) is definitively reduced to form bimetallic NPs in the Au NP/Pd(II) system. The structural fit parameters for the sequentially grown AuPd NPs and the reaction product in the Au NP/Pd(II) system generated from the EXAFS fitting parameters are presented in Table 2.3.

Table 2.3: EXAFS fitting parameters for AuPd NP systems.

Nanoparticle Sample	Shell	N	R (A^o)	ΔE^o(eV)	σ^2($A^{o\,2}$)	R-factor
1:3 AuPd Sequentially Grown NPs	Au-Au	5.9 (0.8)	2.812 (0.008)	4.4 (0.5)	0.010 (0.001)	0.020
	Au-Pd	2.4 (0.4)	2.768 (0.009)		0.008 (0.001)	
	Pd-Pd	6.0 (2.6)	2.73 (0.02)	-4.1 (2.6)	0.008 (0.004)	
	Pd-Au	3.8 (2.5)	2.768 (0.009)		0.008 (0.001)	
1:3 Au NPs/ Pd(II) After Reaction	Au-Au	6.4 (0.7)	2.814 (0.007)	4.9 (0.4)	0.009 (0.001)	0.014
	Au-Pd	3.4 (0.4)	2.777 (0.007)		0.007 (0.001)	
	Pd-Pd	7.0 (3.1)	2.76 (0.02)	3.0 (1.2)	0.008 (0.004)	
	Pd-Au	2.9 (2.7)	2.777 (0.007)		0.007 (0.001)	

In both cases, reasonable fits were obtained; however, higher errors in coordination number for the Pd nearest neighbour were seen, which is likely both due to the lower quality of Pd edge data and inhomogeneities in the actual samples (which are particularly evident in the TEM of the reaction product in the Au NP/Pd(II) system). Higher Pd loadings in sample may allow for quality data acquisition to higher k space values in the future, though heterogeneity problems will likely compromise data quality regardless. We note that because of these errors one cannot make any definitive conclusions regarding the final structures of the AuPd particles; however, the EXAFS data unambiguously indicates that nearly all the Pd is in the zerovalent state in both systems, and that core-shell morphologies are unlikely as the total first shell Au coordination number (e.g. $N_{Au-Au} + N_{Au-Pd}$) is significantly below the bulk fcc value of 12 for both systems. The moderate N_{Au-Pd} and N_{Pd-Au} values (albeit with high errors on the latter) also indicates that significant Au/Pd mixing is seen in both these systems.

2.4.2 Oxidation Reactions in ILs

We have recently shown that trihexyl(tetradecyl)phosphonium chloride (P[6,6,6,14]Cl) ILs are excellent stabilizers for both Au and Pd NPs for hydrogenation reactions[32]. In this IL, the source of NP stabilization is thought to be two-fold: the halide ions that interact with the NP surface, and the long-chain hydrocarbons that provide steric protection. Weaker coordinating anions such as triflate were found to have much lower stabilizing effects in previous work[32]. As AuPd NP recyclability is a major challenge in the water system above (since the products need to be extracted using ethyl acetate or a similar solvent), we were curious as to whether the reaction could proceed in a more recyclable solvent system such as an IL. This system is attractive as it

would allow for the products and un-reacted substrates to be removed from the reaction mixture by vacuum extraction, establishing the potential for re-use of the IL/NP catalyst system.

TEM images in Figure 2.5 show the Au, Pd NPs and sequentially grown 1:3 AuPd NPs before and after reaction.

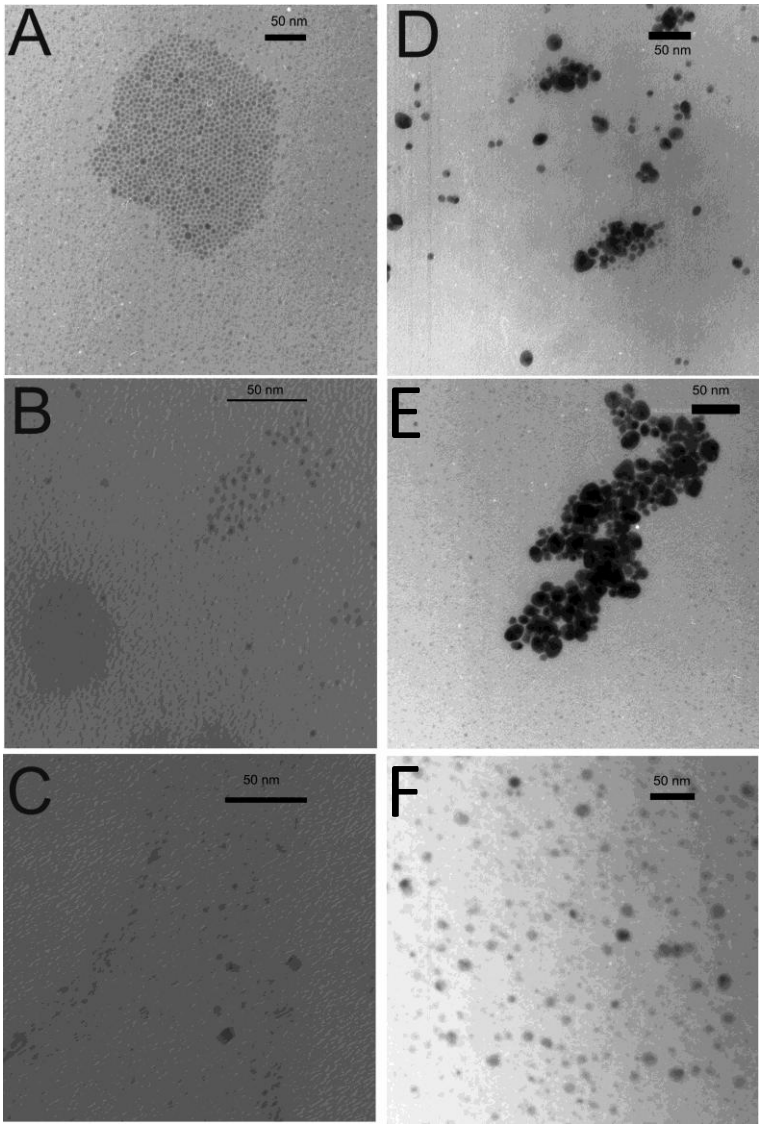

Figure 2.5. TEM images of as-synthesized P[6,6,6,14]Cl IL-stabilized (A) Pd NPs, (B) sequentially-reduced 1:3 AuPd NPs, and (C) Au NPs; and after 24 h reaction with cinnamyl alcohol: (D) Pd NPs, (E) sequentially-reduced 1:3 AuPd NPs, and (F) Au NP/Pd(II) 1:3 mixture.

Before reaction, the Au, AuPd and Pd NPs are 2.2 ± 0.8 nm, 3.7 nm ± 1.0 nm, and 4.3 nm ± 1.3 nm respectively (see Figure 2.1). The Pd NPs are larger than those formed in the aqueous system above, but in general agreement with our previous work[32]. The larger size of the NPs is confirmed by UV-Vis spectroscopy as shown in Figure 2.6; a significant plasmon band at 530 nm is seen for the Au NPs, which dampens significantly upon sequential Pd deposition. However, there is a significant growth of particles during a 12 h catalytic cycle, as seen in Figure 2.5(D, E, F); the Pd and Au NP/Pd(II) system grow to 9.0 nm ± 2.9 nm and 8.7 nm ± 3.9 nm, respectively, while the sequentially grown AuPd system shows a bimodal distribution with a significant number of particles above 10 nm.

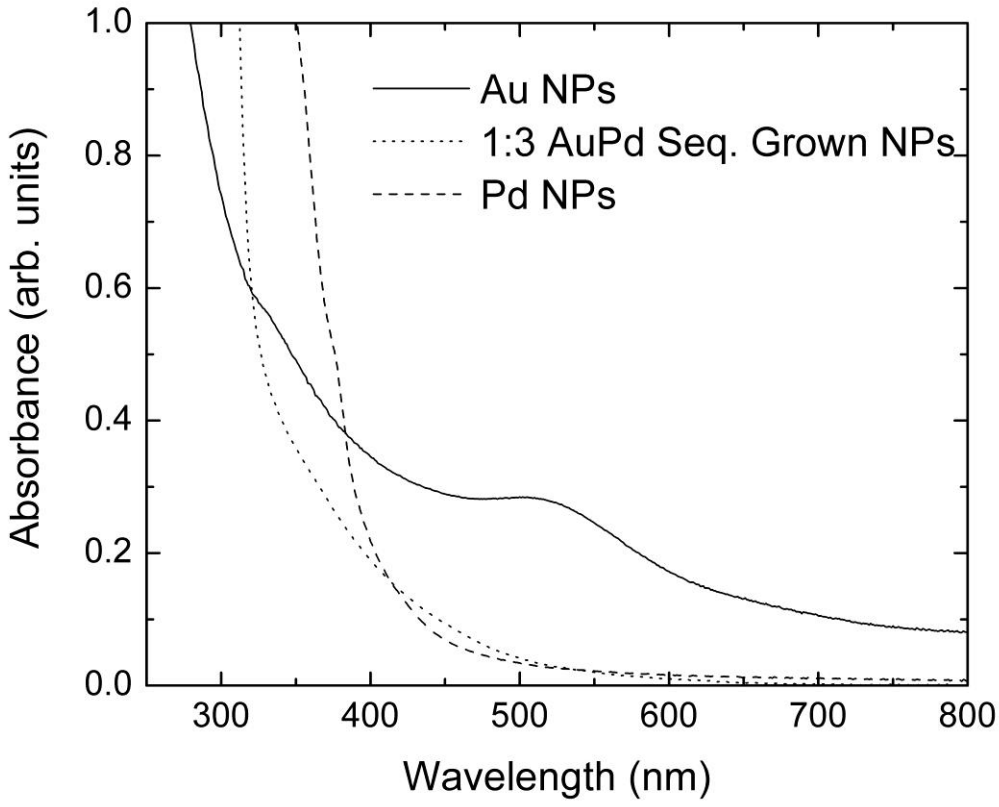

Figure 2.6. UV-Vis spectra of P[6,6,6,14]Cl IL -stabilized Au, Pd, and sequentially-grown 1:3 AuPd NPs.

Since halide ions are also known to promote oxidative etching of Pd, NPs in halide ILs in the presence of oxygen form an unique system in which both Pd and Au oxidation can occur[46]. Evidently an Ostwald ripening mechanism in which Pd (and potentially Au as well) are oxidized and re-reduced upon stoichiometric reactions with the alcohol substrates is occurring to an even greater extent in the IL system as compared to the aqueous system above, due to the extremely high chloride environment in these ILs.

Table 2.4 shows the product distributions for the catalytic oxidations of four of the various α,β-unsaturated alcohols in trihexyl(tetradecyl)phosphonium chloride. We note that 5000:1 ratios of substrate to catalyst were used for the IL work, rather than the 500:1 ratios in the aqueous work, as vacuum stripping of the products and leftover substrates was more reliable at higher substrate levels and IL-stabilized NPs were still quite stable in the presence of larger amounts of substrate.

Table 2.4: Summary of Catalytic Results for the Oxidation of α,β-Unsaturated Alcohols using P[6,6,6,14]Cl -stablized NPs[a]

Substrate	**NP Catalyst**	**Conversion[1]**	**Selectivity (%)**	
			Aldehyde	Other
Allyl Alcohol	Pd NPs	66	17	83[2]
	1:3 AuPd Seq. NPs	47	21	79[2]
	1:3 Au/Pd(II)	45	27	73[2]
Benzyl Alcohol	Pd NPs	97	99	1
	1:3 AuPd Seq. NPs	84	97	3
	1:3 Au/Pd(II)	90	98	2
Cinnamyl Alcohol	Pd NPs	99	70	30
	1:3 AuPd Seq. NPs	81	91	9
	1:3 Au/Pd(II)	98	74	26
Crotyl Alcohol	Pd NPs	53	47	53
	1:3 AuPd Seq. NPs	50	46	54
	1:3 Au/Pd(II)	50	58	42

a Reaction conditions: All reactions are carried out at 60°C with a substrate:catalyst ratio of 5000:1.

1Conversions and selectivities listed over 12h. [2]Major product for allyl alcohol reaction is 1-propanal (isomerization product), α,β-unsaturated ketone (prop-2-en-1-al) was minor product.

While the Au NPs showed almost no catalytic activity in the absence of Pd(II) salts, but were active with Pd(II) salts present, Pd NPs and 1:3 AuPd NPs showed variable degrees of conversion for most of the substrates under the reaction conditions. Several phenomena can be noted from the catalyst data. First, overall conversions over 12 hours for reactions in the IL are

much higher than their respective aqueous systems. In particular, aromatic systems such as benzyl alcohol and cinnamyl alcohol show extremely high conversions with high and moderate selectivities towards the aldehyde, respectively. Again, the major product for the allyl alcohol oxidation reaction is actually the isomerization/tautomerization product, 1-propanal (which could also be formed as a hydrogenation + oxidation product). The activities towards crotyl alcohol oxidation are somewhat similar to that of the aqueous system, albeit with significantly lower selectivities. In order to ensure that the change in substrate:catalyst ratio did not adversely affect the comparison of aqueous/IL systems, crotyl alcohol oxidation was examined in the IL system with a 500:1 substrate:product ratio, and similar yields and selectivities to crotonaldehyde were seen for both Pd NPs (62% conversion, 43% selectivity) and sequentially grown 1:3 AuPd NPs (66% conversion, 56% selectivity) systems . The major finding is that AuPd NPs show no exceptional abilities in terms of catalytic performance and/or product selectivity compared to Pd NPs in this particular system, likely due to the ease at which Pd can be oxidized in this IL as compared to water. Indeed, we have previously noted facile oxidation of Pd NPs upon heating in the P[6,6,6,14]Cl ILs[32]. This easier oxidation of Pd in the IL system allows for higher turnovers of the redox catalytic cycle even in the absence of the Au promoter. Thus the Pd NP/IL system has some promise for the possibility of high activities for mild alcohol oxidations; however, in order to optimize the system, it would be desirable to attempt to minimize the particle growth occurring in the system. Alternatively, we have previously shown that complete oxidation of Pd NPs can allow for a facile reformation of Pd NPs in P[6,6,6,14]Cl systems by re-addition of a reducing agent such as $LiBH_4$[32]. This would, in principle, allow for the recycling of the Pd NP/IL system over a large number of cycles. We will continue to explore this system for recyclable oxidation reactions in the future.

2.5 Conclusions

In summary, the present study considers the NP-catalyzed oxidation of α,β-unsaturated alcohols in water and in a tetraalkylphosphonium IL at 60^{o}C. In water sequentially grown AuPd NPs, either formed intentionally or in situ, were found to be active for most α,β-unsaturated alcohols; although particle size growth due to Ostwald ripening was problematic. TEM and EXAFS studies of sequentially grown AuPd NPs and Au NP/Pd(II) mixtures indicated that both systems led to the formation of AuPd NPs with some mixing of Pd and Au in their structures. Conversely, we found that Pd NPs alone have significant catalytic activity in tetraalkylphosphonium chloride ILs, likely due to the ease of oxidation of Pd in the high chloride environment. As such, Au promoters have little to no effect on Pd catalytic activity in the IL system. The concept of using a recyclable solvent in catalytic alcohol oxidations still remains a problem worthy of intensive research.

2.6 Acknowledgements

The authors would like to thank Dr. Weifeng Chen and Ning Chen at the Canadian Light Source (CLS) for the assistance with EXAFS measurements, Al Robertson at Cytec for donation of tetraalkylphosphonium chloride ionic liquids and NSERC and the University of Saskatchewan for funding. Some of the research described in this paper was performed at the Canadian Light Source, which is supported by the Natural Sciences and Engineering Research Council of Canada, the National Research Council Canada, the Canadian Institutes of Health Research, the Province of Saskatchewan, Western Economic Diversification Canada, and the University of Saskatchewan.

2.7 References

1 J. March, *Advanced Organic Chemistry: Reactions, Mechanisms, And Structure* Editor, Wiley, New York, **1992**.

2 D. G. Lee, U. A. Spitzer, *J. Org. Chem.* **1970**, *35*, 3589-3590.

3 A. Abad, C. Almela, A. Corma, H. Garcia, *Chem. Commun.* **2006**, 3178-3180.

4 P. J. Dyson, T. J. Geldbach, *Metal Catalyzed Reactions in Ionic Liquids*. Editor, Springer, **2005**, pp. p90-91.

5 D. Astruc, F. Lu, J. R. Aranzaes, *Angew. Chem. Int. Ed.* **2005**, *44*, 7852-7872.

6 M. Haruta, *Catal. Today* **1997**, *36*, 153-166.

7 H. Tsunoyama, H. Sakurai, Y. Negishi, T. Tsukuda, *J. Am. Chem. Soc.* **2005**, *127*, 9374-9375.

8 H. Tsunoyama, T. Tsukuda, H. Sakurai, *Chem. Lett.* **2007**, *36*, 212-213.

9 H. Tsunoyama, N. Ichikuni, H. Sakurai, T. Tsukuda, *J. Am. Chem. Soc.* **2009**, *131*, 7086-7093.

10 L. Prati, M. Rossi, *J. Catal.* **1998**, *176*, 552-560.

11 D. I. Enache, D. W. Knight, G. J. Hutchings, *Catal. Lett.* **2005**, *103*, 43-52.

12 H. R. Li, B. T. Guan, W. J. Wang, D. Xing, Z. Fang, X. B. Wan, L. P. Yang, Z. J. Shi, *Tetrahedron* **2007**, *63*, 8430-8434.

13 J. Hu, L. Chen, K. Zhu, A. Suchopar, R. Richards, *Catal. Today* **2007**, *122*, 277-283.

14 O. Casanova, S. Iborra, A. Corma, *J. Catal.* **2009**, *265*, 109-116.

15 H. Liu, Y. Liu, Y. Li, Z. Tang, H. Jiang, *J. Phys. Chem. C* **2010**, *114*, 13362-13369.

16 D. I. Enache, J. K. Edwards, P. Landon, B. Solsona-Espriu, A. F. Carley, A. A. Herzing, M. Watanabe, C. J. Kiely, D. W. Knight, G. J. Hutchings, *Science* **2006**, *311*, 362-365.

17 N. Dimitratos, J. A. Lopez-Sanchez, D. Lennon, F. Porta, L. Prati, A. Villa, *Catal. Lett.* **2006**, *108*, 147-153.

18 W. B. Hou, N. A. Dehm, R. W. J. Scott, *J. Catal.* **2008**, *253*, 22-27.

19 A. Villa, N. Janjic, P. Spontoni, D. Wang, D. S. Su, L. Prati, *Appl. Catal., A* **2009**, *364*, 221-228.

20 S. Marx, A. Baiker, *J. Phys. Chem. C.* **2009**, *113*, 6191-6201.

21 A. F. Lee, S. F. J. Hackett, G. J. Hutchings, S. Lizzit, J. Naughton, K. Wilson, *Catal. Today* **2009**, *145*, 251-257.

22 A. J. Frank, J. Rawski, K. E. Maly, V. Kitaev, *Green Chem.* **2010**, *12*, 1615-1622.

23 Y. T. Chen, H. M. Lim, Q. H. Tang, Y. T. Gao, T. Sun, Q. Y. Yan, Y. H. Yang, *Appl. Catal., A* **2010**, *380*, 55-65.

24 D. Wang, A. Villa, P. Spontoni, D. S. Su, L. Prati, *Chem. Eur. J.* **2010**, *16*, 10007-10013.

25 T. Balcha, J. R. Strobl, C. Fowler, P. Dash, R. W. J. Scott, *ACS Catal.* **2011**, *1*, 425-436.

26 C. P. Vinod, K. Wilson, A. F. Lee, *J. Chem. Tech. Biotech.* **2011**, *86*, 161-171.

27 G. S. Owens, M. M. Abu-Omar, *Chem. Commun.* **2000**, 1165-1166.

28 J. A. Laszlo, D. L. Compton, *J. Mol. Catal. B* **2002**, *18*, 109-120.

29 A. Wolfson, S. Wuyts, D. E. De Vos, I. F. J. Vankelecom, P. A. Jacobs, *Tet. Lett.* **2002**, *43*, 8107-8110.

30 A. Bordoloi, S. Sahoo, F. Lefebvre, S. B. Halligudi, *J. Catal.* **2008**, *259*, 232-239.

31 M. L. Kantam, U. Pal, B. Sreedhar, S. Bhargava, Y. Iwasawa, M. Tada, B. M. Choudary, *Adv. Synth. Catal.* **2008**, *350*, 1225-1229.

32 A. Banerjee, R. Theron, R. W. J. Scott, *ChemSusChem* **2012**, *5*, 109-116.

33 P. Dash, T. Bond, C. Fowler, W. Hou, N. Coombs, R. W. J. Scott, *J. Phys. Chem.C.* **2009**, *113*, 12719-12730.

34 M. Newville, B. Ravel, D. Haskel, J. J. Rehr, E. A. Stern, Y. Yacoby, *Physica B.* **1995**, *208*, 154-156.

35 M. Newville, *J. Synchrotron Radiat.* **2001**, *8*, 322-324.

36 A. Maeland, T. B. Flanagan, *Can. J. Phys.* **1964**, *42*, 2364-&.

37 R. W. J. Scott, O. M. Wilson, S. K. Oh, E. A. Kenik, R. M. Crooks, *J. Am. Chem. Soc.* **2004**, *126*, 15583-15591.

38 S. H. Bergens, B. Bosnich, *J. Am. Chem. Soc.* **1991**, *131*, 5734-5735.

39 C. F. Calver, P. Dash, R. W. J. Scott, *ChemCatChem* **2001**, *3*, 695-697.

40 E. Müller, K. Schwabe, *Z. Elektrochem. Angew. Phys. Chem.* **1928**, *34*, 170-.

41 A. F. Lee, Z. Chang, P. Ellis, S. F. J. Hackett, K. Wilson, *J. Phys. Chem. C.* **2007**, *111*, 18844-18847.

42 K. Zaw, M. Lautens, P. M. Henry, , *Organometallics* **1983**, *2*, 197-199.

43 J. Muzart, *Tetrahedron* **2003**, *59*, 5789-5816.

44 F. Liu, D. Wechsler, P. Zhang, *Chem. Phys. Lett.* **2008**, *461*, 254-259.

45 M. R. Knecht, M. G. Weir, A. I. Frenkel, R. M. Crooks, *Chem. Mater.* **2008**, *20*, 1019-1028.

46 H. A. Kalviri, F. M. Kerton, *Green Chem.* **2011**, *13*, 681-686.

Chapter 3

In situ X-ray Absorption Spectroscopic Analysis of Gold-Palladium Bimetallic Nanoparticle Catalysts

This work has been submitted to ACS Catalysis. A series of Au, Pd, and AuPd catalyst systems under aqueous conditions have been studied by time-resolved *in situ* XAFS analysis. The effects of crotyl alcohol oxidation on Pd in an Au NP/ K_2PdCl_4 mixture have been studied by this method. The change in Pd-L_{III}-edge over the course of the reaction was monitored and examined by linear combination analysis. From this information, insight into the reaction kinetics and active species was gained. EXAFS fitting was also performed on data collected from the *in situ* work, as well as pre-synthesized samples from the lab. This data provided structural information about the NPs formed *in situ* as well as those synthesized in the lab.

This paper was co-authored by Yongfeng Hu and Jeffrey Miller who helped with the *in situ* analyses at the Advanced Photon Source at Argonne National Labs, Illinois. All of the experimental work in this paper was performed by myself. Writing of this paper was also performed by myself, with assistance from Dr. Robert W.J. Scott. Editing was performed by all authors on the paper.

In situ X-ray Absorption Spectroscopic Analysis of Gold-Palladium Bimetallic Nanoparticle Catalysts

Aimee Maclennan,[1] Yongfeng Hu,[2] Jeff Miller,[3] Robert W.J. Scott[1]*

3.1 Abstract

Gold-palladium core-shell nanoparticles have been previously shown to be extremely effective catalysts for a number of oxidation reactions including the aerobic oxidation of alcohol. However, the novel activity and durability of such catalysts are still poorly understood, and there are several putative mechanisms by which oxidation reactions can proceed. Previously we showed that Pd(II) salts in the presence of Au nanoparticles were also effective catalysts for the room temperature oxidation of crotyl alcohol. Herein we show an *in situ* X-ray absorption spectroscopy (XAS) study at both the Pd-K and Pd-L_{III} edges of Au nanoparticle/Pd(II) salt solutions in the presence of crotyl alcohol. Liquid cells with X-ray permeable windows were used to obtain quick-scan XAS data during the oxidation of crotyl alcohol, allowing for time-resolved Pd speciation information and information about the reaction mechanism and kinetics. XAS measurements definitively show that the first step of this reaction involves Pd reduction onto the Au nanoparticles; in addition, further studies of the stability of the resulting Au-Pd core-shell nanoparticles towards oxygen gas suggests that the role of Au in such catalysts is to prevent the re-oxidation of the catalytically active surface Pd atoms.

3.2 Introduction

The extensive and ongoing study of nanoparticle catalysts began when it was first discovered that metal particles less than 10 nm in diameter behaved much differently than their bulk counterparts.[1] Small nanoparticles (NPs), because they possess a large amount of surface area, are often more catalytically active than the bulk material.[1-4] Au is one of the most commonly studied nanoparticle catalyst materials and it is used in reactions such as CO and alcohol oxidations, dehydrogenations, and olefin hydrogenation reactions.[5, 6] In recent years it has been discovered that the size, morphology, and characteristics of Au NPs can be tuned by synthesizing Au NPs with different stabilizers and/or placing them on a variety of supports.[2, 5, 7-10] The catalytic activity of nanoparticle catalysts can also be tuned by mixing Au with other metals such as Pt, Ag, Cu, and Pd.[9-21] In particular, mixing Au with Pd has led to substantially more efficient catalysts for a number of oxidation reactions. For example, AuPd catalysts have recently been used extensively for selective oxidation reactions of both alcohols and toluene as well as the direct formation of hydrogen peroxide from hydrogen and oxygen.[5, 6, 9, 10, 16, 17]

The oxidation of alcohols is important in many pharmaceutical and industrial processes.[6, 22] The AuPd nanoparticle-catalyzed oxidation of both saturated and α-β unsaturated alcohols has been studied in detail by both ourselves[23, 24] and a number of other research groups.[9, 25-38] However, the definitive mechanism by which the reaction takes place remains unclear at this time. Two proposed mechanisms which have received experimental support for the oxidation of α-β unsaturated alcohols include β-hydride (β-H) elimination over a zerovalent surface[3, 23, 24, 39] or a redox mechanism involving Pd(II) formation and re-reduction,[24] which are both shown in Scheme 3.1.

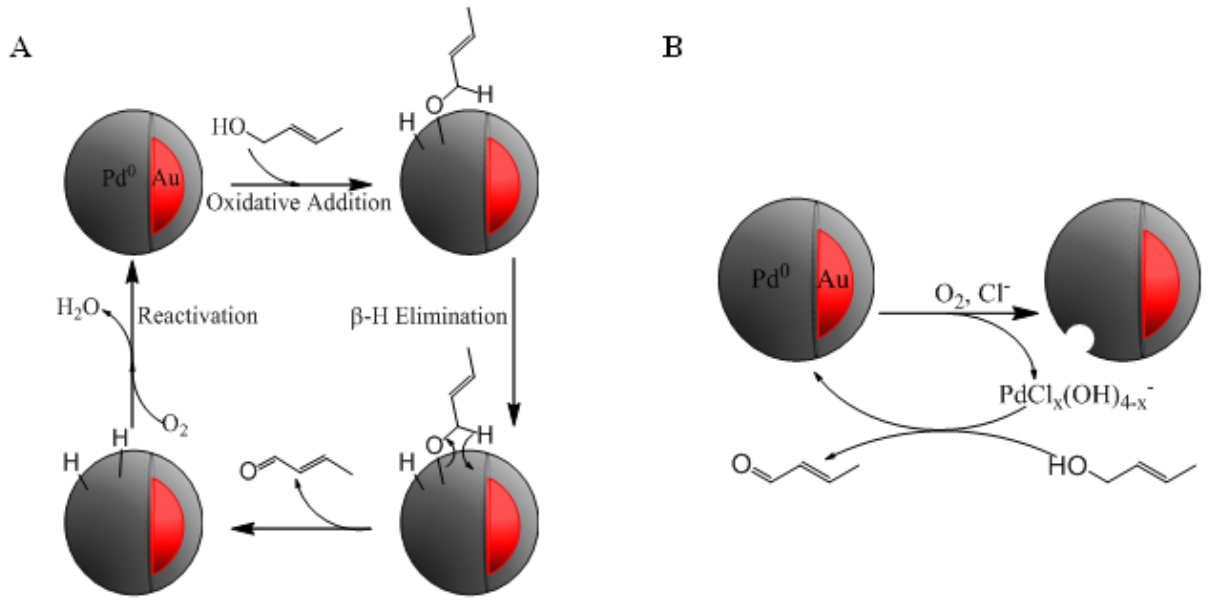

Scheme 3.1. Suggested mechanisms for the oxidation of crotyl alcohol over AuPd nanoparticles in the presence of O_2 (A) β-H elimination mechanism (B) redox mechanism.

β-H elimination occurs by the binding of the alcohol substrate to the nanoparticle surface, where it undergoes a β-H elimination reaction. Upon completion of the alcohol oxidation the product is removed from the NP surface leaving adsorbed hydrogen on the nanoparticle surface. At this point, molecular oxygen is required to strip the hydrogen from the nanoparticle surface (Scheme 1A). Support for this mechanism includes the identification of hydrogenation and isomerization side-products during crotyl alcohol oxidations over AuPd catalysts,[23, 24] although there is evidence that this occurs only in the early stages of the reaction. For the redox mechanism, Pd from the surface of the bimetallic nanoparticle becomes oxidized, followed by the stoichiometric reaction of the oxidized Pd species and the alcohol, upon which the Pd becomes reduced and alcohol is oxidized (Scheme 1B). We previously saw some evidence for this mechanism when we carried out the oxidation of crotyl alcohol in the presence of Au NPs and K_2PdCl_4. Upon introduction of crotyl alcohol into the Au NP/Pd(II) mixture at room temperature, the NPs

significantly grew in size, suggesting Pd(II) reduction onto the Au NPs.[24] This was confirmed by *ex situ* EXAFS analysis of the catalysts after the oxidation reaction. Prati and coworkers showed that monometallic Au and Pd NPs form AuPd catalytic NPs *in situ*, which supports a redox mechanism.[33] In addition, Lee and coworkers have shown that PdO species on the surface of Pd particles are the catalytic species via *in situ* X-ray absorption spectroscopy studies of gas-phase oxidations of crotyl alcohol at temperatures between 80 and 250^{o}C.[34]

In order to gain insight into the mechanism of the oxidation of α-β unsaturated alcohols, a series of reactions were carried out and the effects of Pd in the system were studied *in situ* by X-ray absorption spectroscopy (XAS). XAS analysis is used to determine characteristics such as oxidation state, coordination number, and bond lengths of a material,[10, 40-44] and is traditionally performed on a solid sample. With recent advances in XAS technology it has now become possible to analyze materials under reactive conditions, including samples under *in situ* conditions both in the solid and liquid phase and the ability to study reaction kinetics with fast scans.[45, 46] In order to perform such analyses the experimental set up requires new and innovative designs of sample cells. Liquid and solid cell designs have been fabricated such that samples can be heated and exposed to different atmospheric environments.[46] Such capabilities allow for *in situ* and/or *in operando* verification of the oxidation states and coordination environments of transition metal catalysts. For example, Ishiguro *et al.* and Imai *et al.* have used *in situ* time-resolved XAFS to study platinum cathode catalysts in polymer electrolyte fuel cells,[47-49] and Lee and coworkers have shown PdO formation at higher temperatures during the aerobic oxidation of gas phase alcohols over Pd NP catalysts. [34]

In this study, we have used *in situ* X-ray absorption spectroscopy to follow the Pd(II)/Au NP catalyzed oxidation of crotyl alcohol in aqueous solutions. The Pd-K and Pd-L_{III} edges were

studied by *in situ* XAS in order to examine Pd speciation upon introduction of crotyl alcohol to the aforementioned system. *In situ* X-ray absorption spectroscopy measurements allow valuable information as to the plausible catalytic pathways under appropriate reaction conditions.

3.3 Experimental

3.3.1 Materials

The following chemicals were purchased from Alfa Aesar and used as received: Polyvinylpyrrolidone (PVP) MW 58,000 g/mol, sodium borohydride ($NaBH_4$, 98%), ascorbic acid (99%), tetrachloroauric acid ($HAuCl_4 \cdot 3H_2O$, 99.99%), potassium tetrachloropalladate (K_2PdCl_4, 99.99%), and 2-buten-1-ol (crotyl alcohol, 96%). 18MΩcm Milli-Q water (Millipore, Bedford, MA) was used throughout.

3.3.2 Synthesis of PVP Stabilized Pd, Au, and AuPd NPs in Water

PVP-stabilized monometallic Au and Pd nanoparticles, as well as sequentially reduced bimetallic AuPd nanoparticles were synthesized by previously reported procedures.[23, 24, 50] Monometallic NPs were synthesized using sodium borohydride as a reducing agent, while the sequentially reduced NPs were synthesized by selectively reducing a Pd shell onto Au "core" NP seeds using ascorbic acid.

Synthesis of monometallic Au NPs (also used as "seed" particles in the synthesis of bimetallic NPs) was carried out by mixing 6.30 mL of 10mM $HAuCl_4 \cdot 3H_2O$ (6.30×10^{-5} mol)

with 25 mL of 0.88 mM PVP (2.2×10^{-5} mol) and allowing the mixture to stir at 800 rpm for 30 min at room temperature, under N_2. The mixture was then placed on ice and 6.30 mL of 100 mM $NaBH_4$ (6.30×10^{-4} mol) was added quickly to the solution, stirring at 1200 rpm. The reduced NPs were allowed to stir for 30 min on ice, then an additional 30 min at room temperature. The reaction was quenched by adding 6.30 mL of 100 mM HCl (6.30×10^{-4} mol), and stirring for 30 min. An additional 20 mL of 1.5 mM PVP (3.0×10^{-5} mol) was added to the NP solution in order to further stabilize the particles. The particles were then dialyzed overnight in 1 L of water (changed 4 times) using cellulose dialysis membrane with a molecular cut off of 124000 g/mol, under N2. The dialyzed NPs (*ca*. 1 mM in terms of metal concentration) were then concentrated under vacuum at 25°C to obtain a final Au concentration of 3.13 mM. Monometallic Pd NPs were synthesized in the same manner as the Au NPs, using K_2PdCl_4 instead of $HAuCl_4{\cdot}3H_20$. The Pd NPs were concentrated to 9.44 mM, rather than the 3.13 mM of the Au NPs.

Sequentially reduced NPs were synthesized by mixing 33.11 mL of previously prepared (as aforementioned) 1 mM PVP-stabilized Au NPs (3.13×10^{-5} mol Au) with 4.7 mL of 200 mM ascorbic acid (9.4×10^{-4} mol) and placing the mixture in an ice bath, under N_2. To this mixture, 4.7 mL of 20 mM K2PdCl4 was added and the solution was stirred at 1200 rpm for 1 hour. Ascorbic acid is used in this step for the controlled reduction of Pd(II) onto the Au NP surface. The sequentially reduced NPs were then dialyzed overnight in the same manner as the monometallic NPs. The bimetallic NPs were then concentrated under vacuum at 25°C to achieve final concentrations of 3.13 mM and 9.44 mM in terms of Au and Pd, respectively.

3.3.3 Characterization

TEM analyses of the NPs were conducted using a Philips 410 microscope operating at 100 kV. The samples were prepared by dropcasting a small amount of dilute, aqueous sample onto a plasmon cleaned carbon-coated copper TEM grid (Electron Microscopy Sciences, Hatfield, PA). Average particle diameters were determined by manually measuring 200 NPs from each sample using the ImageJ program.[51]

Pd K edge and Au-L_{III} edge X-ray absorption measurements were conducted on the insertion device beamline of the Materials Research Collaborative Access Team (MRCAT, 10-ID) at the Advanced Photon Source (APS) in Argonne, IL. Full EXAFS measurements were done before and after *in situ* measurements using an energy scan range for the Au-L_{III}-edge of 11,700 to 12,800 eV and an energy scan range for the Pd-K-edge of 24,050 to 25,400 eV while fast XANES measurements of the Pd edge up to k=8 were made every 0.6 seconds. The X-ray measurements were conducted in ion chambers filled with a helium and nitrogen mixture. Pd and Au foils were used for the respective edges as references. All XAFS measurements were conducted in fluorescence mode.

The Sector 9-BM beamline at the APS was used to collect XANES spectra at the Pd-L_{III} edge from 3,140 eV to 3,225 eV. The X-ray measurements were conducted in using helium as the inert atmosphere. *In situ* measurements were taken at this same range and scans were performed every 9.5 minutes. Photoreduction of Pd on the Pd-LIII edge was problematic for aqueous solutions of Pd(II) salts at high beam fluxes; care was taken to lower the beam flux by defocusing and/or filtering the beam with Kapton filters and stir the sample via magnetic stirring such that that photoreduction events were not occurring in the experiments. Such photoreduction

effects were not seen at the higher energy Pd K-edge, likely due to the much greater transparency of water at this energy.

The IFEFFIT software package was used for XAFS data processing and the spectra were analyzed using methods previously stated.[52-54] The background in each post-edge was fit to a cubic spline function while the pre-edge region was fit with a straight line. The EXAFS function, χ, was obtained by subtracting the post-edge background from the overall absorption and then normalizing with respect to the edge jump step. The EXAFS fitting was performed in R-space for the Au and Pd edges. A theoretical AuPd alloy model was constructed based on a AuPd lattice parameters and used for fitting.[55] fcc bulk lattice parameters (i.e., first shell coordination numbers of 12) were used to determine the amplitude reduction factor, S_0^2, for Au and Pd by analyzing Au and Pd reference foils.

3.3.4 General Procedure for *In situ* Reactions

In situ reactions were carried out at the aforementioned beamlines, each beamline employing a different type of liquid cell. The liquid cell used at the 10-ID beamline was fabricated out of polyether ether ketone (PEEK), with Kapton windows on the side of the cell.[46]. The liquid cells used for XANES analysis at the 9-BM beamline were SPEX CertiPrep Disposable XRF X-Cell sample cups with 4 μm Ultralene window film (purchased from Fisher Scientific, Ottawa, ON). Deionized water was used as the liquid medium throughout.

In situ reactions were performed by transferring a determined amount of Au "seed" NPs to the liquid cell then weighing a desired amount of K_2PdCl_4 ("Pd Salt"), suspending it in a minimal amount of water, and transferring to the Au seeds via pipette. To the Au NP / Pd Salt

solution, a determined amount of crotyl alcohol ("substrate") was added via syringe. The mixture was quickly shaken by hand and stirred open to air with a magnet stir bar during XAFS measurements. Au and Pd foils, as well as 10 mM solutions of $HAuCl_4 \cdot 3H_2O$ and K_2PdCl_4 were used as references. During experiments where oxygen was required, a 20% mix of O_2 in He was used.

3.4 Results and Discussion

3.4.1 Nanoparticles Synthesized for Quantitative Analysis of Crotyl Alcohol Oxidation Versus Those Used for XAFS Analysis

The preparation of monometallic and sequentially reduced NPs for liquid XAFS measurements is carried out in the same manner as those prepared for use in the quantitative analysis of the NP-catalyzed oxidation of crotyl alcohol as described previously.[23, 24] However, the concentration of metal needed for liquid XAFS measurements is approximately 20 times more concentrated than those used for catalytic studies of the pseudo-homogeneous oxidation of crotyl alcohol using PVP-stabilized AuPd NPs. During the synthesis of NP samples for XAFS analysis, the NPs are concentrated under vacuum using moderate temperatures. This concentration step inevitably led to some sintering and thus a larger polydispersity in particle sizes. TEM images for Au, Pd, and sequentially reduced AuPd NPs synthesized for liquid XAFS measurements are shown in Figure 3.1 and a summary of NP sizes before and after concentrating is given in Table 3.1.

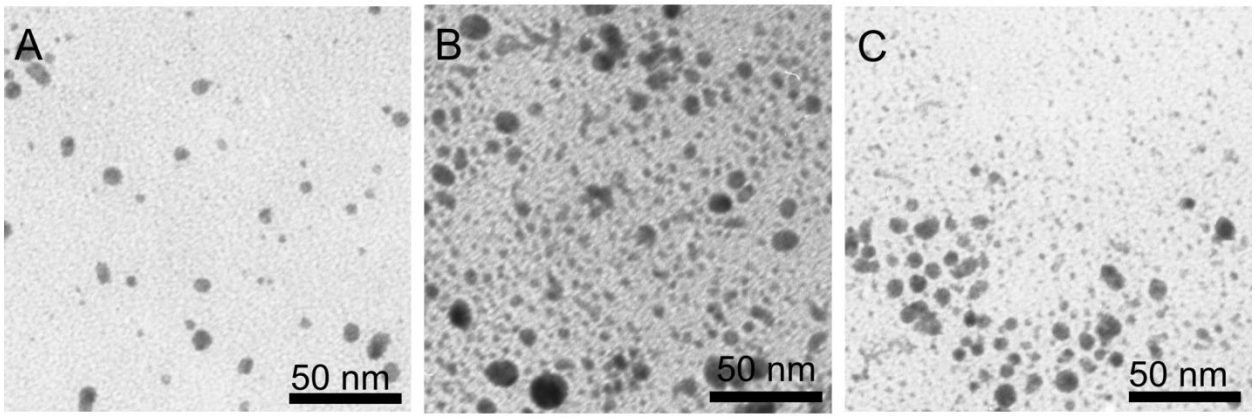

Figure 3.1. TEM images of concentrated PVP-stabilized (A) Au nanoparticles (B) Pd nanoparticles and (C) Sequentially reduced 1:3 Au core: Pd shell nanoparticles.

Table 3.1. Summary of Nanoparticle Sizes

Nanoparticle	Nanoparticle Diameter (nm)
Au	5.5 ± 2.5
Pd	5.8 ± 3.1
1:3 Seq. Grown AuPd	6.0 ± 3.1

The average particle sizes of the final particles are in the 5-6 nm range with moderate polydispersity, which is larger than 3-5 nm particles used in previous catalytic studies. Nevertheless, since in this study we are not performing a quantitative catalytic analysis for the oxidation of crotyl alcohol but rather analyzing the changes in the NP surfaces during the reaction, the larger NPs still allow us to gain valuable information about this system.

3.4.2 *In situ* XANES Analysis of Crotyl Alcohol Oxidation in Water

X-ray absorption near-edge spectroscopy (XANES) analysis was performed on the Pd-L_{III}-edge for a series of Au NPs / Pd salt (K_2PdCl_4) catalyzed oxidation reactions of crotyl alcohol in order to determine the oxidation state of Pd in the system. The oxidation state of Pd is related to the intensity of the white line absorption peak, as well as the energy at which the absorption peak arises. The absorption peak arises from the excitation of electrons from the 2p core into unfilled 4d states.[56, 57] As empty 4d states of the Pd in the system become occupied, or the Pd becomes reduced, a decrease in white line intensity will occur.[58] In addition, a shift in the absorption maximum is expected with Pd reduction. For *in situ* XANES analysis, linear combination analysis fitting was done using two standards which represented fully reduced and fully oxidized Pd. The standard used to determine Pd(II) was a 10 mM solution of the K_2PdCl_4 in water, while that for Pd(0) was a fully reduced sample of sequentially reduced 1:3 AuPd NPs. The standard spectras were used to calculate the extent of the reduction of Pd(II) in the system during *in situ* reactions.

In order to determine if the reduction of Pd onto the Au NP surface occurs spontaneously, or if a reductant is required, an initial XANES measurement of Au NPs in the presence of Pd salt was taken. The spectrum obtained for this mixture (not shown) produced an edge-jump with a large white line intensity which was identical in intensity to the pure K_2PdCl_4 salt solution, indicating that the Pd was still in the Pd(II) oxidation state and did not spontaneously reduce to Pd(0) in the presence of Au NPs. To this solution, crotyl alcohol substrate was added into the liquid cell to give a substrate: metal molar ratio of 250:1. Figure 3.2 shows the comparison of the Pd-L_{III}-edge XANES of Au NPs and Pd(II) salt in solution before the addition of crotyl alcohol (black).

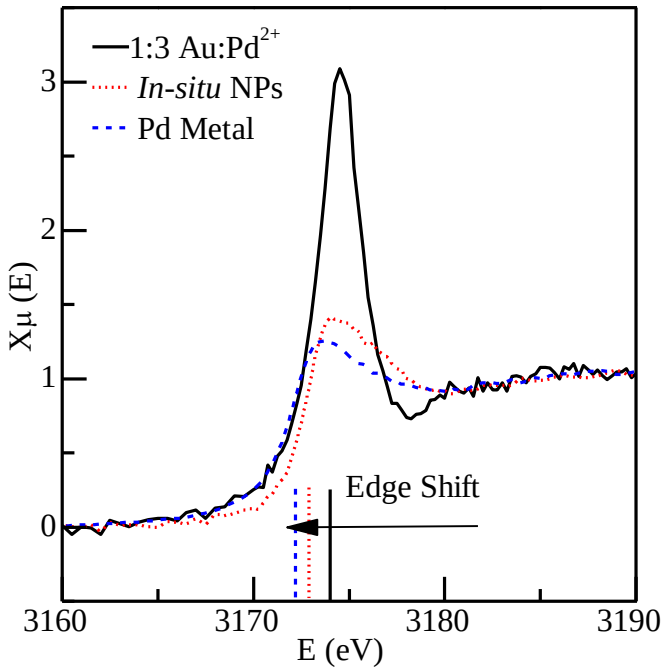

Figure 3.2. XANES Pd-L_{III} spectra comparing 1:3 Au:Pd^{2+} in water, NPs formed *in situ* after the addition of crotyl alcohol to 1:3 Au:Pd^{2+} in water in a 250:1 substrate:metal ratio, and pure Pd metal. The shifts in respective absorption edges are shown at the bottom of the spectra.

The large excess of substrate caused the Pd(II) to reduce quickly, therefore the reaction was complete before the first XANES scan was completed (subsequent scans were identical to the first). The decrease in the amplitude of the edge jump after the addition of crotyl alcohol to the Au NP / Pd(II) salt mixture can be clearly seen in Figure 3.2. The absorption edge of each spectrum was also determined by taking the derivative of the spectrum. The absorption edges of each spectra are depicted at the bottom of Figure 3.2, showing that the edge shifts to lower energies from the Pd(II) starting material, to the final reduced sample formed *in situ* and to the metal foil. The edge shift to lower energies is also an indication of Pd reduction. As the empty d states are filled, the energy gap between the 2p and empty 4d states becomes smaller, therefore the energy required to excite a core electron from the 2p state to an empty d state also becomes smaller.[59] The shift towards lower excitation energy between the before and after addition of

crotyl alcohol to the Au NPs /Pd salt solution signifies that the Pd is reduced by the crotyl alcohol. However, it can be seen that the absorption energy of the AuPd NPs formed after the addition of crotyl alcohol is at a slightly higher energy than the metallic Pd foil. The difference in absorption energies may be due to an electronic effect occurring between the Au NPs and Pd Shell, in which electron density is drawn away from the Pd by Au, causing the absorption edge to occur at a slightly higher energy. Alternatively, it is also possible this shift is due to Cl- absorption on the Pd surface. Thus, the Pd L_{III} edge data is consistent with the reduction of Pd on the Au NP surfaces upon exposure to crotyl alcohol, but do not rule out the possibility of secondary Pd nucleation. This result is consistent with the observations of others who have shown stoichiometric reactions of Pd(II) salts with allylic alcohols, typically giving the aldehyde and a Pd metal precipitate after the reaction.[61] Later EXAFS studies are more definitive with regards to bimetallic AuPd NP formation.

3.4.3 *In situ* XAS Analysis of Crotyl Alcohol Oxidation in Water

The reduction of Pd(II) onto Au NPs by the addition of crotyl alcohol was also studied *in situ* by Pd-K-edge XANES, an excitation of a core 1s electron to an unoccupied 4p state. Quick XAS scans of each sample were taken from 150 eV before the absorption edge to 445 eV (k=8) after every 36 seconds. Time-resolved normalized XANES data in E space for the *in situ* reaction of 1:1 Au NPs:Pd(II) and 1:1 Pd: substrate ratios is shown in Figure 3.3.

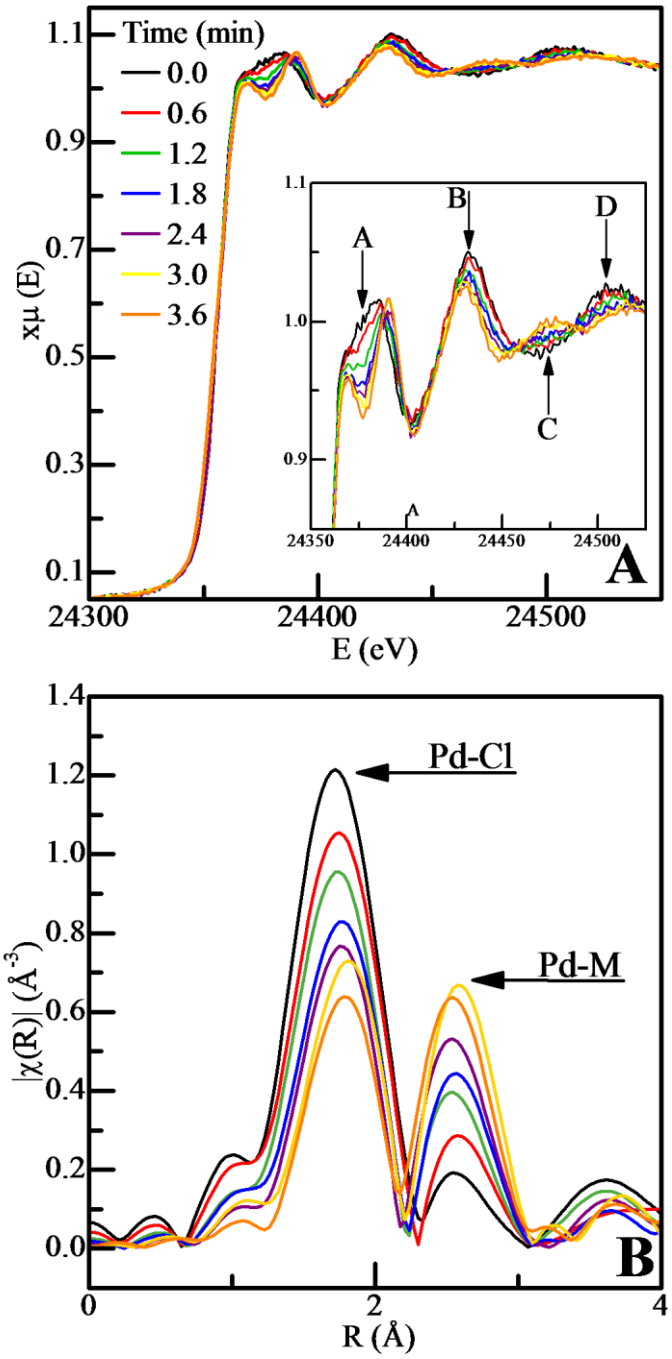

Figure 3.3. Time resolved Pd K-edge XAFS in (A) E-space with inset of enlarged post-edge image and (B) R-space for the nanoparticles formed *in situ* during the oxidation of crotyl alcohol in water. Au:Pd = 1:1, Pd: Substrate = 1:1/2

Time-resolved spectra in E space (Figure 3B) clearly shows spectral changes with reaction progress. As the reaction proceeds the first feature after the absorbance edge (labeled A) slowly transforms into two narrow peaks. Comparison to references confirms that this spectral change corresponds to the Pd(II) in solution being reduced to Pd(0) upon the addition of crotyl alcohol. Small changes in further XANES features (B-D) can also be seen as the reaction progresses. The same data set is also shown in R-space in Figure 3B. Two significant features in this spectrum are seen which correlates to the Pd-Cl bond and the Pd-M bond, a mixture of Pd-Pd and Pd-Au bonding. As the reaction progresses the Pd-Cl peak decreases in amplitude while the Pd-M feature increases. Because the Pd-Cl peak decreases as the Pd-M increases it can be said that Pd(II) is indeed being reduced. Linear combination analysis was also performed on the E space data for this reaction from 30 eV before to 30 eV after the edge. Reference spectra used were K_2PdCl_4 mixed with Au NPs and a fully reduced, pre-synthesized sample of AuPd NPs. The Pd-K-edge XANES were fit with a linear combination of that for K2PdCl4 and fully reduced AuPd NPs and is shown in Figure 3.4. The reduction of Pd(II) occurs quickly for ca. 4 minutes then begins to plateau, and after 8 minutes the Pd is fully reduced. Kinetic treatment of the data indicates that the reduction of Pd(II) onto the Au surface is a first order reaction with a rate constant of 0.0468 min^{-1}.

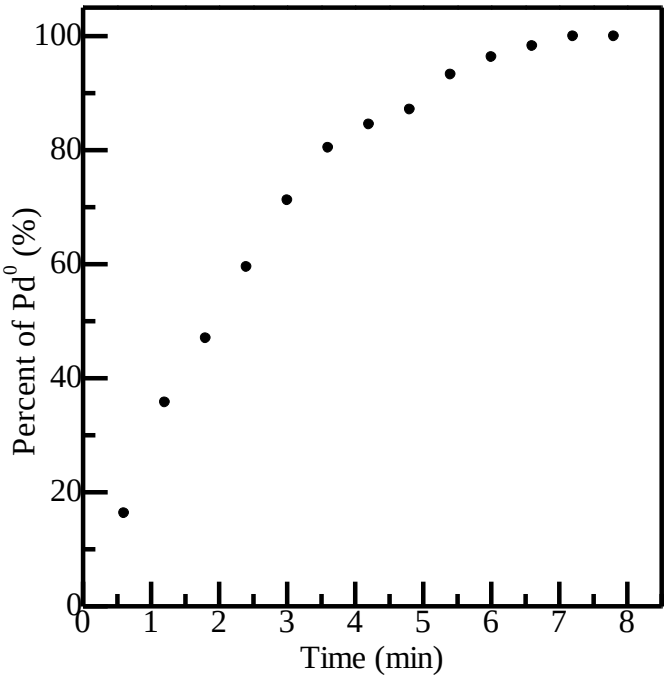

Figure 3.4. Linear combination of the Pd-K-Edge EXAFS spectra for the nanoparticles formed *in situ* during the oxidation of crotyl alcohol. Au:Pd = 1:1, Pd: Substrate = 1:1/2

3.4.4 Oxidation of Nanoparticles

According to the redox mechanism for the oxidation of crotyl alcohol, the presence of molecular oxygen is required in order to oxidize Pd(0) from the surface of the nanoparticle, forming a catalytically active Pd(II) species either in solution or on the surface of the nanoparticle. If the reaction proceeds by this mechanism, a sample of AuPd NPs which has been exposed to oxygen for long time periods should show signs of oxidation. A sample of the nanoparticles formed *in situ* during the reaction of 1:1 Au NPs: Pd(II), and a 1:1 substrate to Pd ratio was treated with a mixture of 20% oxygen in helium for variable amounts of time. The spectra of the Pd-L_{III}-edge in E space for each scan of the nanoparticles after oxygen treatment are shown in Figure 3.5.

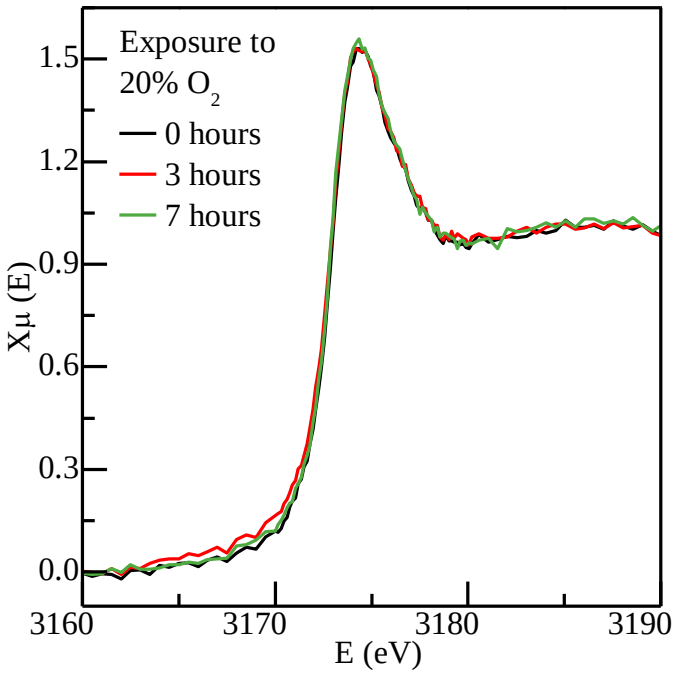

Figure 3.5. Pd-L_{III}-Edge in E-space for nanoparticles formed *in situ* which have subsequently been exposed to a 20% mixture of O_2 in He for varying amounts of time.

XANES analysis is more sensitive to changes in oxidation state than EXAFS, therefore we compared these spectra in order to determine if the NPs are easily oxidized. Only very minute changes can be seen in the spectra even after exposure to oxygen for 7 h. EXAFS fitting analysis was also performed on similarly collected Pd K-edge data, and a summary of the fitting results is shown in Table 3.2.

Table 3.2. EXAFS fitting of nanoparticles exposed to oxygen for varying amounts of time.

Time Exposed to 20% O_2 (min)	Shell	N	R(Å)	ΔEo (eV)	R-factor
0	Pd-Pd	6.8(0.2)	2.748(0.003)	-5.2(0.3)	0.003
	Pd-Au	2.8(0.3)	2.77(0.02)		
180	Pd-Pd	6.3(0.2)	2.745(0.004)	-4.9(0.4)	0.008
	Pd-Au	3.3(0.4)	2.76(0.02)		

Values of σ^2 for the Pd-Pd and Pd-Au shells were fixed at 0.0079 $Å^2$ and 0.012 $Å^2$, respectively. A S_o^2 value of 0.93, determined from Pd foil was used for Pd fitting

It can be seen that there are no significant changes in coordination number or bond distances, even after 3 hours of oxygen treatment. Thus, both sets of data show that no significant Pd oxidation is occurring during treatment with molecular oxygen, thus it is unlikely the alcohol oxidation reaction proceeds via a redox mechanism at room temperature. Others have shown, upon exposure to allylic alcohols, Pd(II) does reduce into Pd black.[60, 61] Small monometallic Pd NPs are very susceptible to oxidation;[62] thus if pure Pd NPs were formed by secondary nucleation *in situ*, we would expect large changes in the Pd-L_{III}-edge from Pd(0) oxidation to Pd(II) upon exposure to oxygen. Since there is no significant change in the Pd-L_{III} spectra, or the Pd-K EXAFS fitting, the formation of small Pd NPs can likely be ruled out.

3.4.5 EXAFS Fitting and Structural Analysis of AuPd Nanoparticles

EXAFS structural analysis was performed on solution-phase NPs formed at the end of three different *in situ* liquid reactions at the Pd K edge. The Pd-K-edge EXAFS of solutions of pre-synthesized 1:3 sequentially reduced AuPd NPs and monometallic Pd NPs were also analyzed. Models for the 1:1 and 1:3 Au:Pd NPs were prepared based on weighted values of pure Au and Pd fcc structures and the EXAFS data was fit to the model in R-space. Quality fits for all the samples were obtained, with the fits for the AuPd NPs formed *in situ* shown in Figure 3.6.

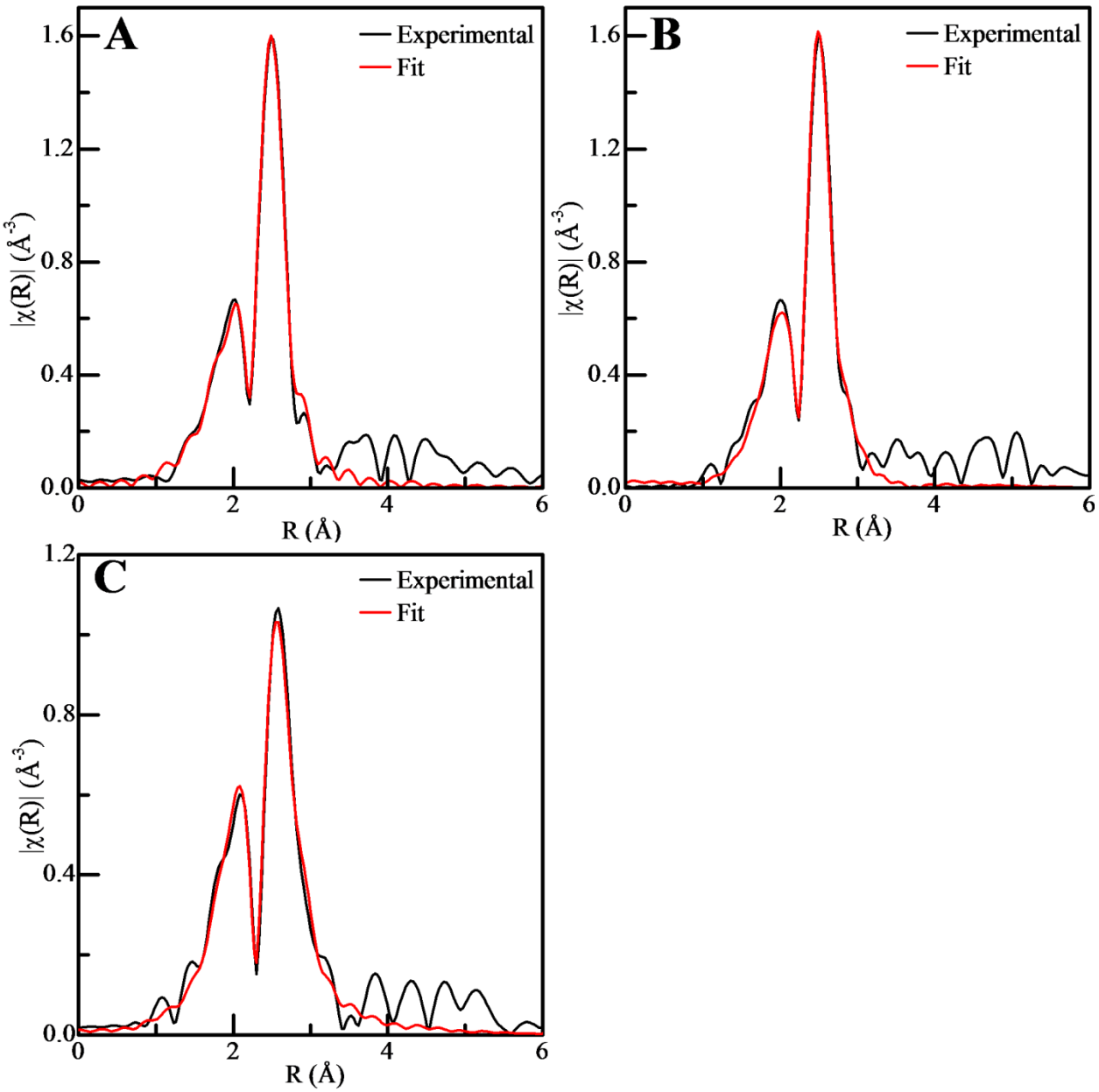

Figure 3.6. EXAFS spectra in R space and their respective fits to determine characteristics of the nanoparticles formed *in situ* for (A) 1:3 AuPd, 250:1 substrate:metal ratio (B) 1:3 AuPd, 1:1 Pd: substrate, and (C) 1:1 AuPd, 1:1/2 Pd: substrate.

A summary of the data determined by EXAFS fitting is given in Table 3.3. Due to time constraints it was not possible to collect Au L_{III} edge data after each *in situ* measurement, thus only Pd edge data was fit for *in situ* samples. The monometallic Pd and Au "core" NPs synthesized have a 1st shell coordination numbers of 7.8 and 9.2, respectively.

Table 3.3. Summary of EXAFS Fits.

Nanoparticle	Shell	N	R(Å)	ΔEo (eV)	R-factor
Au:Pd = 1:3 Sub:Cat = 250:1	Pd-Pd	7.0(0.2)	2.741(0.003)	-5.2(0.3)	0.003
	Pd-Au	2.7(0.3)	2.75(0.02)		
Au:Pd = 1:3 Pd : Sub = 1:1	Pd-Pd	6.8(0.2)	2.748(0.003)	-3.9(0.3)	0.003
	Pd-Au	2.8(0.3)	2.77(0.02)		
Au:Pd = 1:1 Pd : Sub = 1 :1/2	Pd-Pd	4.9(0.2)	2.721(0.004)	-3.1(0.3)	0.006
	Pd-Au	4.8(0.4)	2.73(0.01)		
1:3 AuPd Core-shell	Pd-Pd	3.9(0.3)	2.74(0.01)	-5.5(0.8)	0.022
	Pd-Au	4.5(0.7)	2.75(0.02)		
	Au-Au	8.2(0.6)	2.84(0.01)	6.4(0.6)	
	Au-Pd	2.4(0.3)	2.79(0.01)		
Pd NPs	Pd-Pd	7.8(0.3)	2.740(0.005)	-4.8(0.4)	0.017
Au NPs	Au-Au	9.2(1.6)	2.83(0.01)	4.6(1.3)	0.029

The σ^2 ($Å^2$) values for the Pd-Pd, Pd-Au, Au-Au, and Au-Pd shells were fixed at 0.0079, 0.012, 0.012, and 0.009 respectively. S_o^2 values of 0.93 and 0.91, determined from Pd and Au foils, was used for Pd and Au fitting, respectively.

For all three *in situ* reactions, it is also apparent from EXAFS analyses that the Pd(II) reduction is complete as no significant Pd-Cl or Pd-O contributions were seen in the final spectra.

In the bulk material, a coordination number of 12 would be expected for a material composed of Pd and Au metals. Because NPs exhibit such a high degree of surface area, many surface atoms are left without neighbouring atoms. Therefore, a coordination number less than 12 is expected for the NPs analyzed. For each spectrum, the Pd-Pd and Pd-Au coordination numbers were obtained ((N_{Pd-Pd}) and (N_{Pd-Au}), respectively). For the two *in situ* reactions performed at a Au NP:Pd(II) ratio of 1:3 there is no significant difference in coordination numbers. Finally, the NPs formed with an Au:Pd ratio of 1:1 have lower Pd-Pd and higher Pd-Au coordination numbers than the 1:3 AuPd NPs. With less Pd in the system it would be expected that a thinner shell of Pd can be reduced onto the Au NP surface. The smaller Pd-Pd coordination number of the 1:1 NPs suggests that there are more surface Pd atoms in this system than the 1:3 AuPd system, but the larger Pd-Au coordination number suggests that more Au-Pd mixing is also seen in this sample. The Pd-Pd 1st shell coordination numbers in all the samples are significantly below that of pure Pd NPs (particularly for the 1:1 Au:Pd ratio; while it is possible that there may be some secondary nucleation of Pd NPs in the system, it is apparent from EXAFS data that most of the Pd is deposited on existing Au nanoparticles in the solution.

Finally, a comparison was made between the *in situ* formed AuPd nanoparticles via crotyl alcohol reduction and sequentially formed 1:3 Au:Pd NPs synthesized *ex-situ* using an ascorbic acid secondary reductant. A lower N_{total} value for Pd of 9.4 was seen for the sequentially formed particles via ascorbic acid reduction compared to the AuPd particles made *in situ* via crotyl alcohol reduction. This indicates that NPs made by the controlled reduction of Pd onto Au seeds by ascorbic acid produced smaller NPs. However, the higher degree of Pd-Au bonding in these same particles suggests that these NPs have significant AuPd mixing, which potentially is an aging effect (the ascorbic acid nanoparticles were made approximately one week before analysis).

We are planning to more thoroughly examine the effect of aging on nanoparticle structure in future studies.

3.5 Conclusions

We have shown that quick scan, *in situ* X-ray absorption spectroscopic experiments can yield valuable information on nanoparticle-catalyzed reactions in solution. The AuPd nanoparticle-catalyzed oxidation of crotyl alcohol in water was studied by *in situ* XAS analysis. It was found that, when using Au(0) nanoparticles in the presence of Pd(II) as the reaction catalyst, the Pd(II) becomes reduced to Pd(0) upon exposure to the crotyl alcohol. In addition, the products from the this reaction (*in situ* formed AuPd NPs) were treated with O_2 for up to three hours, and no significant changes in the spectra or coordination numbers were seen. This suggests that the Pd on the surface of the Au nanoparticles is quite stable to oxidation under these conditions.

3.6 Acknowledgements

The authors would like to thank NSERC and the University of Saskatchewan for funding. The authors would also like to thank Drs. Tianpin Wu, Jeremy Kropf, and Trudy Bolin at the Advanced Photon Source (APS) for the assistance with EXAFS and XANES measurements. Use of the Advanced Photon Source is also supported by the U. S. Department of Energy, Office of Science, Office of Basic Energy Sciences, under Contract DE-AC02-06CH11357. PNC/XOR facilities at the Advanced Photon Source, and research at these facilities, are supported by the US

Department of Energy - Basic Energy Sciences, a Major Resources Support grant from NSERC, the University of Washington, Simon Fraser University, and the Advanced Photon Source. MRCAT operations are supported by the Department of Energy and the MRCAT member institutions. Funding for JTM is based upon work supported as part of the Institute for Atom-efficient Chemical Transformations (IACT), an Energy Frontier Research Center funded by the U.S. Department of Energy, Office of Science, Office of Basic Energy Sciences.

3.7 References

1 M. Haruta, Y. Yamada, T. Kobayashi, S. Iijima, *J. Catal.* **1989**, *115*, 301-309.

2 M. Haruta, *Catal. Today* **1997**, *36*, 153-166.

3 H. Tsunoyama, H. Sakurai, Y. Negishi, T. Tsukuda, *J. Am. Chem. Soc.* **2005**, *127*, 9374-9375.

4 N. Dimitratos, J. A. Lopez-Sanches, D. Lennon, F. Porta, L. Prati, A. Villa, *Catal. Lett.* **2006**, *108*, 147-153.

5 S. Kanaoka, N. Yagi, Y. Fukuyama, S. Aoshima, H. Tsunoyama, T. Tsukuda, H. Sakurai, *J. Am. Chem. Soc.* **2007**, *129*, 12060-12061.

6 N. Dimitratos, J. A. Lopez-Sanches, J. M. Anthonykutty, G. Brett, A. F. Carley, R. C. Tiruvalam, A. A. Herzing, C. J. Kiely, D. W. Knight, G. J. Hutchings, *Phys. Chem. Chem. Phys.* **2009**, 4952-4961.

7 D. I. Enache, D. W. Knight, G. J. Hutchings, *Catal. Lett.* **2005**, *103*.

8 A. Abad, C. Almela, A. Corma, H. Garcia, *Chem. Commun.* **2006**, 3178-3180.

9 P. Miedziak, M. Sankar, N. Dimitratos, J. A. Lopez-Sanches, A. F. Carley, D. W. Knight, S. H. Taylor, C. J. Kiely, G. J. Hutchings, *Catal. Today* **2011**, *164*, 315-319.

10 C. Evangelisi, E. Schiavi, L. A. Aronica, A. M. Caporusso, G. Vitulli, L. Bertinetti, G. Martra, A. Balerna, S. Mobilio, *J. Catal.* **2012**, *286*, 224-236.

11 M. P. Mallin, C. J. Murphy, *Nano Lett.* **2002**, *2*, 1235-1237.

12 M. Kim, H. Na, K. C. Lee, E. A. Yoo, M. Lee, *J. Mater. Chem.* **2003**, *13*, 1789-1792.

13 V. V. Agrawal, P. Mahalakshmi, G. U. Kulkarni, C. N. R. Rao, *Langmuir* **2005**, *22*, 1846-1851

14 W. Lee, M. G. Kim, J. Choi, J. Park, S. J. Ko, S. J. Oh, J. Cheon, *J. Am. Chem. Soc.* **2005**, *127*, 16090-16097.

15 R. Rapallo, G. Rossi, R. Ferrando, A. Fortunelli, B. C. Curley, L. D. Lloyd, G. M. Tarbuck, R. L. Johnston, *J. Chem. Phys.* **2005**, *122*, 194308.

16 N. Dimitratos, A. Villa, D. Wang, F. Porta, D. Su, L. Prati, *J. Catal.* **2006**, *244*, 113-121.

17 E. I. Enache, J. K. Edwards, P. Landon, B. Solsona-Espriu, A. F. Carley, A. A. Herzing, M. Watanabe, C. J. Kiely, D. W. Knight, G. J. Hutchings, *Science* **2006**, *311*, 362-365.

18 N. K. Chaki, H. Tsunoyama, Y. Negishi, H. Sakurai, T. Tsukuda, *J. Phys. Chem. C.* **2007**, *111*, 4885-4888.

19 X. Liu, A. Wang, X. Wang, C. Mou, T. Zhang, *Chem. Commun.* **2008**, 3187-3189.

20 C. L. Bracey, P. R. Ellis, G. J. Hutchings, *Chem. Soc. Rev.* **2009**, *38*, 2231-2243.

21 M. Tsuji, M. Matsunaga, T. Ishizaki, T. Nonaka, *CrystEngComm* **2012**, *14*, 3623-3632.

22 S. Caron, R. W. Dugger, S. G. Ruggeri, J. A. Ragan, D. H. B. Ripin, *Chem. Rev.* **2006**, 2943-2989.

23 W. Hou, N. A. Dehm, R. W. J. Scott, *J. Catal.* **2008**, *253*, 22-27.

24 T. Balcha, J. R. Strobl, C. Fowler, P. Dash, R. W. J. Scott, *ACS Catal.* **2011**, *1*, 425-436.

25 S. Carrettin, P. McMorn, P. Johnston, K. Griffin, G. J. Hutchings, *Chem. Commun.* **2002**, 696-697.

26 Y. Kon, Y. Usui, K. Sato, *Chem. Commun.* **2007**, 4399-4400.

27 A. F. Lee, S. F. J. Hackett, G. J. Hutchings, S. Lizzit, J. Naughton, K. Wilson, *Catal. Today* **2009**, *145*, 251-257.

28 A. Villa, N. Janjic, P. Spontoni, D. Wang, D. S. Su, L. Prati, *Appl. Catal., A* **2009**, *364*, 221-228

29 A. J. Frank, J. Rawski, K. E. Maly, V. Kitaev, *Green Chem.* **2010**, *12*, 1615-1622.

30 A. F. Lee, C. V. Ellis, K. Wilson, N. S. Hondow, *Catal. Today* **2010**, *157*, 243-249

31 J. Naughton, A. F. Lee, S. Thompson, C. P. Vinod, K. Wilson, *Phys. Chem. Chem. Phys.* **2010**, *12*, 2670-2678.

32 A. Villa, D. Wang, P. Spontoni, R. Arrigo, D. Su, L. Prati, *Catal. Today* **2010**, *157*, 89-93.

33 D. Wang, A. Villa, P. Spontoni, D. Su, L. Prati, *Chem. Euro. J.* **2010**, *16*, 10007-10013.

34 A. F. Lee, C. V. Ellis, J. N. Naughton, M. A. Newton, C. M. A. Parlett, K. Wilson, *J. Am. Chem. Soc.* **2011**, *133*, 5724-5727

35 L. Prati, A. Villa, C. E. Chan-Thaw, R. Arrigo, D. Wang, D. S. Su, *Faraday Discuss.* **2011**, *152*, 353-365.

36 M. Sankar, E. Nowicka, R. Tiruvalam, Q. He, S. H. Taylor, C. J. Kiely, D. Bethell, D. W. Knight, G. J. Hutchings, *Chem. Euro. J.* **2011**, *17*, 6524-6532.

37 M. Alhumaimess, Z. Lin, W. Weng, N. Dimitratos, N. F. Dummer, S. H. Taylor, J. K. Bartley, C. J. Kiely, G. J. Hutchings, *ChemSusChem* **2012**, *5*, 125-131.

38 N. Dimitratos, J. A. Lopez-Sanchez, G. J. Hutchings, *Chem. Sci.* **2012**, *3*, 20-44.

39 C. Keresszegi, D. Ferri, T. Mallat, A. Baiker, *J. Phys. Chem. B* **2005**, *109*, 958-967.

40 G. Meitzner, G. H. Via, F. W. Lytle, J. H. Sinfelt, *J. Chem. Phys.* **1985**, *83*, 4793-4799.

41 N. Toshima, M. Harada, T. Yonezawa, K. Kushihashi, K. Asakura, *J. Phys. Chem.* **1991**, *95*, 7448-7453.

42 B. Hwang, L. S. Sarma, J. Chen, C. Chen, S. Shih, G. Wang, D. Liu, J. Lee, M. Tang, *J. Am. Chem. Soc.* **2005**, *127*, 11140-11145.

43 Y. Mikhlin, M. Likhatski, Y. Tomashevich, A. Romanchenko, S. Erenburg, S. Trubina, *J. Electron. Spectrosc. Relat. Phenom.* **2010**, *177*, 24-29.

44 F. Liu, P. Zhang, *Appl. Phys. Lett.* **2010**, *96*,043105.

45 A. F. Lee, C. V. Ellis, J. N. Naughton, M. A. Newton, C. M. A. Parlett, K. Wilson, *J. Am. Chem. Soc.* **2011**, *133*, 5724-5727.

46 R. C. Nelson, J. T. Miller, *Catal. Sci. Technol.* **2011**, *2*, 461-470.

47 H. Imai, K. Izumi, M. Matsumoto, Y. Kubo, K. Kato, Y. Imai, *J. Am. Chem. Soc.* **2009**, *131*, 6293-6300.

48 H. Imai, M. Matsumoto, T. Miyazaki, K. Kato, H. Tanida, T. Uruga, *Chem. Commun.* **2011**, *47*, 3538-3540.

49 N. Ishiguro, T. Saida, T. Uruga, S.-i. Nagamatsu, O. Sekizawa, K. Nitta, T. Yamamoto, S.-i. Ohkoshi, Y. Iwasawa, T. Yokoyama, M. Tada, *ACS Catal.* **2012**, *2*, 1319-1330.

50 P. Dash, T. Bond, C. Fowler, W. Hou, N. Coombs, R. W. J. Scott, *J. Phys. Chem. C.* **2009**, *113*, 12719-12730.

51 M. D. Abramoff, P. J. Magalhaes, S. J. Ram, *Biophotonics Int.* **2004**, *11*, 36-42.

52 M. Newville, *J. Synchrotron Radiat.* **2001**, *8*, 322-324.

53 B. Ravel, *J. Synchrotron Radiat.* **2001**, *8*, 314-316.

54 B. Ravel, M. Newville, *J. Synchrotron Radiat.* **2005**, *12*, 537-541.

55 A. Maeland, T. B. Flanagan, *Can. J. Phys.* **1964**, *42*, 2364-2366.

56 G. Meitzner, J. H. Sinfelt, *Catal. Lett.* **1995**, *30*, 1-10.

57 D. C. Huang, K. H. Chang, W. F. Pong, P. K. Tseng, K. J. Hung, W. F. Huang, *Catal. Lett.* **1998**, *53*, 155-159.

58 T. K. Sham, S. J. Naftel, I. Coulthard, *J. Appl. Phys.* **1996**, *79*, 7134-7138.

59 D. H. Pearson, C. C. Ahn, B. Fultz, *Physical Review B* **1993**, *47*, 8471-8478.

60 J. Tsuji, H. Nagashima, K. Hori, *Chem. Lett.* **1980**, 257-260.

61 K. Zaw, M. Lautens, P. M. Henry, *Organometallics* **1983**, *2*, 197-199.

62 R. W. J. Scott, H. Ye, R. R. Henriquez, R. M. Crooks, *Chem. Mater.* **2003**, *15*, 3873-3878.

Chapter 4

Summary, Conclusions and Future Work

4.1. Summary, Conclusions, and Future Work for the Aerobic Oxidation of α,β-Unsaturated Alcohols

4.1.1. Summary and Conclusions

In this work a series of catalyst systems consisting of Au and Pd were used in the oxidation of a series of α,β-unsaturated alcohols. This work followed up with earlier work with specific substrates, by examining a larger scope of substrates. In addition, parallel reactions were performed and compared between water and ionic liquid solvents. For aqueous reactions it was determined that the catalyst system was influential on the conversion and selectivity of the reaction. Monometallic Au and Pd nanoparticles showed little to no selectivity for all substrates. The only significant conversion provided by a monometallic catalyst was 12% conversion of allyl alcohol by Pd nanoparticles. Active catalysts for these reactions were the bimetallic pairings of Au and Pd. AuPd nanoparticles and Au nanoparticles paired with Pd(II) salt were active catalysts for all of the substrates with selectivity towards the aldehyde product for benzyl alcohol, cinnamyl alcohol, and crotyl alcohol. The catalysts were not as efficient at 60°C compared to previous studies performed at room temperature. Ostwald ripening of the nanoparticles was determined to be a factor in nanoparticle deactivation. This was determined by studying the particles via TEM imaging before and after the reactions. The nanoparticles were also studied by EXAFS analysis. Due to poor-quality data, definitive conclusions about the morphologies could not be drawn, however, EXAFS analysis did conclusively demonstrate all the metal was in the

zerovalent state. It is likely that the nanoparticle structure for both the AuPd nanoparticles and the AuPd particles formed from Au and Pd(II) were of the random bimetallic alloy morphology. Identical reactions were performed in ionic liquids (ILs) and the results were compared between the water and IL system. Monometallic Pd NPs showed significantly higher activities in the ILs than in water. These catalysts likely have higher activities in ILs due to the ease of oxidation of Pd in the high chloride environment. Therefore, Au promoters have little influence on the NPs in ILs, making the monometallic nanoparticles much more active.

The large scope of substrates used for these reactions have presented some interesting results. Although the major product for the reactions was commonly the corresponding aldehyde, there were also significant conversions towards the hydrogenation and isomerization/ tautomerization products for allyl alcohol, crotyl alcohol, and 1-hexen-3-ol. These products may be due to partial atomic hydrogen speciation on the nanoparticle surface during the catalytic reaction, but further analysis on these side reactions needs to be performed.

4.1.2. Future Work

4.1.2.1. Prevention of Ostwald Ripening

The high surface area of nanoparticles is a major contributing factor to their efficiency as catalysts. The growth of nanoparticles during a reaction will result in a decrease of surface area, which can lead to the deactivation of NP catalysts. Ostwald ripening is a common cause of nanoparticle growth in which atoms from a NP surface are oxidized from the surface and redeposited onto another NP, resulting in the growth of NPs in solution.[1-5] In order to maintain the efficiency of the nanoparticle catalysts one must find a way to prevent Ostwald ripening from

occurring. One solution for preventing Ostwald ripening or nanoparticle sintering/aggregation is to isolate the nanoparticles from one another by inorganic nanocapsules[6]. A common and effective material for nanocapsules is silica. Surrounding nanoparticles with silica is effective in keeping the particles from interacting with one another, while allowing the reaction to occur[6]. This method of stabilization may be beneficial for AuPd nanoparticles used at high temperatures.

4.1.2.2. Looking into the Mechanism of Isomerization and Tautomerization Products

The formation of isomerization and tautomerization products during the oxidation of α,β-unsaturated alcohols is an interesting result. The mechanism by which these products occur is unclear, but other research groups have seen the formation of these products as well[7]. Future work on the determination of the isomerization and tautomerization product mechanism should be pursued. One method to analyze the mechanism by which these products occur could be *in situ* XAFS, via monitoring the hydrogen saturation on the surface material of the nanoparticles. If hydrogen is present on the surface of the nanoparticles, as proposed by Bergens *et al.*, a shift in absorption energy will occur. One could also study hydrogenation reactions of α,β-unsaturated alcohols, using molecular H_2 as the reducing agent. If the isomerization and tautomerization products are the predominant species, it is highly likely that the surface of the nanoparticles is easily saturated with hydrogen, making this mechanism plausible.

4.1.2.3. AuPd Nanoparticle Catalysts for Diol and Glycerol Oxidation

The information gathered from the oxidation of α,β-unsaturated alcohols may be valuable in determining which catalyst systems are useful for the selective oxidation of certain alcohols, *ie* primary, secondary, tertiary. Allyl, benzyl, cinnamyl, and crotyl alcohols are all primary alcohols, while 1-hexen-3-ol is a secondary alcohol. From the oxidation study it was seen that AuPd catalyst systems have the highest conversion for alcohols that contain aromatic rings in their aldehyde product. Allyl and crotyl alcohols showed lower conversions towards the aldehyde product than the benzyl and cinnamyl alcohols. The oxidation of 1-hexen-3-ol, a secondary alcohol, showed high conversions to the ketone using K_2PdCl_4, while the other catalysts systems showed low conversions to the ketone. Therefore, the resulting product of the oxidation reaction is dependent on the type of alcohol and the catalyst system used. If these features of the oxidation reactions can be methodically studied, one could develop a reaction which selectively oxidizes a certain alcohol into a desired product. This could be applied to alcohols which contain multiple –OH bonds. One important reaction would be the oxidation of glycerol. Glycerol contains three –OH groups, two primary alcohols and one secondary alcohol, as seen in Figure 4.1.

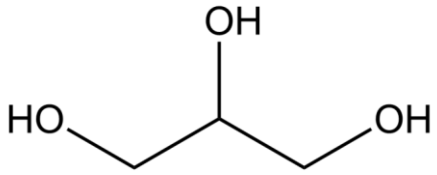

Figure 4.1. Molecule of Glycerol.

Glycerol can be oxidized into many different products depending on which alcohol or alcohols are oxidized. Products of glycerol oxidation include dihydroxyacetone, hydroxypyruvic acid, glycolic acid, glyceraldehyde, and glyceric acid.[8] The formation of these products from glycerol is important because glycerol is a byproduct of biofuel formation, and with the increase in biofuel production, a surplus of glycerol may occur.[8] An efficient means to deal with the surplus glycerol must be determined. If one can synthesize a catalyst which selectively oxidizes one or multiple –OH groups of glycerol into a desired material, the amount of excess or waste glycerol will be less substantial. Many groups are currently studying the oxidation of glycerol.[8-17] However, only a few catalysts with high conversion and selectivity towards one product have been identified. Catalyst materials which have shown promise are Au, Pd, and Pt.[16] Au combined with either Pt or Pd has shown moderate conversions (20 to 40%) with high selectivity towards glyceric acid formation.[15, 16] The formation of dihydroxyacetone from glycerol has also been achieved in moderate yields with high selectivity using Pt-Bi complexes.[9, 11, 13] It also been shown that tuning the ratio of Pt to Bi changes the rate of the reaction as well as the selectivity towards dihydroxyacetone.[9, 11] The above samples show promising results for the formation of useful products from the selective oxidation of glycerol. Therefore, it is imperative that catalysis research continues in this direction.

4.2. Summary, Conclusions, and Future Work for *In situ* XAFS Analysis of AuPd Nanoparticle Systems

4.2.1. Summary and Conclusions

This focus of this work was to study the catalyst system of Au nanoparticles and Pd(II) salts on the oxidation of crotyl alcohol. We successfully studied this system by *in situ* XAFS, obtaining information about the mechanism and kinetics of the reaction. By monitoring the oxidation state of Pd in the system we were able to obtain information about what is happening upon exposure of crotyl alcohol to the catalyst. The treatment of nanoparticles with oxygen was also studied by EXAFS analysis in gain insight on the mechanism of the reaction. Sequentially reduced nanoparticles and the *in situ* product formed from the Au/Pd(II) system were studied by EXAFS in order to determine the structure and morphology of the nanoparticles.

In order to analyze the nanoparticles by *in situ* XAFS, it was required that the metal be present in high concentrations. Upon concentrating the samples, agglomeration was seen which resulted in large particles. Large particles are not ideal for catalytic analyses, but they were usable for the purpose of this study. For future analyses, a method of synthesizing small, monodisperse Au and AuPd nanoparticles at metal concentrations of 10 mM or higher should be investigated.

Studying the oxidation of crotyl alcohol by Au NPs and Pd(II) salt by *in situ* XAFS and EXAFS yielded interesting results. It was seen that upon the addition of crotyl alcohol to the system, all of the Pd(II) had reduced to Pd(0). If any Pd(II) had remained in the system, a significant Pd-Cl contribution in the resulting spectrum would be seen. However, no significant Pd-Cl features remained at the end of reaction, signifying the full reduction of Pd(II) in the

system. Kinetic information on the rate of Pd(II) reduction by the addition of crotyl alcohol was also studied by *in situ* XANES. It was noted that, varying the ratio of Pd to crotyl alcohol changed the rate at which the Pd was reduced. The reaction which produced the best results was had a 1:1 ratio of Pd to crotyl alcohol. This reaction provided a series of time-resolved data which was easily transformed into a linear combination plot of percent Pd(II) reduction versus time. From this information the kinetics of the reaction were studied. The reduction of Pd(II) by an equivalent of crotyl alcohol was determined to be a first order reaction with a rate of 0.468 min^{-1}.

EXAFS fitting was performed on samples pre-synthesized in the lab and the nanoparticles formed *in situ* during the reaction of Au NPs and Pd(II) salt with crotyl alcohol. It was found that, as the ratio of crotyl alcohol to Pd(II) was reduced, the Pd-Pd contributions decreased suggesting a more uniform deposition of Pd onto the Au seed particles was achieved. The monometallic samples synthesized in the lab showed M-M coordination numbers much less than the bulk number of 12, indicating that the particles are very small, consisting of many surface atoms. Sequentially reduced 1:3 Au:Pd nanoparticles synthesized in the lab had larger Au-M coordination numbers than Pd-M, suggesting that the majority of gold is situated inside the particle while Pd composes the outer shell. However, there is some mixing of the metals within the nanoparticles, suggest by the Pd-M value being much higher than 6, and the Au-M value being lower than 12. This signifies that some Pd has migrated inside the particle while some Au is situated on the particle surface. Therefore the sequentially reduced particles have likely adopted a random or cluster in cluster morphology. This morphology may have occurred during nanoparticle synthesis, may be a result of concentrating the sample to 10 mM, or due to temporal evolution over a 10 day period.

4.2.2. Future Work

In situ XAFS analysis is an exciting and novel way of analyzing many reactions, including catalytic systems. It has the potential to provide invaluable information about the mechanism and kinetics of reactions. However, there are still some limitations and obstacles that must be overcome in order to perfect this analysis. Further uses for *in situ* XAFS and the limitations which need to be overcome will be discussed below.

4.2.2.1. *In situ* Analysis of Catalytic Reactions; Following the Kinetics of a Reaction

Using *in situ* XAFs we successfully determined the kinetics for the reduction of Pd(II) onto Au seeds by crotyl alcohol. Applying the same strategy of analysis, we have the potential to gain insight into the kinetics of other catalytic and nanoparticle reactions. It would be beneficial to study a variety of substrates and catalyst systems by *in situ* XAFS in order to determine the active species of the catalyst and how the catalyst works with certain substrates. Understanding a variety of catalysts and how they work with certain substrates will help in the development of more efficient catalysts. This reflects back on important reactions such as glycerol oxidation. Gaining new information on reaction kinetics and active species of catalysts, we may be able to develop some very important catalysts in the future.

4.2.2.2. *In situ* Analysis of Galvanic Exchange Reactions

Preliminary work has been done on the *in situ* study of the galvanic exchange reaction between Pd nanoparticles and $HAuCl_4$. Galvanic exchange reactions involve the replacement of atoms from a nanoparticle with those from a metal salt precursor.[18] The driving force of this reaction is the difference in electrochemical potential of the two species. The metal salt must have a standard reduction potential greater than the nanoparticle species in order to oxidize the sacrificial nanoparticle.

The galvanic exchange between Pd nanoparticles and Au salts was analyzed by quick scan, *in situ* XAFS on the Pd-L_{III}-Edge. $HAuCl_4$ dissolved in water was added in 5 different aliquots to a liquid sample of Pd nanoparticles. Quick scans were taken of the solution after each addition of Au salt to the nanoparticles and the oxidation of Pd was monitored. The time-resolved data for this analysis is presented in Figure 4.2. Initial results have shown that upon each addition of Au, the Pd was oxidized from the nanoparticles. The oxidation of Pd is indicated by an increase in the white line intensity of the Pd-L_{III}-absorption edge. After each addition of Au, the absorption edge increased indicating that more Pd has been oxidized from the nanoparticles. As Pd is oxidized Au is simultaneously reduced onto the nanoparticle, presumably forming a shell on the surface of the particle. However, the Au edge was not analyzed in this experiment and EXAFS fitting was not performed. Therefore, a definitive conclusion cannot be drawn about the nanoparticles morphology at this time.

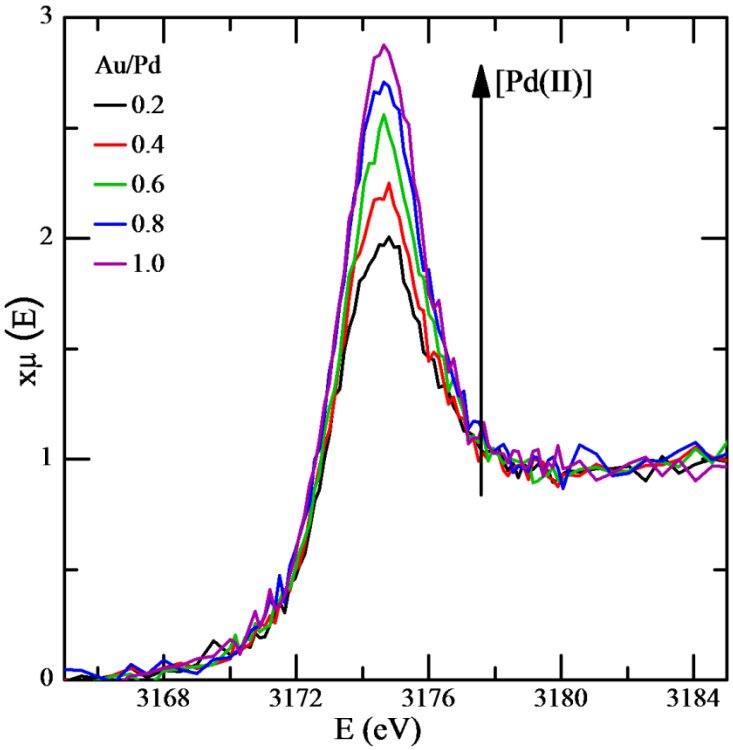

Figure 4.2. Time resolved EXAFS of the Pd-L_{III}-Edge for the galvanic exchange reaction between Pd NPs and $HAuCl_4$.

The preliminary results obtained from this experiment show promise on the *in-situ* analysis of galvanic exchange reactions. This type of reaction has been used to synthesize many different types of bimetallic nanoparticles. Therefore, it would be beneficial to continue our research on these reactions in order to gain insight into what is occurring during galvanic displacement and the kinetics by which these types of reactions occur.

4.2.2.3. Overcoming Beam-induced Photoreduction

Although *in situ* analysis has proven to be a very desirable technique there are still a few faults that need to be overcome in order to routinely perform this analysis. One of the most

troublesome problems that we encountered during our *in situ* studies was the beam-induced photoreduction of the liquid phase samples. However, photoreduction of the sample appears to have only occurred at lower energies. When analyzing the Pd-K-Edge (24,350 eV) there was no evidence of photoreduction of the Pd(II) salt, but when studying the Pd-L_{III}-Edge (3,173 eV) photoreduction of the Pd(II) salt appeared to occur quite rapidly. While we were able to reduce the rate of photoreduction to negligible amounts via diffusing the beams and using energy filters to cut down the beam intensity, this leads to a loss of spectral resolution. Figure 4.3 shows a series of scans of the Pd-L_{III}-edge for a solution of Pd(II) salt in water. As the sample is held under the beam for increasing periods of time it is seen that formation of Pd(0) increases. At this time it remains unknown as to why photoreduction is only seen at lower energies; it is likely due to the high absorption of the X-rays by the aqueous solvent at these energies, leading to the photooxidation of water.

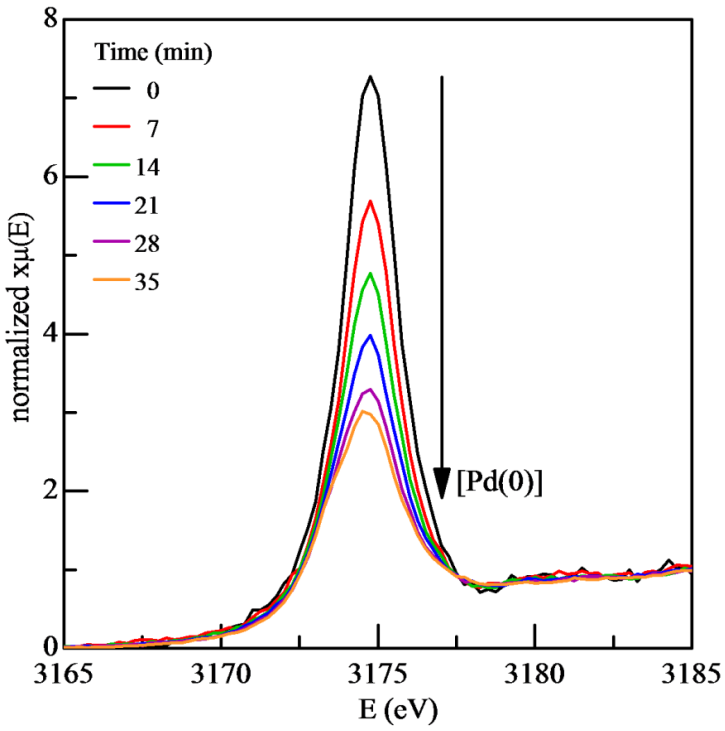

Figure 4.3. Time resolved Pd-L_{III}-Edge data for a series of spectra of Pd(II) salt in water.

One possible method to inhibit the photoreduction of the sample is to add an oxidant into the system which re-oxidizes any photoreduced material. However, this is not an ideal way to treat the sample because it alters the reaction conditions, preventing one from analyzing the reaction under true *in situ* parameters. In order to make *in situ* XAFS analysis a more precise technique, future development for the prevention or inhibition of beam induced photoreduction needs to be explored. This is particularly important given that *in situ* XAFS analysis is one of the most novel techniques that can be used to study a variety of different systems, including NP catalysts.

4.3 References

1 R. Narayanan, M. A. El-Sayed, *J. Am. Chem. Soc.* **2003**, *125*, 8340-8347.

2 S. B. Simonsen, I. Chorkendorff, S. Dahl, M. Skoglundh, J. Sehested, S. Helveg, *J. Am. Chem. Soc.* **2010**, *132*, 7968-7975.

3 S. B. Simonsen, I. Chorkendorff, S. Dahl, M. Skoglundh, J. Sehested, S. Helveg, *J. Catal.* **2011**, *281*, 147-155.

4 J. A. Jiménez, M. Sendova, *Mater. Chem. & Phys.* **2012**, *135*, 282-286.

5 E. M. Larsson, J. Millet, S. Gustafsson, M. Skoglundh, V. P. Zhdanov, C. Langhammer, *ACS Catal.* **2012**, *2*, 238-245.

6 X. W. Lou, C. Yuan, E. Rhoades, Q. Zhang, L. A. Archer, *Adv. Funct. Mater.* **2006**, *16*, 1679-1684.

7 S. H. Bergens, B. Bosnich, *J. Am. Chem. Soc.* **1991**, *113*, 958-967.

8 S. Hirasawa, Y. Nakagawa, K. Tomishige, *Catalysis Science & Technology* **2012**, *2*, 1150-1152.

9 R. Garcia, M. Besson, P. Gallezot, *Appl. Catal., A* **1995**, *127*, 165-176.

10 S. Carrettin, P. McMorn, P. Johnston, K. Griffin, C. J. Kiely, G. A. Attard, G. J. Hutchings, *Top. Catal.* **2004**, *27*, 131-136.

11 A. Brandner, K. Lehnert, A. Bienholz, M. Lucas, P. Claus, *Top. Catal.* **2009**, *52*, 278-287.

12 M. Sankar, N. Dimitratos, D. W. Knight, A. F. Carley, R. Tiruvalam, C. J. Kiely, D. Thomas, G. J. Hutchings, *ChemSusChem* **2009**, *2*, 1145-1151.

13 W. Hu, D. Knight, B. Lowry, A. Varma, *Ind. Eng. Chem. Res.* **2010**, *49*, 10876-10882.

14 A. Villa, A. Gaiassi, I. Rossetti, C. L. Bianchi, K. van Benthem, G. M. Veith, L. Prati, *J. Catal.* **2010**, *275*, 108-116.

15 A. Villa, G. M. Veith, L. Prati, *Angew. Chem. Int. Ed.* **2010**, *49*, 4499-4502.

16 G. L. Brett, Q. He, C. Hammond, P. J. Miedziak, N. Dimitratos, M. Sankar, A. A. Herzing, M. Conte, J. A. Lopez-Sanchez, C. J. Kiely, D. W. Knight, S. H. Taylor, G. J. Hutchings, *Angew. Chem. Int. Ed.* **2011**, *50*, 10136-10139.

17 L. Prati, A. Villa, C. E. Chan-Thaw, R. Arrigo, D. Wang, D. S. Su, *Faraday Discuss.* **2011**, *152*, 353-365.

18 T. Huang, R. W. Murray, *J. Phys. Chem. B* **2003**, *107*, 7434-7440.